

EPA-650/4-74-040

NOVEMBER 1974

Environmental Monitoring Series

# **MATHEMATICAL SIMULATION OF SMOG CHAMBER PHOTOCHEMICAL EXPERIMENTS**



Office of Research and Development  
U.S. Environmental Protection Agency  
Washington, DC 20460

EPA-650/4-74-040

# **MATHEMATICAL SIMULATION OF SMOG CHAMBER PHOTOCHEMICAL EXPERIMENTS**

by

Thomas A. Hecht, Mei-Kao Liu, and David C. Whitney

Systems Applications, Inc.  
950 Northgate Drive  
San Rafael, California 94903

Contract No. 68-02-0580  
ROAP 21AKC  
Task 23  
Program Element No. 1A1008

EPA Project Officer: Marcia C. Dodge

Chemistry and Physics Laboratory  
National Environmental Research Center  
Research Triangle Park, North Carolina 27711

Prepared for

OFFICE OF RESEARCH AND DEVELOPMENT  
U.S. ENVIRONMENTAL PROTECTION AGENCY  
WASHINGTON, D.C. 20460

November 1974

This report has been reviewed by the Environmental Protection Agency and approved for publication. Approval does not signify that the contents necessarily reflect the views and policies of the Agency, nor does mention of trade names or commercial products constitute endorsement or recommendation for use.

# CONTENTS

PREFACE . . . . .	v
ABSTRACT . . . . .	vi
ACKNOWLEDGMENT . . . . .	vii
LIST OF ILLUSTRATIONS . . . . .	viii
LIST OF TABLES . . . . .	xi
LIST OF ABBREVIATIONS . . . . .	xiii
I INTRODUCTION . . . . .	1
A. Investigating the Phenomenology of Smog Formation . . . . .	1
B. Smog Chamber Experiments . . . . .	2
C. Studies of Elementary Reactions . . . . .	6
D. Kinetic Simulation . . . . .	7
E. Mathematical Techniques Useful in Kinetic Simulation . . . . .	8
PART 1--THE PHENOMENOLOGY OF SMOG FORMATION . . . . .	11
II DEVELOPMENT, ANALYSIS, AND APPLICATION OF THE KINETIC MECHANISM . . . . .	12
III EVALUATION OF THE GENERAL MECHANISM USING NAPCA DATA . . . . .	15
A. Predictions for Propylene/ $\text{NO}_x$ , n-Butane/ $\text{NO}_x$ , and Propylene/n-Butane/ $\text{NO}_x$ Experiments . . . . .	16
1. Changes in the General Kinetic Mechanism . . . . .	17
2. Results and Discussion . . . . .	25
B. Simulation of a Multiparaffin/ $\text{NO}_x$ Smog Chamber Experiment . . . . .	38
1. Choice of Rate Constants and Reaction Mechanism . . . . .	40
2. Results and Discussion . . . . .	41

III	EVALUATION OF THE GENERAL MECHANISM USING NAPCA DATA (Continued)	
C.	Simulation of a Multiolefin/ $\text{NO}_x$ Smog Chamber Experiment . . .	46
1.	Choice of Rate Constants for the Oxidant-Olefin Reactions . . . . .	53
2.	Changes in the General Mechanism . . . . .	53
3.	Results and Discussion . . . . .	60
IV	SENSITIVITY AND UNCERTAINTY OF REACTIONS IN THE GENERAL MECHANISM . . . . .	69
A.	The Mechanism Employed . . . . .	70
B.	Sensitivity Analysis . . . . .	74
1.	Criterion of Sensitivity . . . . .	76
2.	Procedure . . . . .	78
3.	Results . . . . .	80
C.	The Implications of Combined Sensitivity and Uncertainty Data . . . . .	82
1.	Rate Constants That Should Be Determined with Great Accuracy . . . . .	82
2.	Reactions That Can Possibly Be Eliminated From the General Mechanism . . . . .	85
D.	Concluding Comments . . . . .	86
V	ANALYSIS OF UCR DATA	
A.	Characteristics of the Chamber System That Affect the Chemical Kinetics . . . . .	88
1.	Light Intensity . . . . .	88
2.	Homogeneity of Reactants . . . . .	93
3.	Temperature . . . . .	93
4.	Water Concentration . . . . .	93
5.	Wall Effects . . . . .	96
6.	Analytical Methods and Dilution Due to Sampling . . . . .	102
B.	Simulation of UCR Propylene/ $\text{NO}_x$ Experiments . . . . .	105
PART 2--	METHODOLOGY . . . . .	124
VI	TECHNIQUES FOR EVALUATING THE KINETIC MECHANISM . . . . .	125
VII	AN AUTOMATIC COMPUTER PROGRAM FOR EVALUATION OF KINETIC MECHANISMS . . . . .	126
A.	Chamber Effects . . . . .	127
B.	Computational Aspects . . . . .	129
C.	Ease of Changing Reactions . . . . .	130

VIII	THE QUASI-STEADY-STATE ASSUMPTION OF CHEMICAL KINETICS . . . . .	132
A.	The Need for the Quasi-Steady-State Assumption . . . . .	133
B.	The Validity of the Quasi-Steady-State Assumption When Applied to a Simple Kinetic Mechanism . . . . .	134
1.	Exact Solutions . . . . .	136
2.	Quasi-Steady-State Solutions . . . . .	137
3.	Comparison of the Exact and the Quasi-Steady-State Solutions . . . . .	138
C.	A General Theory on the Validity of the Quasi-Steady-State Assumption . . . . .	143
D.	Some Numerical Experiments Using the General Mechanism . . . .	149
E.	Conclusions . . . . .	151
IX	TREATMENT OF COMPLEX MIXTURES OF ORGANIC REACTANTS IN THE KINETIC MECHANISM . . . . .	153
A.	Exact Solutions . . . . .	158
B.	Approximate Solutions . . . . .	162
PART 3--	OVERVIEW AND PROSPECT . . . . .	170
X	OVERVIEW AND PROSPECT . . . . .	171
REFERENCES	. . . . .	174
EPA TECHNICAL REPORT DATA FORM	. . . . .	178

## PREFACE

As part of its program to clarify the roles of organic compounds and oxides of nitrogen in the production of photochemical smog, the U.S. Environmental Protection Agency (EPA) has supported and is continuing to support the study of irradiation-induced air pollution in environmental chambers and the determination of the rate constants and mechanisms of elementary reactions thought to be important in smog formation. However, experimental work cannot by itself lead to a complete understanding of the smog formation process. Consequently, the EPA is sponsoring SAI's work on the development of a chemical kinetic mechanism for photochemical smog formation. The mechanism incorporates the experimentally measured rate constants and is presently being tested in relation to data obtained during smog chamber experiments. Ultimately, the mechanism should be capable of predicting the kinetics of the chemical transformations that take place in photochemical smog. Our initial efforts to formulate and evaluate a kinetic mechanism for photochemical smog formation were summarized in a detailed planning document (Seinfeld et al., 1973) and in a 1973 final report (Hecht et al., 1973). In the present report, we describe the results of our continued efforts to improve this kinetic mechanism.

## ABSTRACT

This report deals with the continued development and testing of a general kinetic mechanism for photochemical smog formation. In line with recent experimental measurements, several rate constant values were updated, and simulations of several n-butane/ $\text{NO}_x$ , propylene/ $\text{NO}_x$ , and n-butane/propylene/ $\text{NO}_x$  smog chamber experiments were repeated. The predictions made vary in their agreement with experimental observations, but they tend to be best at high ratios of initial hydrocarbons to  $\text{NO}_x$ . The mechanism also reproduced reasonably well the behavior of a complex mixture of paraffins and  $\text{NO}_x$ , and of a mixture of six olefins and  $\text{NO}_x$ . A sensitivity analysis of the mechanism was carried out, and the results were combined with uncertainty estimates of the rate constants to quantify the importance of determining individual rate constants with greater accuracy. Operating parameters of the University of California, Riverside, (UCR) evacuable smog chamber were considered in detail; experimental data from this chamber will soon be used to test the mechanism further. Finally, the report discusses the validity of the steady-state approximation in simulating smog chamber experiments and some techniques for mathematically combining a number of similar organic species into general groupings.



## ACKNOWLEDGMENT

We wish to express our appreciation to the individuals who contributed to the computational aspects of this work. The sensitivity calculations in Section II-B were carried out by John Overton of EPA; the other computer runs used for the study were done by Gary Lundberg of SAI.

## ILLUSTRATIONS

1	Results of Smog Chamber Simulation for Run EPA 306 . . . . .	26
2	Results of Smog Chamber Simulation for Run EPA 325 . . . . .	27
3	Results of Smog Chamber Simulation for Run EPA 329 . . . . .	27
4	Results of Smog Chamber Simulation for Run EPA 459 . . . . .	28
5	Results of Smog Chamber Simulation for Run EPA 307 . . . . .	29
6	Results of Smog Chamber Simulation for Run EPA 333 . . . . .	30
7	Results of Smog Chamber Simulation for Run EPA 348 . . . . .	31
8	Results of Smog Chamber Simulation for Run EPA 349 . . . . .	32
9	Results of Smog Chamber Simulation for Run EPA 352 . . . . .	33
10	Simulation of the Multiparaffin/ $\text{NO}_x$ Run--Predictions for $\text{NO}$ , $\text{NO}_2$ , $\text{O}_3$ , and 2-Methyl-Pentane . . . . .	43
11	Simulation of the Multiparaffin/ $\text{NO}_x$ Run--Predictions for 2,2,4-Tri-Methyl-Pentane, n-Pentane, and Aldehyde . . . . .	44
12	Simulation of the Multiparaffin/ $\text{NO}_x$ Run--Predictions for Iso-Pentane, 2,4-Di-Methyl-Pentane, and PAN . . . . .	45
13	Simulation of the Multiolefin/ $\text{NO}_x$ Experiment Using the Mechanism in Table 1--Predictions for $\text{NO}$ , $\text{NO}_2$ , and $\text{O}_3$ . . . . .	49
14	Simulation of the Multiolefin/ $\text{NO}_x$ Experiment Using the Mechanism in Table 1--Predictions for Aldehyde, Cis-2-Butene, and Ethylene . . . . .	50
15	Simulation of the Multiolefin/ $\text{NO}_x$ Experiment Using the Mechanism in Table 1--Predictions for PAN, 1-Butane, and 2-Methyl-2-Butene . . . . .	51
16	Simulation of the Multiolefin/ $\text{NO}_x$ Experiment Using the Mechanism in Table 1--Predictions for 2-Methyl- 1-Butene and Propylene . . . . .	52

17	Simulation of the Multiolefin/ $\text{NO}_x$ Experiment Using the Revised Mechanism (Table 8)--Predictions for $\text{NO}$ , $\text{NO}_2$ , and $\text{O}_3$ . . . . .	64
18	Simulation of the Multiolefin/ $\text{NO}_x$ Experiment Using the Revised Mechanism (Table 8)--Predictions for Formaldehyde, Aldehyde, Cis-2-Butene, and Ethylene . . . . .	65
19	Simulation of the Multiolefin/ $\text{NO}_x$ Experiment Using the Revised Mechanism (Table 8)--Predictions for PAN, 1-Butene, and 2-Methyl-2-Butane . . . . .	66
20	Simulation of the Multiolefin/ $\text{NO}_x$ Experiment Using the Revised Mechanism (Table 8)--Predictions for 2-Methyl-1-Butene and Propylene . . . . .	67
21	Base Case for the Sensitivity Study--Run EPA 329 . . . . .	75
22	Spatial Distribution of Light Within the Evacuatable Chamber Without a Reflector . . . . .	89
23	Water Concentration as a Function of Time for Run EC-11, and Constant Value (Solid Line) Used for Simulating This Experiment . . . . .	94
24	Water Concentration as a Function of Time for Run EC-16, and Constant Value (Solid Line) Used for Simulating This Experiment . . . . .	95
25	Simulation of Run EC-11 Using the Mechanism in Table 1--Predictions for $\text{NO}$ , $\text{NO}_2$ , and PAN . . . . .	110
26	Simulation of Run EC-11 Using the Mechanism in Table 1--Predictions for Olefin, Aldehyde, and $\text{O}_3$ . . . . .	111
27	Simulation of Run EC-12 Using the Mechanism in Table 1--Predictions for $\text{NO}$ , $\text{NO}_2$ , and PAN . . . . .	112
28	Simulation of Run EC-12 Using the Mechanism in Table 1--Predictions for Olefin, Aldehyde, and $\text{O}_3$ . . . . .	113
29	Simulation of Run EC-14 Using the Mechanism in Table 1--Predictions for $\text{NO}$ , $\text{NO}_2$ , and PAN . . . . .	114
30	Simulation of Run EC-14 Using the Mechanism in Table 1--Predictions for Olefin, Aldehyde, and $\text{O}_3$ . . . . .	115
31	Simulation of Run EC-16 Using the Mechanism in Table 1--Predictions for $\text{NO}$ , $\text{NO}_2$ , and PAN . . . . .	116
32	Simulation of Run EC-16 Using the Mechanism in Table 1--Predictions for Olefin, Aldehyde, and $\text{O}_3$ . . . . .	117

33	Simulation of Run EC-17 Using the Mechanism in Table 1-- Predictions for NO, NO <sub>2</sub> , and PAN . . . . .	118
34	Simulation of Run EC-17 Using the Mechanism in Table 1-- Predictions for Olefin, Aldehyde, and O <sub>3</sub> . . . . .	119
35	Simulation of Run EC-18 Using the Mechanism in Table 1-- Predictions for NO, NO <sub>2</sub> , and PAN . . . . .	120
36	Simulation of Run EC-18 Using the Mechanism in Table 1-- Predictions for Olefin, Aldehyde, and O <sub>3</sub> . . . . .	121
37	Simulation of Run EC-21 Using the Mechanism in Table 1-- Predictions for Olefin, NO, NO <sub>2</sub> , and Aldehyde . . . . .	122
38	Simulation of Run EC-21 Using the Mechanism in Table 1-- Predictions for O <sub>3</sub> and PAN . . . . .	123
39	Comparisons of the Exact and the QSSA Solutions for Stable Species . . . . .	138
40	Comparisons of the Exact and the QSSA Solutions for the Reaction Intermediate . . . . .	140
41	The Rate Constant for HC + O . . . . .	167
42	The Rate Constant for HC + O <sub>3</sub> . . . . .	168
43	The Rate Constant for HC + OH . . . . .	169

## TABLES

1	A Lumped Kinetic Mechanism for Photochemical Smog Formation . . . . .	19
2	Validation Values of the Rate Constants and Their Comparison with the Recommended Values of Other Investigations . . . . .	22
3	Initial Conditions Associated with Experimental Chamber Data . . . . .	25
4	Reactions That Can Be Eliminated from the General Mechanism Shown in Table 1 . . . . .	37
5	Values of T, H, and M Before and After Removal of the Reactions in Table 4 . . . . .	38
6	Rate Constants for the O and OH Oxidation Reactions . . . . .	42
7	Experimental Values for the Simulation of Oxidant-Olefin Reactions . . . . .	48
8	Revised General Mechanism Used To Simulate the Multiolefin/ NO <sub>x</sub> Experiment . . . . .	61
9	The Kinetic Mechanism Used for the Sensitivity Analysis . . . . .	71
10	Sensitivity of the Reactions . . . . .	81
11	Combined Sensitivity and Uncertainty of the Reactions . . . . .	84
12	Reactions Participating in the Total Ozone Decay Process . . . . .	99
13	Physical and Chemical Parameters Measured . . . . .	103
14	Initial Conditions for Experiments in the Propylene/ NO <sub>x</sub> Block . . . . .	109
15	Error Resulting from the Use of the QSSA . . . . .	141
16	Percentage Errors Incurred by Using the Quasi-Steady-State Assumption . . . . .	150
17	Percentage Errors Incurred by Using the Photostationary State Assumption . . . . .	152

18	Comparison of Hydrocarbon Consumption for Different Lumping Schemes . . . . .	161
19	Comparison of Ozone Production for Different Lumping Schemes . . . . .	161
20	Comparison of Hydrocarbon Consumption in the Multiparaffin Run . . . . .	163
21	Comparison of Ozone Production in the Multiparaffin Run . . . . .	163
22	Comparison of Hydrocarbon Consumption in the Multiolefin Run . . . . .	164
23	Comparison of Ozone Production in the Multiolefin Run . . . . .	164

## ABBREVIATIONS

cc	Cubic centimeters
EC	Evacuable chamber
EPA	Environmental Protection Agency
GC	Gas chromatograph
NAPCA	National Air Pollution Control Administration
NBS	National Bureau of Standards
ppb	Parts per billion
pphm	Parts per hundred million
ppm	Parts per million
SAI	Systems Applications, Incorporated
SAPRC	Statewide Air Pollution Research Center
SM	Sensitivity measure
UCR	University of California at Riverside

## I INTRODUCTION

In contrast to the two earlier documents describing a kinetic mechanism for photochemical smog formation mentioned previously (Seinfeld et al., 1973; Hecht et al., 1973), this report distinguishes between the analysis of the phenomenology of the chemical process and the mathematical and computational methodology used to carry out the simulations. This chapter discussed the concepts of phenomenology and methodology as they relate in general to the work described in this report. In addition, this chapter briefly reviews the aspects of experimental investigations of the smog formation process that are relevant to kinetic modeling. Special consideration is given to the manner in which kinetic simulation with a chemical mechanism complements smog chamber experiments and reaction kinetics studies in investigations of the chemistry of smog formation. We conclude this chapter with a discussion of the role of kinetic simulation in understanding the nature of photochemical smog formation and a summary of the uses of mathematical techniques for kinetic simulation that have been developed during the reported work.

### A. INVESTIGATING THE PHENOMENOLOGY OF SMOG FORMATION

In a system as complex as the atmosphere, isolation and characterization of the chemical processes that occur are virtually impossible. Thus, two fundamental approaches have been devised for controlled study of the chemistry of smog formation: irradiation of known concentrations of pollutants in a large reactor (smog chamber) and determination of the rates and mechanisms of elementary reactions thought to occur in polluted air. Data obtained during a smog chamber experiment include the concentrations of a limited number of reactants ( $\text{NO}_2$ ,  $\text{NO}$ , organics) and products ( $\text{NO}_2$ ,  $\text{O}_3$ , PAN) with time. However, one is unable to gain insight into the details of the chemical transformations taking place; only the macroscopic effects of the overall chemical process are observed. On the other hand,



detailed information concerning the rate and course of a single reaction, such as that obtained in a reaction kinetics study, reveals little concerning the nature of the overall smog formation process. Indeed, one has difficulty knowing whether all the important reactions have been identified.

Kinetic simulation provides a means of comparing the results of these two experimental approaches for investigating the chemistry of smog formation. Studies of several elementary reactions can be drawn together, yielding a chemical mechanism. The mathematical rate equations describing the mechanism can then be solved numerically to obtain predictions of the concentrations of the reactants and products with time. In principle, therefore, kinetic simulation takes the results of elementary reaction studies as input data and produces results of a form identical to the data obtained in smog chamber experiments as output. By comparing the predictions of the mechanism with actual chamber data, one is able to determine the degree of agreement between the two experimental approaches.

In practice, the comparison process is somewhat more complicated than that just described. For example, it has been shown that the surfaces of smog chambers can and do affect the overall rate of the chemical transformations. This and other systematic effects must be included in the kinetic simulation. Uncertainties in the values of experimentally measured rate constants are equally perplexing. These can range from 20 per cent in the most favorable case to a factor of 5 or greater. The major sources of uncertainty in both types of experimental data are addressed here in detail, and the value and role of kinetic simulation for understanding the chemistry of smog formation are examined in light of these difficulties.

## B. SMOG CHAMBER EXPERIMENTS

A smog chamber experiment is generally conducted in the following manner. A reactor (ranging in size from a few liters to thousands of liters) is charged with a known number of moles of organic compound(s)

and  $\text{NO}_x$  in air. After the reactants are homogeneously distributed throughout the chamber, the system is irradiated. During the irradiation, the concentrations of various reactants and products are determined at several points in time.

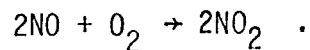
Replicate runs carried out in a particular environmental chamber are generally reproducible to within a difference of 10 percent. When the same experiment is carried out in different chambers, however, the agreement between the observed concentration-time profiles is erratic. The reasons for these "anomalies" have been discussed at some length by Seinfeld et al. (1973), but the major causes are reviewed briefly here.

Some of the discrepancies can be accounted for simply in terms of operating characteristics of the various chambers. For example, key radical chain initiating reactions, such as the dissociation of  $\text{NO}_2$ , are photolytic. Thus, depending on the magnitude of variations between chambers, differences in the intensity and the spectral and spatial distribution of the light can have a significant effect on the rate of smog formation. The majority of reactions occurring in smog, however, are thermal. Most of these are known to have small positive activation energies (0 to 5 kcal/mole), although a few have small negative activation barriers (0 to -2 kcal/mole). Smog chamber experiments are generally carried out at ambient temperatures. But, depending upon the placement of the lights (outside or inside the chamber) and the adequacy of the air conditioning available, temperatures within a chamber can rise to  $50^\circ\text{C}$  during a six-hour irradiation. The variation of the rate of smog formation with temperature has not yet been systematically investigated in chambers. However, it is unlikely that a temperature rise of  $25^\circ\text{C}$  would have a negligible effect on the kinetics. Fortunately, while variations in light intensity and temperature can affect the observed rate of the chemical transformations, these sources of uncertainty can largely be eliminated through careful measurement, control, and chamber design procedures.

Interactions of the walls or material on the walls with the reactants and products in the gas phase are less easily quantified causes of disagreement between chambers. Gay and Bufalini (1971) have shown that

nitric acid accumulates on the walls of a small reactor when ppm levels of organic and  $\text{NO}_x$  are irradiated. As a result, it is not possible to account for all of the "nitrogen" introduced into the chamber in terms of nitrogen-containing products measured in the gas phase at the end of an experiment. Ozone, on the other hand, is known to decompose directly on the walls. The loss rate varies from chamber to chamber, but the destruction of 20 percent of an initial  $\text{O}_3$  charge over a six-hour irradiation of  $\text{O}_3$  in air is not uncommon. The observed rate probably depends upon the surface-to-volume ratio and the type of wall materials used in the reactor (Jaffe, 1972).

In their study of the thermal oxidation of NO, Bufalini et al. (1972) have shown that if NO and air are photolyzed in an unpurified chamber, NO will be oxidized to  $\text{NO}_2$  at a faster rate than one would predict based on the thermal air oxidation reaction alone:



They have suggested that this is due in part to the liberation of organic contaminants from the walls of the reactor. If this occurs, the organics then participate in a chain process resulting in the additional oxidation of NO above that due to the thermal reaction. In a related experiment, Bufalini et al. have also shown that if air containing a reactive organic compound such as biacetyl is irradiated in a dirty chamber, small concentrations of  $\text{O}_3$  will form. Presumably, this  $\text{O}_3$  forms as a result of a series of reactions involving the organic compound and  $\text{NO}_x$  liberated from the walls.

A final class of chamber uncertainties are those associated with the analytical instrumentation. Errors due to inaccurate calibration of the instruments and chemical interferences in the measurements (lack of specificity) are well known and need not be discussed here. A somewhat more subtle source of uncertainty is attributable to the large volume of sample gas that must be withdrawn from the chamber to obtain accurate

measurements, thus leading to a continuous reduction in the concentrations of both the reactants and the products over the course of an experiment. For example, the analytical instruments commonly used for the measurement of NO/NO<sub>2</sub>, O<sub>3</sub>, organics, PAN, and CO require samples to be withdrawn at an average rate of about 1.5 liters/minute. Thus, during a six-hour experiment, about 10 percent of the original molar charge of reactants would, for example, be lost from a 5000 liter reactor. The percentage of charge lost for a particular chamber depends on the following:

- > The volume of the chamber
- > The type and number of analyzers employed
- > The periodicity of the measurements.

This so-called dilution effect (the volume withdrawn is normally replaced by an equal volume of "clean" air to maintain a constant pressure in the reactor) can be taken into account easily in the analysis of the chamber results if the sampling rates and chamber volume are known. The magnitude of the effect, however, demonstrates the need for the development and application of in situ measurement methods for chamber studies.

Sources of uncertainties in the interpretation of smog chamber data--whether due to imprecise measurements of light intensity, lack of control over temperature, wall reactions, wall contaminants, or other factors--are generally recognized by chamber scientists. In many cases, the data quality can be strengthened simply by keeping careful records of the operating conditions of the chamber, by calibrating instruments with increasing frequency, and by modifying the system design. Unfortunately, wall contamination problems and heterogeneous reactions remain very difficult to characterize. In current programs, the rates of a few particular effects attributable to the walls, such as ozone decomposition, are determined periodically. A detailed chamber characterization study is presently being carried out by Jaffe at Lockheed under contracts with the Coordinating Research Council and EPA. Hopefully, that work will lead to a greater understanding of the magnitude and nature of surface effects.

### C. STUDIES OF ELEMENTARY REACTIONS

The primary criterion used to decide whether a reaction involving reactants present in photochemical smog should be included in a chemical mechanism is the rate of the reaction. The speed at which an elementary reaction proceeds is, of course, proportional to the product of the concentrations of the reactants, and the proportionality factor is usually called the "rate constant" of the reaction. In actual fact, many of the rate constants of the nonphotolytic reactions in smog vary with temperature, pressure, or both and with the concentrations of other gases present. Thus, one must take care to note the conditions under which a rate constant is measured. If necessary, suitable correction of the value for the desired temperature and pressure must be made before the rate constant is used for a kinetic simulation.

Unfortunately, the determination of many gas phase reaction rate constants is extremely difficult because measurements must frequently be carried out near the detection limits of the analytical apparatus. Thus, even though investigators are generally able to achieve a high level of precision in their measurements, the study of the same reaction in other laboratories or by different experimental techniques often leads to very different values of the rate constant, as shown later in this report.

To be sure, the complete kinetic analysis of a reaction entails more than the measurement of the rate constant; the mechanism and products of the elementary reaction must be determined as well. Certainly, most of the reactions considered in this report are well characterized in this regard, but there are some significant exceptions. For example, the detailed fate of the various intermediates of the OH-propylene reaction is still unclear. (Little is known about the behavior of the OH-propylene adduct; for present purposes, the species has been assumed to react in the same fashion as an alkyl radical and has been included in the  $RO_2$  class.) The OH oxidation is the most significant chain transfer step involving organics during a propylene- $NO_x$  smog chamber

experiment. Thus, the uncertainty as to the role of the adduct in smog formation is particularly significant. Another weak link in the mechanism involves the lack of knowledge of the products of the  $O_3$ -olefin reaction. These two deficiencies, however, are well recognized and are being addressed in current research programs.

#### D. KINETIC SIMULATION

Smog chamber data constitute a standard against which the accuracy of predictions of a kinetic mechanism can be measured. But because of wall effects and other operating characteristics of the system, the observed time-varying chemical distribution in the chamber cannot be accounted for entirely in terms of the reactions occurring in the gas phase. Thus, the use of chamber results as a standard or reference for judging the accuracy of a mechanism must be carefully qualified.

As a collection of individual elementary reactions, a chemical mechanism represents the chemistry that one would presumably observe in an infinitely large reactor that is irradiated by a uniform source of light and is maintained at constant temperature. Of course, a typical smog chamber does not meet all of these criteria. Therefore, before predictions and experimental results can be compared, terms must be added to the mechanism to represent operating characteristics of each particular smog chamber. The most important corrections involve the following:

- > Accounting for the dilution of reactants and products due to sampling.
- > Specifying the rate of decomposition of  $O_3$  and the formation of  $HNO_3$  on the walls.
- > Expressing rate constants in the temperature-dependent (exponential) format so that the effects of temperature variations in a chamber on the rate of reactions are properly represented.

In essence, then, the chemical kinetic mechanism actually is an integral component of a mathematical model that simulates a smog chamber system.

A major goal of the chemical and mathematical investigations of smog formation is to gain a level of understanding sufficient to allow prediction of the atmospheric photochemical process. As has been noted, however, there are considerable uncertainties with which one must contend, even in the prediction of the kinetics of a propylene-NO<sub>x</sub> experiment. Inaccuracies in measurements and unknown effects of walls and wall contaminants on the gas phase chemistry create sources of uncertainty in the chamber data. Similarly, large error bounds on the values of many reaction rate constants and unknown reaction mechanisms provide a dis-comforting number of degrees of freedom with which to "tune" the predictions of the model into agreement with the chamber data.

#### E. MATHEMATICAL TECHNIQUES USEFUL IN KINETIC SIMULATION

To obtain predictions of concentration as a function of time, for comparison with smog chamber data, one must fulfill the following requirements:

- > The initial state of the system must be specified (e.g., concentrations of all chemical species present, temperature, and irradiation intensity and spectral distribution).
- > A rate constant value must be assigned to each reaction in the mechanism.
- > The chemical rate equations for each reactant, intermediate, and product must be derived.
- > The resultant differential equations must be solved.

The differential rate equations can be derived manually from the mechanism, but the process is cumbersome. In this report, we describe a computer program (MODKIN), prepared during this study, that automatically formulates the rate equations that mathematically represent a chemical mechanism. Reactions are submitted to this program in standard notation, e.g.,



Since the addition (or deletion) of a single reaction of this form results in changes to four rate equations, the convenience of MODKIN over manual coding is readily apparent.

Because the characteristic time scales of formation of the individual reactants and intermediates in the mechanism usually vary greatly, the resultant set of coupled differential equations are often "stiff."\* When this is the case, small integration time steps are required to obtain accurate solutions of the equations for the most rapidly varying species. Recently, numerical integration routines have been developed that automatically increase the integration time step as the stiffness of the system of equations decreases, thereby reducing the computing time required for a complete smog chamber simulation run. We have incorporated such an algorithm, that of Gear (1971), in MODKIN.

Other mathematical techniques can also result in computer time or storage savings. For example, by invoking the steady-state approximation for cases in which it is valid, the pertinent coupled differential rate equations can be replaced with algebraic equations. Such a change in representation usually results in a reduction in the computing time required for a simulation. However, the magnitude of the savings, if any, depends on the degree to which the stiffness of the system of differential equations is relieved and the number of iterations required to solve the algebraic equations.

Computational time can also be shortened by employing "lumping" techniques. Consider the simulation of a multiorganic/ $\text{NO}_x$ /air experiment. For this system to be represented exactly, each organic species would have to be assigned its individual rate equation. If the number of organic species were large, a significant amount of computer core and time would be required to obtain predictions of the behavior of the system. Although computer storage needs are not of direct concern in the

---

\* A set of differential equations are called "stiff" when the magnitudes of the eigenvalues of the system differ by several orders of magnitude.



development of a chemical mechanism, the mechanism will ultimately be applied to the atmosphere. Exact representation of the hundreds of different reactive organic species at every "grid point" simulated by an airshed model would tax even the largest computers. Consequently, a means of combining or lumping a number of organic species that react in similar ways into a single, fictitious species is needed. We discuss one possible lumping scheme in this report.

PART 1  
THE PHENOMENOLOGY OF SMOG FORMATION

## II DEVELOPMENT, ANALYSIS, AND APPLICATION OF THE KINETIC MECHANISM

A general kinetic mechanism for smog formation has several possible uses. Such a model might be used to calculate the reactivity of individual organic compounds in terms of their ability to "form" smog. Or, imbedded in an airshed dispersion model, the chemical mechanism might be instrumental in evaluating alternative emission control strategies and in assessing the impact of planned urban growth. These uses, however, are contingent upon the accuracy of the mechanism. Thus, the development of a substantially complete and reliable model is of considerable importance.

The qualitative nature of the smog formation process has been understood for a number of years (Leighton, 1961). However, prediction of the chemical process depends on detailed knowledge of both the pathways and the rate constants of the reactions in the mechanism. During the past decade, great progress has been made in measuring the rate constants of gas phase reactions involving short-lived or transient species. The rates of many of the reactions thought to occur in smog have been measured for the first time only recently. Even now, several heretofore speculative reactions are being scrutinized, and the values of other rate constants are being confirmed (e.g.,  $\text{HO}_2 + \text{NO} \rightarrow \text{OH} + \text{NO}_2$ ).

In such a dynamic scientific environment, it would be presumptuous to suggest that any given set of reactions and rate constants is the chemical mechanism for smog formation. Even this report reflects a continuous updating of the mechanism as new knowledge of reaction kinetics became available; several similar forms of the general mechanism appear in conjunction with the different tasks of the project. Only one formulation of the kinetic mechanism (presented later in Table 1) has been tested over an extensive range of initial conditions and reactant ratios. Further evolutionary changes in this mechanism, in the form of a more

detailed treatment of aldehydes,  $O_3$ -olefin reaction mechanisms, and reactions of PAN, were made when we simulated the behavior of a multi-olefin- $NO_x$ -air smog chamber experiment (these are presented later in Table 8). Similarly, before carrying out the sensitivity study reported in Chapter IV, we modified the mechanism in Table 1 to augment the agreement between the predictions and the data for the particular smog chamber experiment that was simulated. The modified scheme is presented later in Table 9. Because these latter sets of reactions are ad hoc formulations that have not yet been tested extensively, we recommend, for the time being, that prospective users of these general mechanisms select the form in Table 1 for their applications.

Although the mechanism is presented in three forms, most of these changes were made to replace overly general representations with more detailed descriptions and to substitute sound experimental measurements--as they became available--for speculative estimates.

The development of the mechanism during this project followed two complementary paths. The first approach involved testing the quality of predictions in relation to smog chamber data. By adding, modifying, or deleting reactions and then varying the values of rate constants within their bounds of uncertainty, we sought to increase the accuracy of prediction of the mechanism over a wide range of organic compound-to- $NO_x$  ratios. For these runs, we reevaluated many of the NAPCA propylene/ $NO_x$ , and propylene/n-butane/ $NO_x$  experiments that we had reported previously (Hecht et al., 1973). In addition to these experiments, however, we examined two multiorganic- $NO_x$  smog chamber experiments. One of these was conducted with five different paraffins present initially; the other contained six different olefins in the initial charge.\* The results of these chamber simulations are discussed in Chapter III.

---

\* The multiolefin/ $NO_x$  experiment was the last set of data to be modeled during the contract year. In attempting to simulate this run, we found it desirable to introduce several changes into the kinetic mechanism to reduce discrepancies between predictions and observed concentration time data. Though tested against only one set of experimental data, the resulting mechanism shows promise and will serve as the springboard for our analysis of UCR propylene- $NO_x$  experiments next year.

The second approach focused on quantifying the influence of uncertainties in the values of individual reaction rate constants on the predictions of the mechanism. We first carried out a detailed sensitivity analysis of the mechanism, calculating the change in the predictions of the model with the change in each rate constant. The sensitivity values (S) were then combined with uncertainty estimates (U) for each rate constant to create a new index (S\*U). The combined index reflects the importance of obtaining more accurate rate constant measurements as a means of reducing the uncertainties in the predictions of the model. In addition to identifying reaction rate constants for which accurate measurements are particularly important, we were able to point out insensitive reactions that can possibly be deleted from the mechanism without significant loss of accuracy. This effort is described in Chapter IV.

In Chapter V, we describe our work using data from the new UCR evacuable smog chamber. The exercises carried out thus far deal primarily with our attempts to model the chamber characteristics properly, but they include simulations of the first seven UCR propylene/ $\text{NO}_x$  photochemistry experiments using the mechanism in Table 1.

Unfortunately, the photochemistry data arrived too late in the project to permit us to begin a formal mechanism development and evaluation program. These propylene experiments, along with many more runs involving n-butane and toluene that are yet to be carried out, will provide the principal chamber data base for our model refinement work next year.

### III EVALUATION OF THE GENERAL MECHANISM USING NAPCA DATA

During the past decade, the National Air Pollution Control Administration\* (NAPCA) conducted an extensive experimental program to investigate the rate of formation of secondary air pollutants (e.g.,  $\text{NO}_2$ ,  $\text{O}_3$ , PAN, aldehydes) in an irradiated system initially containing organic reactants,  $\text{NO}_x$ , and air. We used a number of these experiments involving the irradiation of propylene, n-butane, or both, in  $\text{NO}_x$  and air to test the general kinetic mechanism in its initial configuration (Hecht et al., 1973). Since our 1973 report discussed the experimental techniques and apparatus used, the sources of experimental uncertainty, and the adequacy of these particular experiments as a data base for model evaluation, our comments in this chapter focus chiefly on the continued development and testing of the general mechanism with reference to the NAPCA chamber data.

As noted earlier, one of the principal goals of this project was to refine the general mechanism so as to achieve greater accuracy and confidence in prediction. Toward this end, we have kept abreast of current kinetic and mechanistic studies of relevant elementary reactions, incorporating the results of these studies into the mechanism as soon as possible. Our progress in modeling photochemical smog has been, and will continue to be, limited principally by the rate at which knowledge of uncertain rate constants and elementary reaction mechanisms is established experimentally.

A total of five different combinations of organic compounds were represented in the eleven different NAPCA organic- $\text{NO}_x$ -air irradiation experiments that we used to evaluate the mechanism. The data base was distributed as follows:

---

\* Now part of EPA.

<u>System</u>	<u>No. of Runs</u>
propylene-NO <sub>x</sub>	3
n-butane-NO <sub>x</sub>	1
propylene/n-butane-NO <sub>x</sub>	5
n-pentane/iso-pentane/2-Me-pentane/ 2,4-di-Me-pentane/2,2,4-tri-Me-pentane-NO <sub>x</sub>	1
ethylene/propylene/1-butene/cis-2-butene/ 2-Me-1-butene/2-Me-2-butene-NO <sub>x</sub>	1

As previously noted, the propylene, n-butane, and propylene-n-butane experiments were first considered during last year's mechanism development program. Our interest in the multiolefin/NO<sub>x</sub> and multiparaffin/NO<sub>x</sub> experiments was twofold. First, these experiments provided an opportunity to explore the generality of the mechanism, particularly with respect to reactions of general classes of organic molecules and free radicals. Second, these experiments were well suited for testing our mathematical technique for lumping (or combining) individual organic compounds into general classes.

In this chapter, we restrict our comments to a discussion of changes introduced into the general mechanism during the simulation of the NAPCA experiments. The details and validity of the lumping techniques are considered in Chapter IX.

#### A. PREDICTIONS FOR PROPYLENE/NO<sub>x</sub>, n-BUTANE/NO<sub>x</sub>, AND PROPYLENE/n-BUTANE/NO<sub>x</sub> EXPERIMENTS

Shortly after completion of the previous report, we learned that three of the rate constants in the mechanism had been measured or estimated to be significantly lower than the values we were using. These reactions and their associated rate constants are tabulated as follows:

Reaction	New Value (ppm <sup>-1</sup> min <sup>-1</sup> )	Old Value (ppm <sup>-1</sup> min <sup>-1</sup> )
$O_3 + NO_2 \xrightarrow{k_7} NO_3 + O_2$	0.046 (Ghormley et al., 1973)	0.11
$NO + HNO_3 \xrightarrow{k_{12}} NO_2 + HNO_2$	$2.5 \times 10^{-4}$ (Jaffee and Ford, 1967)	10.0
$HNO_2 + HNO_3 \xrightarrow{k_{13}} 2NO_2 + H_2O$	0.2 (Westberg, 1973)	5.0

Two of the new rate constants,  $k_7$  and  $k_{12}$ , were of particular concern to us because we had recently determined that these reactions influenced the predictions of the mechanism. Reaction 13 was unimportant, however, even when the substantially higher "old" rate constant value was used in the simulations. Decreasing  $k_7$  to its new value resulted in a 15 percent increase in the magnitude of the  $NO_2$  peak and an 18 percent reduction in the time before the  $NO_2$  peak was reached. Finally, a simulation of the experiment with all three rate constants at their revised values resulted in predictions of unacceptably low peak  $NO_2$  and  $O_3$  levels and an unsatisfactorily premature time before the  $NO_2$  peak was reached when compared with the experimental data.

The general mechanism, as presented in the previous report, had been "tuned" into good agreement with experimental data through the adjustment of uncertain rate constants. The deterioration in accuracy of prediction caused by the introduction of the new values of the three rate constants, however, forced a serious reconsideration of the rate constants and reactions in the kinetic mechanism.

#### 1. Changes in the General Kinetic Mechanism

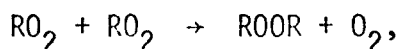
In addition to the three rate constant modifications discussed above, we altered three other rate constants and selected new products for two other reactions.



Reactions 38 and 39, formerly chain termination reactions



and



were modified to produce OH and RO and two RO radicals, respectively, rather than peroxides. This is in line with current thinking regarding peroxy-radical/peroxy-radical reactions involving  $\text{RO}_2$ .

In addition to  $k_7$ ,  $k_{12}$ , and  $k_{13}$ , the following rate constants were revised:

Reaction	New Value	Old Value
$\text{O}_3 + \text{NO} \xrightarrow{k_3} \text{NO}_2 + \text{O}_2$	$20.8 \text{ ppm}^{-1} \text{ min}^{-1}$	$23 \text{ ppm}^{-1} \text{ min}^{-1}$
$\text{NO} + \text{NO}_2 + \text{H}_2\text{O} \xrightarrow{k_{14}} 2\text{HNO}_2$	$2.1 \times 10^{-6} \text{ ppm}^{-2} \text{ min}^{-1}$	$4.3 \times 10^{-6} \text{ ppm}^{-2} \text{ min}^{-1}$
$\text{ALD} + h\nu \xrightarrow{k_{29}} \beta \text{RO}_2 + (2-\beta)\text{HO}_2$	$2.5 \times 10^{-3} \text{ min}^{-1}$	$2.0 \times 10^{-3} \text{ min}^{-1}$

The rate of Reaction 3 was revised to the recently measured value of Ghormley et al. (1973). The rate constants for the heterogeneous formation of nitrous acid and the photodissociation of aldehydes were modified within their bounds of uncertainty (see Chapter IV) because such changes improved the agreement between predictions and experimental data.

We present in Table 1 the general mechanism as it was used for the propylene/, n-butane/, and propylene-n-butane/ $\text{NO}_x$  simulations. The rate constants used for these calculations ("validation values") are summarized in Table 2, along with recommended values of several other investigators.

Table 1

## A LUMPED KINETIC MECHANISM FOR PHOTOCHEMICAL SMOG FORMATION

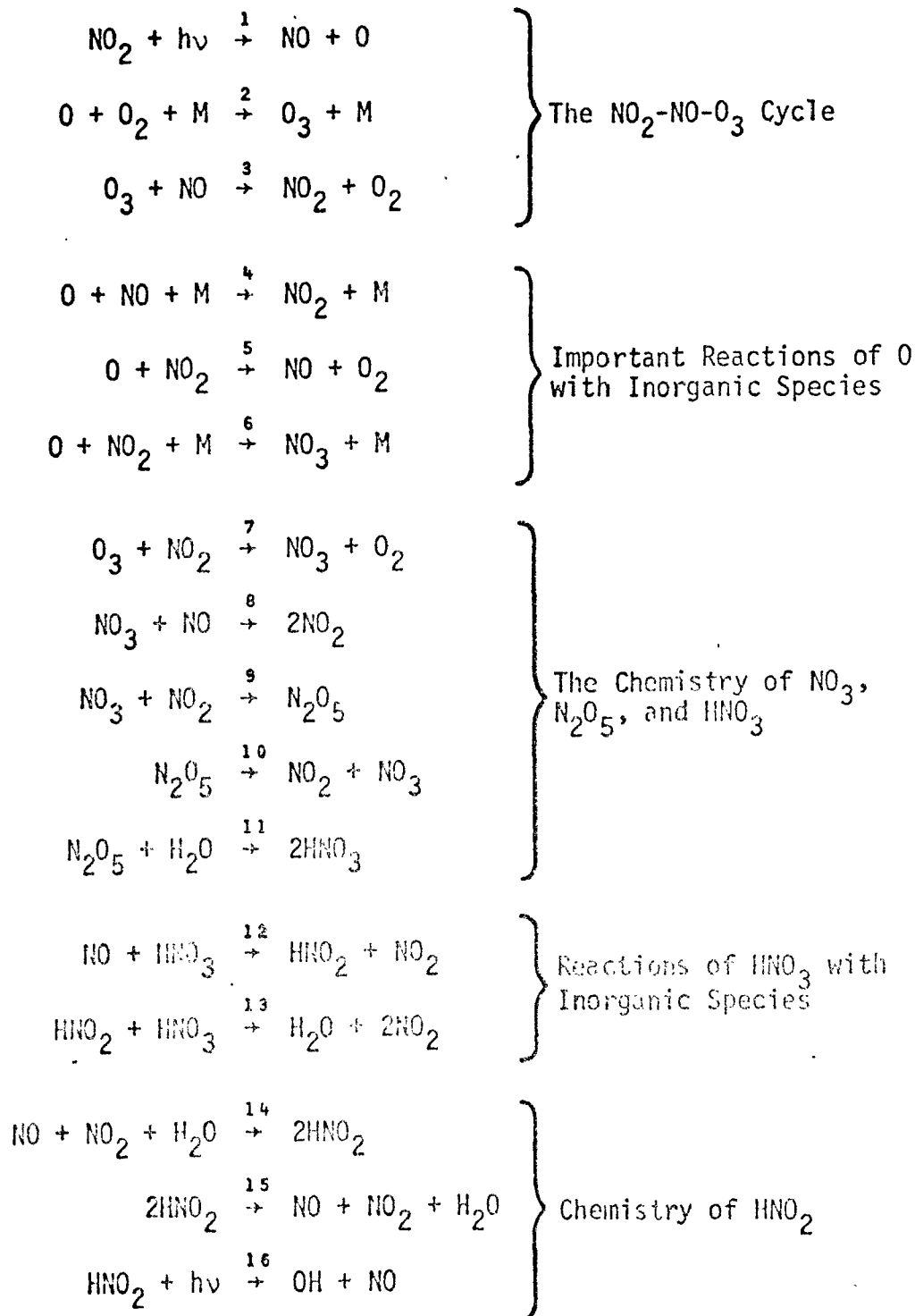
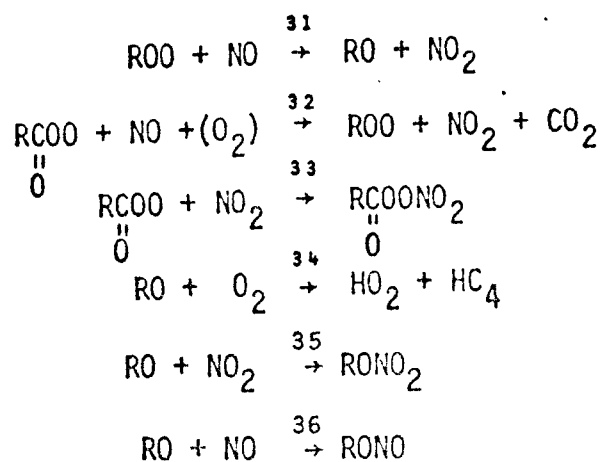


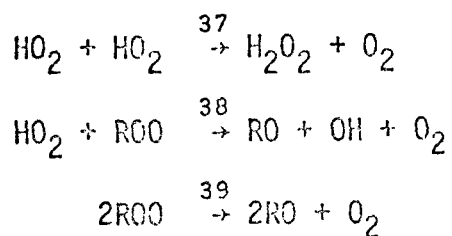
Table 1 (Continued)

$\text{OH} + \text{NO}_2$	$\xrightarrow{17}$	$\text{HNO}_3$	} Important Reactions of OH with Inorganic Species
$\text{OH} + \text{NO} + \text{M}$	$\xrightarrow{18}$	$\text{HNO}_2 + \text{M}$	
$\text{OH} + \text{CO} + (\text{O}_2)$	$\xrightarrow{19}$	$\text{CO}_2 + \text{HO}_2$	
$\text{HO}_2 + \text{NO}$	$\xrightarrow{20}$	$\text{OH} + \text{NO}_2$	} Oxidation of NO by $\text{HO}_2$
$\text{H}_2\text{O}_2 + h\nu$	$\xrightarrow{21}$	$2\text{OH}$	} Photolysis of $\text{H}_2\text{O}_2$
$\text{HC}_1 + \text{O}$	$\xrightarrow{22}$	$\text{ROO} + \alpha \text{RCOO} + (1-\alpha) \text{HO}_2$	} Organic Oxidation Reactions  $\text{HC}_1$ = Olefins $\text{HC}_2$ = Aromatics $\text{HC}_3$ = Paraffins $\text{HC}_4$ = Aldehydes
$\text{HC}_1 + \text{O}_3$	$\xrightarrow{23}$	$\text{RCOO} + \text{RO} + \text{HC}_4$	
$\text{HC}_1 + \text{OH}$	$\xrightarrow{24}$	$\text{ROO} + \text{HC}_4$	
$\text{HC}_2 + \text{O}$	$\xrightarrow{25}$	$\text{ROO} + \text{OH}$	
$\text{HC}_2 + \text{OH}$	$\xrightarrow{26}$	$\text{ROO} + \text{H}_2\text{O}$	
$\text{HC}_3 + \text{O}$	$\xrightarrow{27}$	$\text{ROO} + \text{OH}$	
$\text{HC}_3 + \text{OH}$	$\xrightarrow{28}$	$\text{ROO} + \text{H}_2\text{O}$	
$\text{HC}_4 + h\nu$	$\xrightarrow{29}$	$\beta \text{ROO} + (2-\beta) \text{HO}_2$	
$\text{HC}_4 + \text{OH}$	$\xrightarrow{30}$	$\beta \text{RCOO} + (1-\beta) \text{HO}_2 + \text{H}_2\text{O}$	

Table 1 (Concluded)



Reactions of Organic  
Free Radicals with NO,  
NO<sub>2</sub>, and O<sub>2</sub>



Other Peroxy Radical  
Reactions

Table 2

VALIDATION VALUES OF THE RATE CONSTANTS AND THEIR COMPARISON  
WITH THE RECOMMENDED VALUES OF OTHER INVESTIGATIONS

Reaction	Validation Value*	Demerjian et al. (1974)	Johnston et al. (1970)	Niki et al. (1972)	Others
1	0.266 min <sup>-1</sup>	+	+	+	+
2	$2.0 \times 10^{-5}$ ppm <sup>-2</sup> min <sup>-1</sup>	$2.0 \times 10^{-5}$	$2.3 \times 10^{-5}$	$2.2 \times 10^{-5}$	
3	20.8	$2.3 \times 10^1$	$2.9 \times 10^1$	$2.9 \times 10^1$	20.8s
4	$3.5 \times 10^{-3}$ ppm <sup>-2</sup> min <sup>-1</sup>	$3.4 \times 10^{-3}$	$2.5 \times 10^{-3}$		
5	$1.38 \times 10^4$	$8.1 \times 10^3$	$8.1 \times 10^3$		$1.38 \times 10^{4**}$
6	$2.2 \times 10^{-3}$ ppm <sup>-2</sup> min <sup>-1</sup>	$2.2 \times 10^{-3}$			
7	$4.6 \times 10^{-2}$	$0.48-1.1 \times 10^{-1}$	$1.1 \times 10^{-1}$	$1.1 \times 10^{-1}$	$4.6 \times 10^{-2s}$
8	$1.5 \times 10^4$	$0.66-1.47 \times 10^4$	$1.5 \times 10^4$	$1.5 \times 10^4$	
9	$4.5 \times 10^3$	$6.8 \times 10^3$	$4.5 \times 10^3$	$4.4 \times 10^3$	
10	$1.5 \times 10^1$ min <sup>-1</sup>	$1.5 \times 10^1$	$1.4 \times 10^1$	$1.4 \times 10^1$	
11	$1.0 \times 10^{-5}$	$2.5 \times 10^{-3}$	$3.0 \times 10^{-3}$	$1.5 \times 10^{-6}$	$\leq 2 \times 10^{-5++}$
12	$2.5 \times 10^{-4}$				$2.5 \times 10^{-4ss}$
13	0.2				$\leq 0.2\Box$
14	$2.1 \times 10^{-6}$ ppm <sup>-2</sup> min <sup>-1</sup>	$\leq 4.3 \times 10^{-6}$	$6.9 \times 10^{-6}$	$3.6 \times 10^{-8}$	
15	4.5	$\leq 4.5$		$2.8 \times 10^{-2}$	
16	$1.3 \times 10^{-2}$ min <sup>-1</sup>	$1/4 \times k_1$	$1/10 \times k_1$	$1/2000 \times k_1$	
17	$1.5 \times 10^4$	$\geq 1.5 \times 10^4$	$1.5 \times 10^3$	$6.0 \times 10^3$	

Table 2 (Continued)

Reaction	Validation Value*	Demerjian et al. (1974)	Johnston et al. (1970)	Niki et al. (1972)	Others
18	$1.2 \times 10^4 \Delta$	$0.8 \times k_{17}$		$2.1 \times 10^3$	
19	$2.5 \times 10^2$	$2.5 \times 10^2$	$2.2 \times 10^2$	$2.6 \times 10^2$	
20	$7.0 \times 10^2$	$2.0 \times 10^2$		$2.9 \times 10^2$	$7.0 \times 10^{20}$
21	$1/250 \times k_1 \text{ min}^{-1}$	$1/160 \times k_1$			$1/250 \times k_1^D$
22	$6.8 \times 10^3$	$6.8 \times 10^3$	$3.7-4.4 \times 10^3$	$4.4 \times 10^3$	
23	$1.6 \times 10^{-2}$	$1.5 \times 10^{-2}$	$0.9-1.6 \times 10^{-2}$	$1.7 \times 10^{-2}$	
24	$2.5 \times 10^4$	$2.5 \times 10^4$		$2.5 \times 10^4$	
25	$1.07 \times 10^2 \square \square$		$1.07 \times 10^2$		
26	$8 \times 10^3 \square \square$				
27	$6.5 \times 10^1$	$3.2 \times 10^1$	$0.16-6.5 \times 10^1$		$6.0 \times 10^3 \Delta \Delta$
28	$3.8 \times 10^2$	$6.4 \times 10^3$	$5.7 \times 10^3$		$3.8 \times 10^3 \square \square$
29	$2.5 \times 10^{-3} \text{ min}^{-1}$	$0.4-2.5 \times 10^{-3}$		$1/1000 \times k_1$	
30	$2.3 \times 10^4$	$2.2 \times 10^4$		$2.3 \times 10^4$	
31	$9.1 \times 10^2$	$9.1 \times 10^2$		$2.9 \times 10^2$	
32	$9.1 \times 10^2$	$4.7 \times 10^2$		$1.5 \times 10^3$	
33	$1.0 \times 10^2$	$4.9 \times 10^2$		$2.2 \times 10^1$	
34	$2.4 \times 10^{-2}$	$2.4-5.6 \times 10^{-2}$		$4.4 \times 10^{-3}$	
35	$4.9 \times 10^2$	$3.0-4.9 \times 10^2$		$2.9 \times 10^3$	
36	$2.5 \times 10^2$	$2.0-2.5 \times 10^2$		$9.9 \times 10^2$	

Table 2 (Concluded)

Reaction	Validation Value*	Demerjian et al. (1974)	Johnston et al. (1970)	Niki et al. (1972)	Others
37	$5.3 \times 10^3$	$5.3 \times 10^3$	$5.3 \times 10^3$	$5.3 \times 10^3$	
38	$1.0 \times 10^2$	$1.0 \times 10^2$		$5.3 \times 10^3$	
39	$1.0 \times 10^2$	$1.0 \times 10^2$		$4.4 \times 10^3$	

\* In units of  $\text{ppm}^{-1} \text{min}^{-1}$  unless otherwise indicated.

† Depends on the experimental system.

§ Ghormley et al. (1973).

\*\* Schuck et al. (1966).

†† Morris and Niki (1973).

§§ Jaffe and Ford (1957).

□ Based on thermodynamic considerations. This reaction probably proceeds heterogeneously, and the reverse reaction may be important, although it was not included here.

Δ Pseudo-second-order value.

○ Davis et al. (1972).

◇ Unpublished value measured in the Chemistry and Physics Laboratory of EPA.

□□ These values are for toluene. Since the experimental data considered did not include aromatic hydrocarbons, these two values were not used in the validation exercises.

ΔΔ Morris and Niki (1971).

○○ Demerjian et al. (1974) employed  $6.4 \times 10^3 \text{ ppm}^{-1} \text{min}^{-1}$  in their modeling studies, since that value provided a better fit to the rate of removal of n-butane than the value of  $3.8 \times 10^3 \text{ ppm}^{-1} \text{min}^{-1}$  measured by Greiner (1970).

## 2. Results and Discussion

The results of nine smog chamber simulations are displayed graphically in Figures 1 through 9. In all figures in this report, the experimental data are represented by symbols, and the simulated results, by solid lines. Except for the revisions in the mechanism and rate constants already noted, these runs were carried out in the manner, and under the assumptions, described in Chapter V of the previous report. The initial conditions associated with the experimental chamber data are listed in Table 3.

Table 3  
INITIAL CONDITIONS ASSOCIATED WITH  
EXPERIMENTAL CHAMBER DATA

<u>EPA Run</u>	<u>(NO<sub>2</sub>)<sub>0</sub>*</u>	<u>(NO)<sub>0</sub>*</u>	<u>(n-Butane)<sub>0</sub>*</u>	<u>(Propylene)<sub>0</sub>*</u>
306†	0.03	0.30	1.60	
325	0.04	0.32		0.45
329	0.06	0.26		0.24
459	0.06	1.14		0.78
307	0.05	1.23	3.06	0.36
333	0.08	1.25	3.41	0.23
348	0.08	1.23	3.39	0.44
349	0.08	0.31	3.25	0.44
352	0.07	0.27	3.29	0.26

\* Initial concentrations in units of ppm.

† 0.12 ppm of aldehyde also present initially.

### a. Analysis of Chamber Simulation Results

It is difficult to draw broad, general conclusions about the adequacy and accuracy of the kinetic mechanism. Although many of the predicted concentration-time profiles match the experimental data very well, other profiles show poor agreement. Some of the discrepancies may be due to



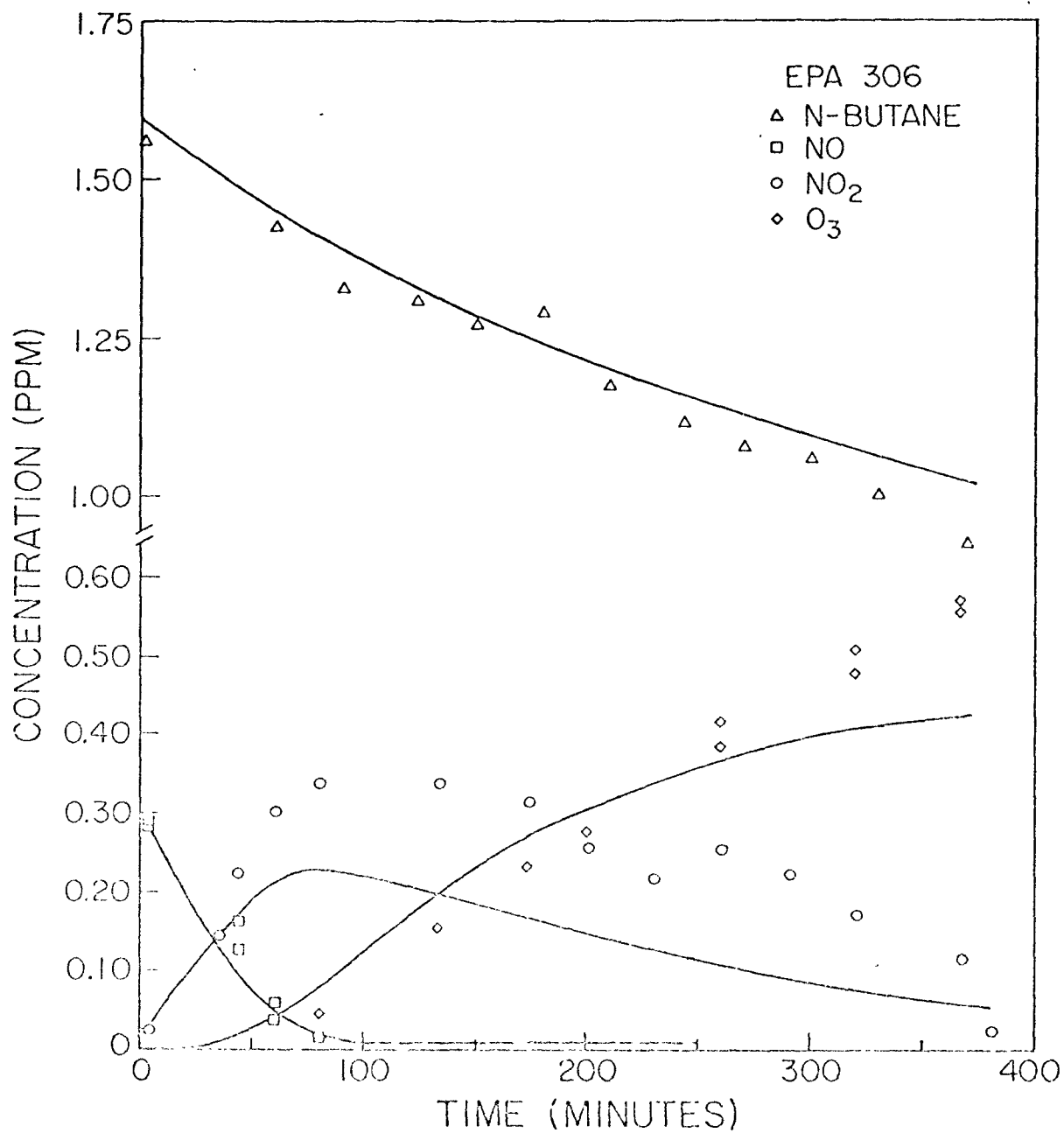


FIGURE 1. RESULTS OF SMOG CHAMBER SIMULATION  
FOR RUN EPA 306

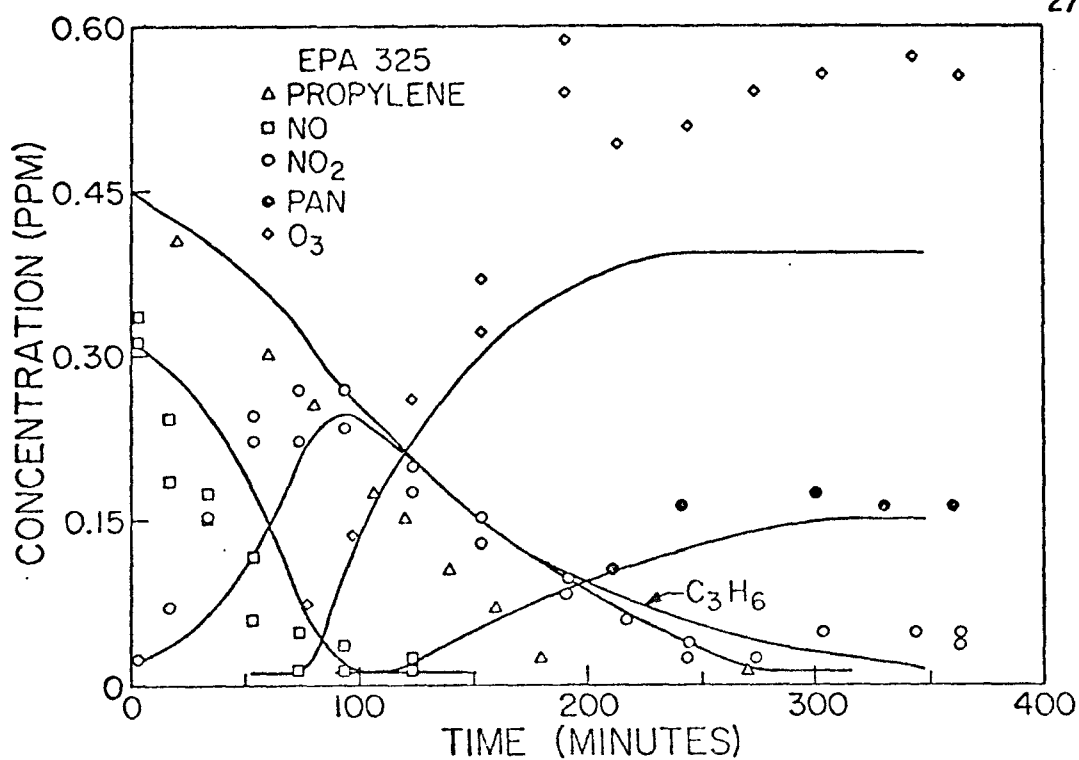


FIGURE 2. RESULTS OF SMOG CHAMBER SIMULATION  
FOR RUN EPA 325

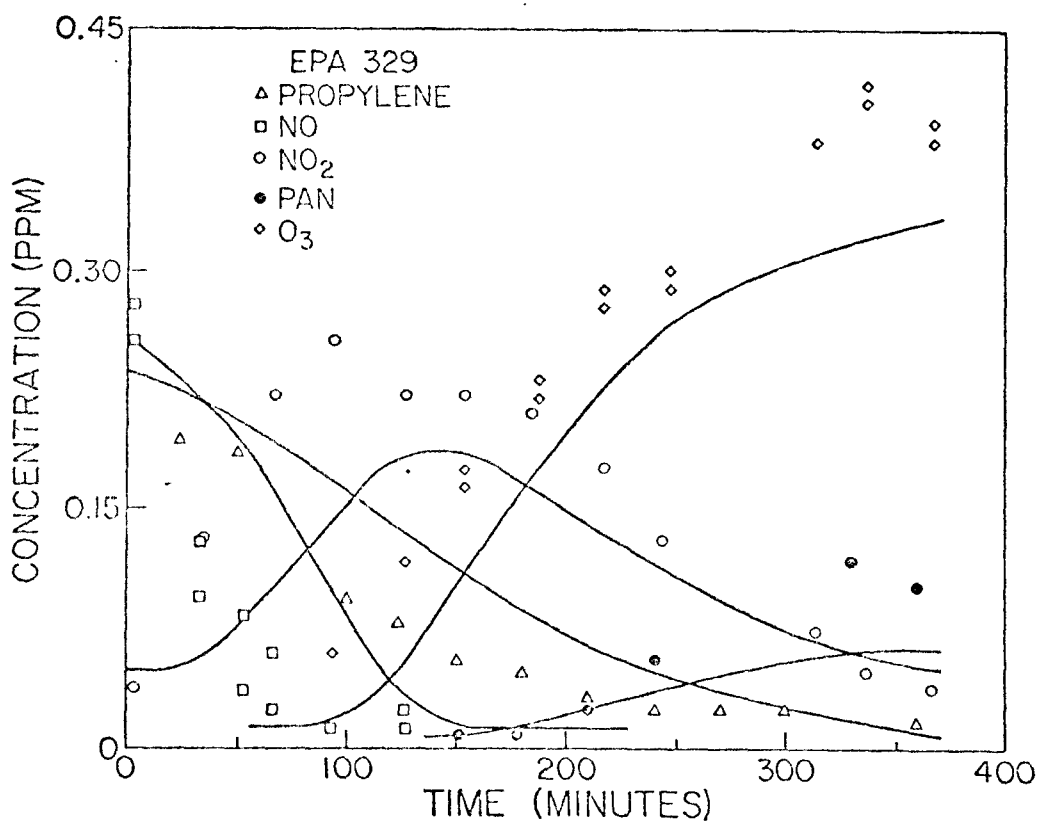


FIGURE 3. RESULTS OF SMOG CHAMBER SIMULATION  
FOR RUN EPA 329

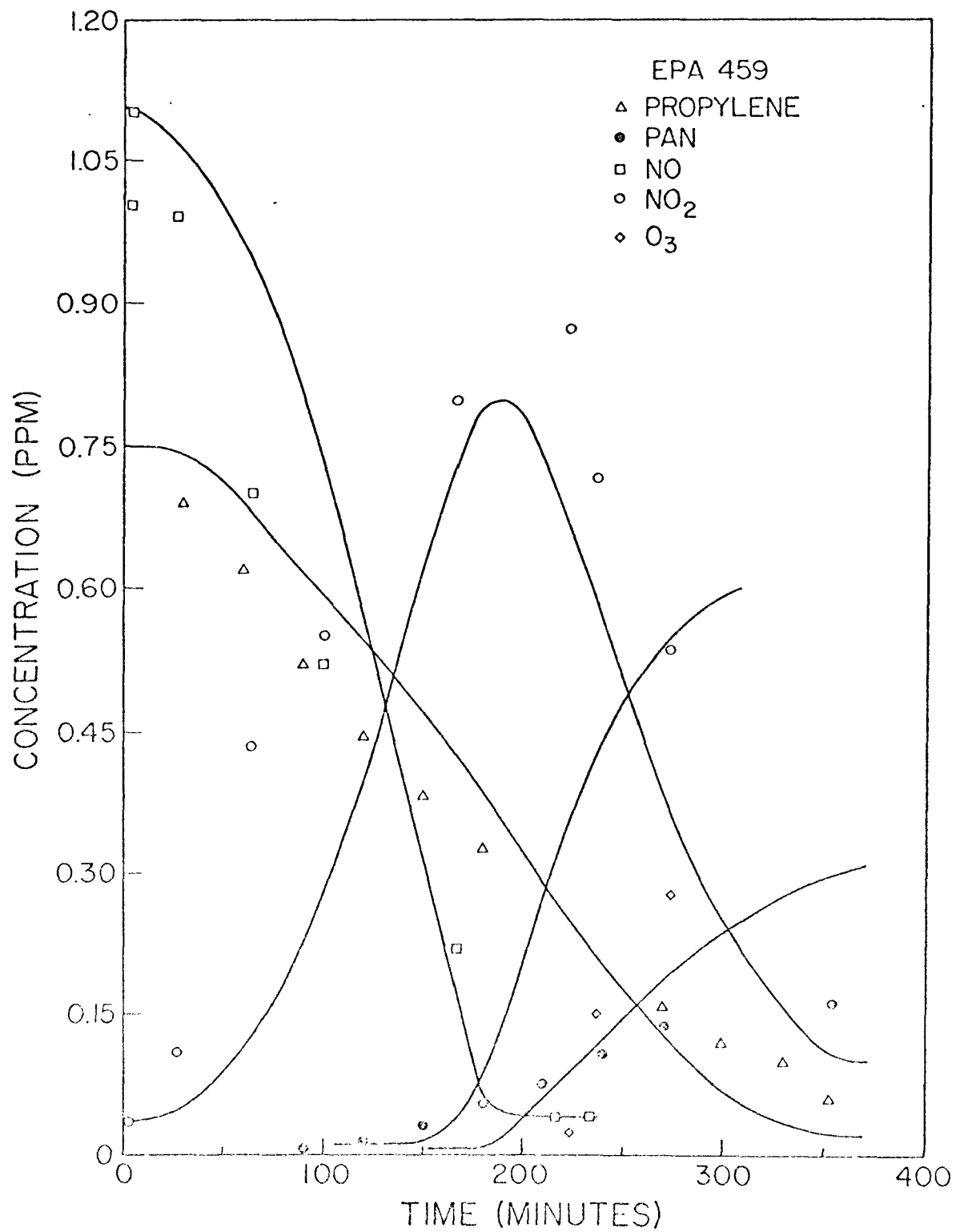


FIGURE 4. RESULTS OF SMOG CHAMBER SIMULATION FOR RUN EPA 459

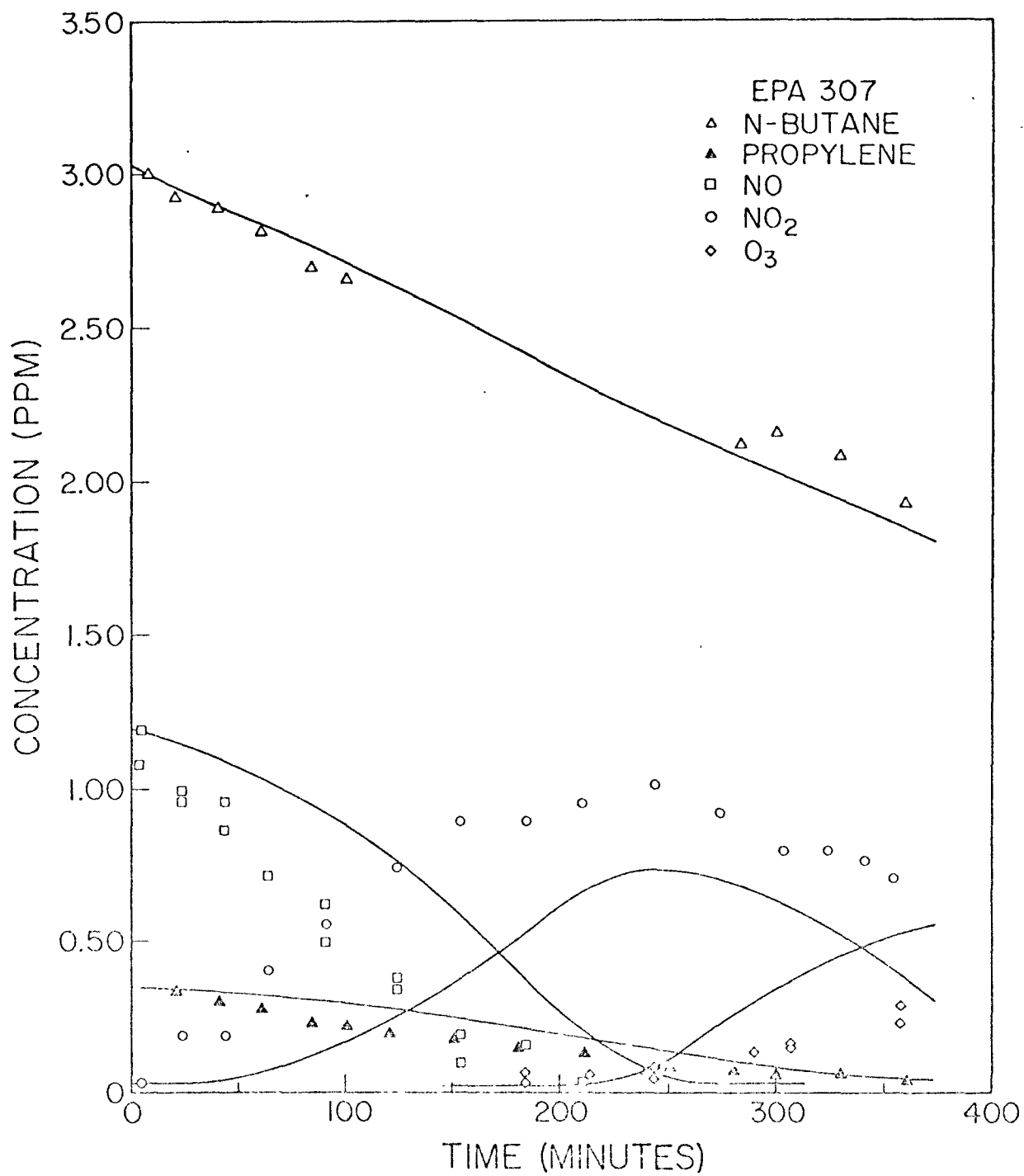


FIGURE 5. RESULTS OF SMOG CHAMBER SIMULATION FOR RUN EPA 307

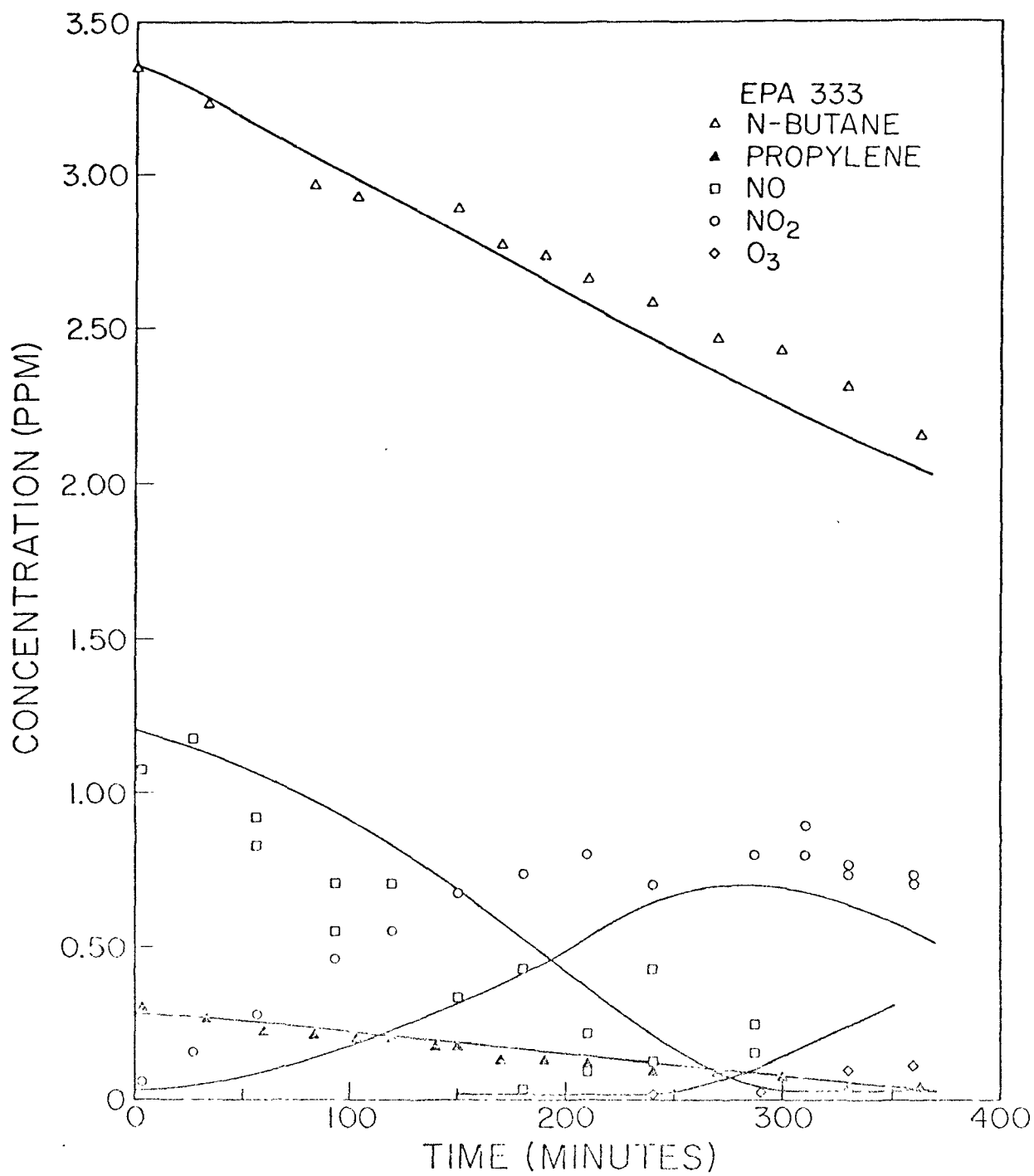


FIGURE 6. RESULTS OF SMOG CHAMBER SIMULATION FOR RUN EPA 333

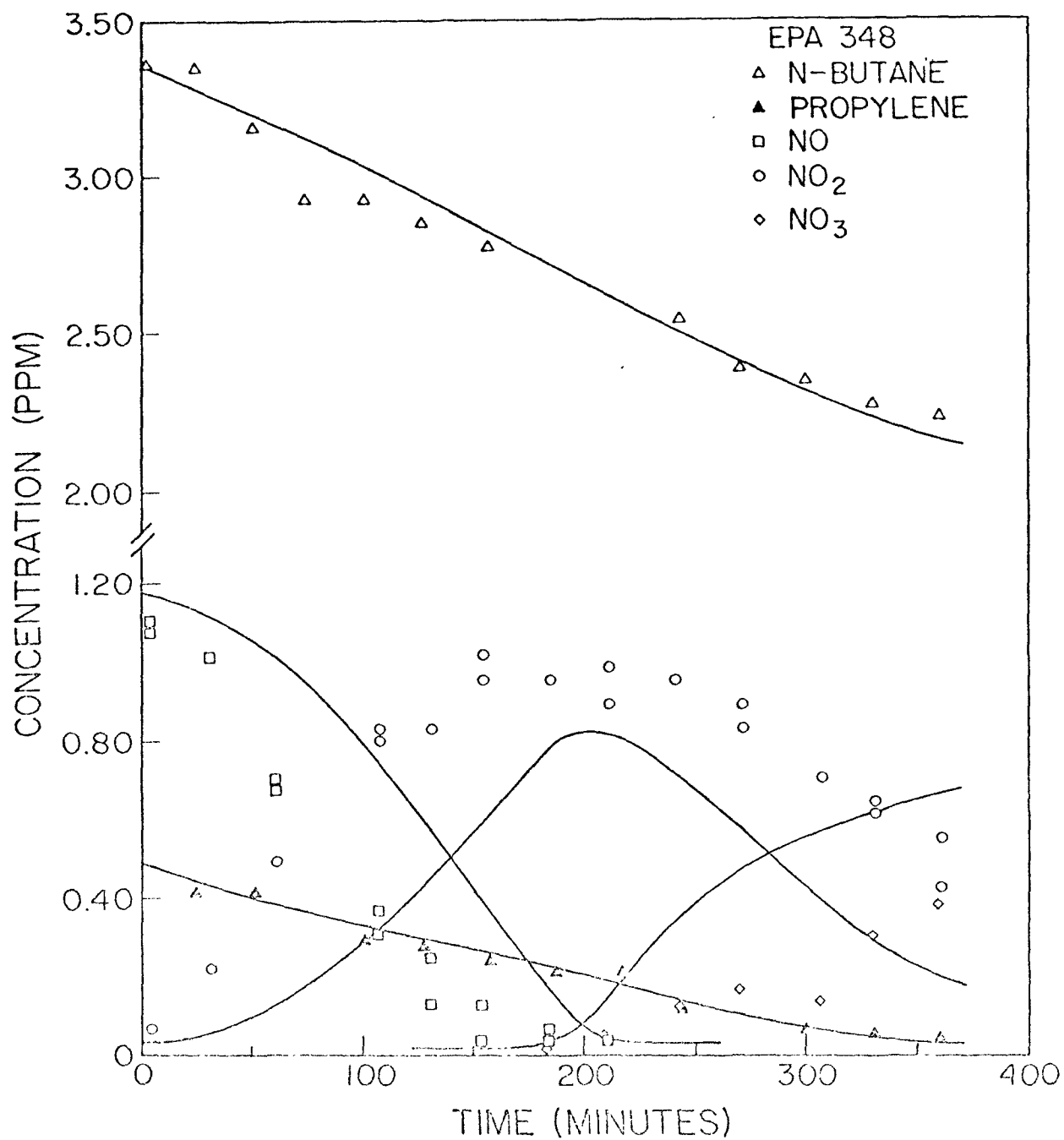


FIGURE 7. RESULTS OF SMOG CHAMBER SIMULATION FOR RUN EPA 348

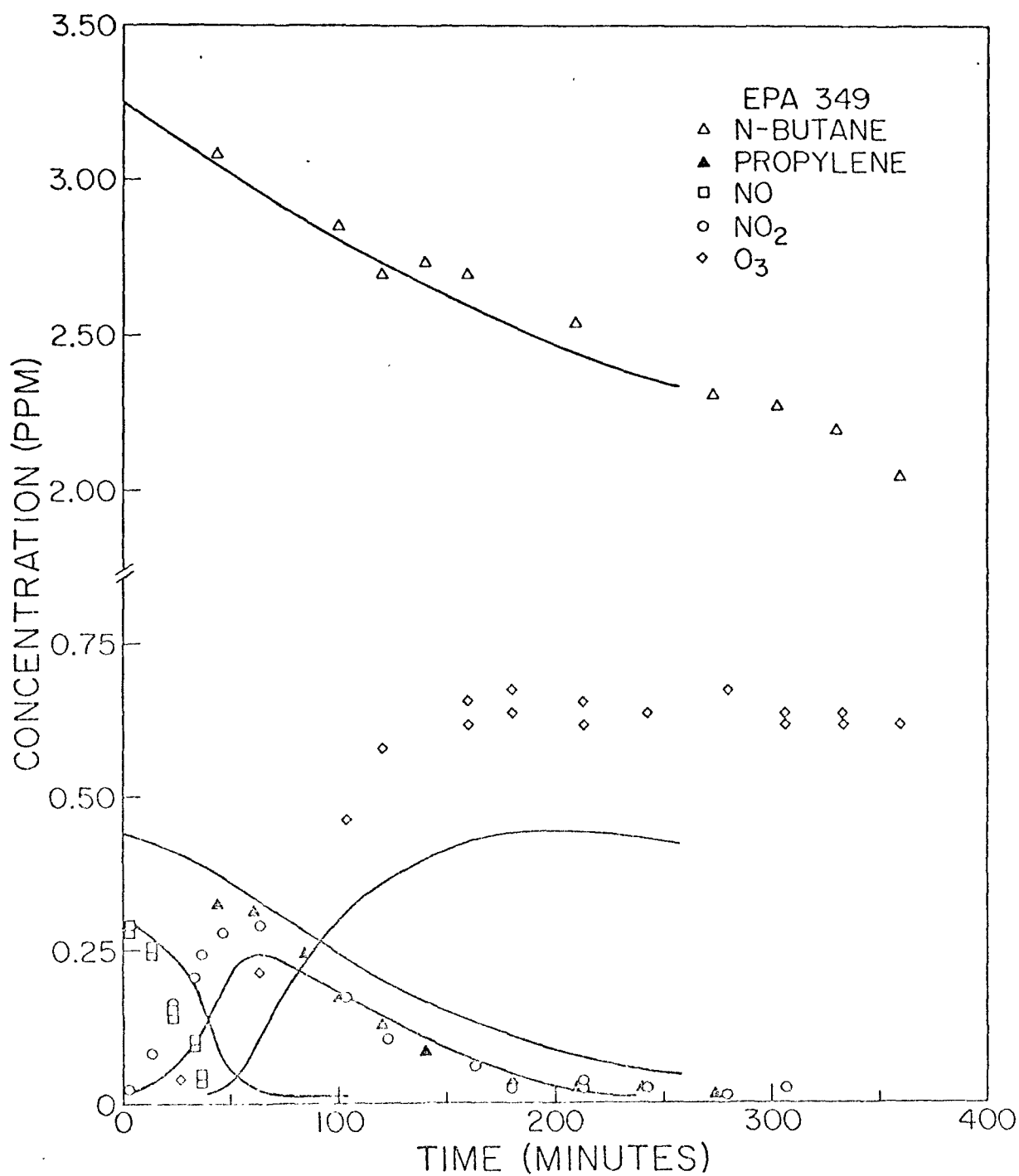


FIGURE 8. RESULTS OF SMOG CHAMBER SIMULATION FOR RUN EPA 349

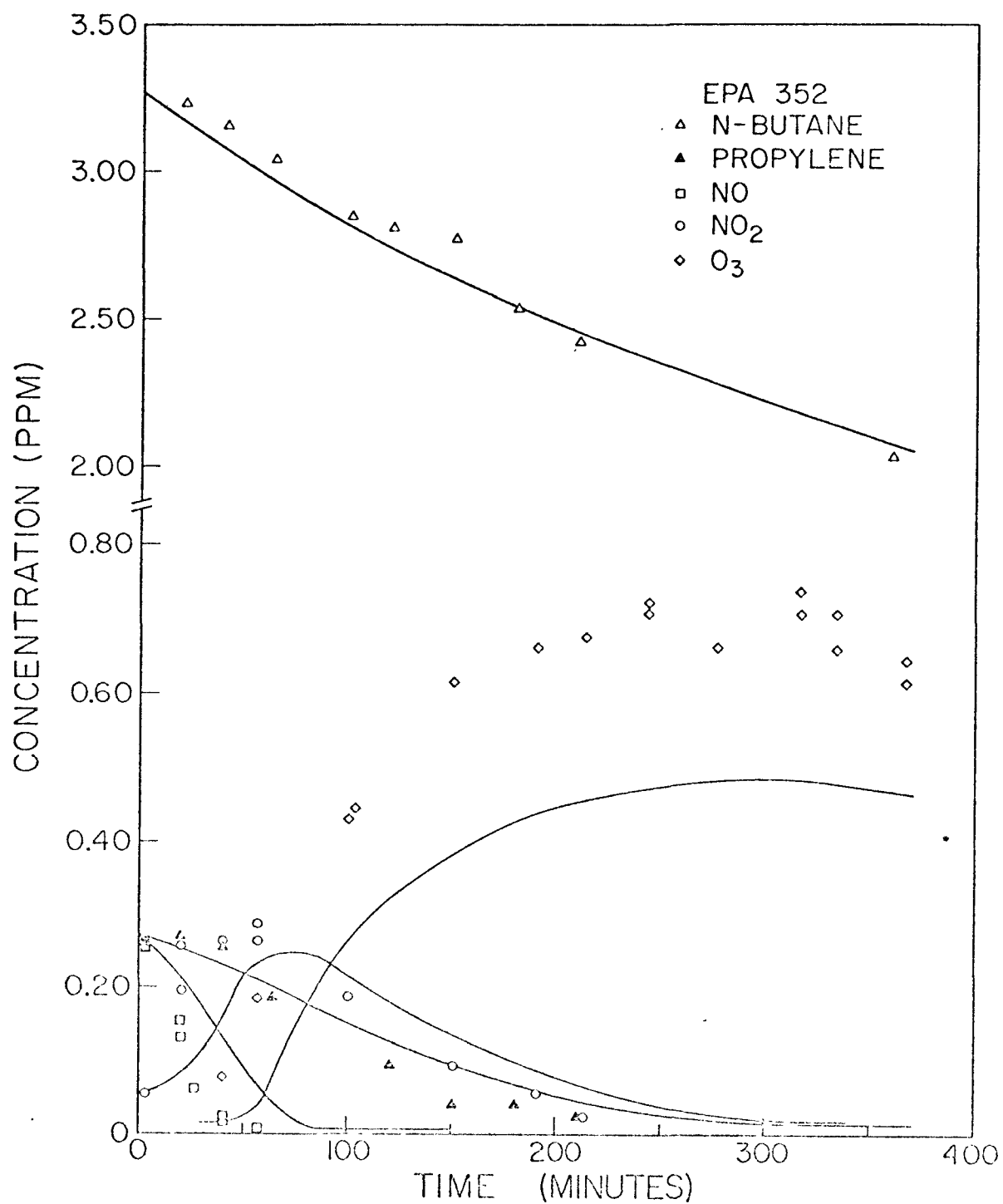


FIGURE 9. RESULTS OF SMOG CHAMBER SIMULATION FOR RUN EPA 352



inaccuracies or interferences in the chemical measurements or to incomplete characterization of the chamber operating conditions (e.g., light intensity). We considered these possibilities in some detail in the previous report and shall not, therefore, discuss them here.\*

Complete omission or inaccurate specification of products of key reactions, along with inaccuracies and uncertainties in the values of many rate constants, are probably the causes of a major portion of the disagreement between predictions and experimental data. Resolution of these types of uncertainties is a slow and painstaking process. In the absence of experimental measurements, provisional rate constant values can be estimated and elementary reactions and reaction mechanisms can be hypothesized on the basis of thermochemical principles (Benson, 1968). However, because of the large uncertainty associated with most estimates, we depend mainly on experimental studies to justify the changes introduced into the mechanism.

Analyzing the predicted concentration-versus-time profiles for organics,  $\text{NO}_x$ ,  $\text{O}_3$ , and PAN, as shown in Figures 1 through 9, we can make the following observations:

- > The rates of oxidation of n-butane and propylene predicted by the mechanism match the data uniformly well over the full range of initial concentrations studied.
- > The predicted rate of oxidation of NO and the time to the  $\text{NO}_2$  maximum agree well with the data. At initial concentrations of  $\text{NO}_x$  greater than 1 ppm, however, the rates of

---

\* EPA's decision to support a new program of chamber experiments (see Chapter V) was based in part on the poor characterization of many chamber operating parameters in previous studies. Although early experiments generally provided answers to many of the qualitative and semiquantitative questions about the chemistry of smog formation, they were not performed with model evaluation purposes in mind and are not, therefore, ideally suited for use in such work.

$O_3$  accumulation and  $NO_2$  oxidation are predicted to be more rapid than those observed (e.g., Figures 5 through 7). Under these conditions, the predicted rate of accumulation of  $NO_2$  was lower, and the magnitude of the  $NO_2$  maximum was smaller, than the corresponding experimental values. Conceivably, interferences by  $HNO_2$  and  $HNO_3$  in the  $NO_2$  measurements could have resulted in artificially high experimental values for  $NO_2$ . And as we have already noted, important reactions may be missing from the mechanism, or rate constants may be in error. Decreases in  $k_{11}$  and  $k_{12}$  (heterogeneous and homogeneous formation of  $HNO_3$ ) would slow the consumption of  $NO_2$  after the  $NO_2$  peak, as would the introduction of other reactions that consume OH (a reactant in Reaction 17)--or generators of OH--after the  $NO_2$  peak. Another possible explanation for the discrepancies is that reactions involving nitrogen-containing products (such as  $HNO_3$  and PAN) that lead to  $NO_2$  formation might be occurring. We considered one reaction of this type, the reaction of  $NO + HNO_3$  ( $k_{12}$ ), but it is too slow to be important in the kinetics. Possible reactions of PAN are discussed in Section III-C. As of this time, however, it is not possible to pinpoint specific errors--whether they involve experimental data, reactions, or rate constants--that lead to inaccurate predictions under conditions of high initial  $NO_x$ .

- >  $O_3$  reached an asymptotic level in only five of the nine experiments (Figures 1, 2, 3, 8, and 9). The predicted maxima were somewhat lower than the measured values in each case, but the technique used to determine  $O_3$  suffered from interferences, as described in the previous report. In the four experiments in which more than 0.5 ppm NO was present initially, the  $O_3$  concentration did not reach a plateau during the irradiation. In most of those simulations, the predicted onset of  $O_3$  accumulation was in good agreement with the data.

- > Measurements of PAN were made in only three of the experiments (see Figures 2 through 4). For the first two of these runs, the predicted PAN concentrations are in good agreement with the data. For Run 459 (Figure 4), however, the predicted onset of PAN formation occurred too early and the levels reached were too high compared with the data. We discuss possible causes of high PAN predictions in Section III-C, where we consider a reaction that may be important in consuming PAN.

b. Elimination of Insensitive Reactions from the General Mechanism

We have stated several times in this section that certain reactions are insensitive and that varying particular rate constants has only a minor effect on predictions. Because the general mechanism may ultimately be used in complex atmospheric air pollution simulation models, the mechanism should be as concise as possible to reduce the computing time required for evaluation of the models. Roth et al. (1974) have carried out a detailed sensitivity analysis of the mechanism presented in Table 1. Since we have included an analogous sensitivity study of a modified version of the general mechanism in Chapter IV, we do not repeat the discussion by Roth et al. here. Nevertheless, because of the importance of their results, which show that the mechanism can, indeed, be simplified, we summarize their findings in the following pages.

In the Roth study, reactions were considered to be "insensitive" if, upon their removal from the mechanism, both individually and as a group, the remaining set of reactions was able to predict the following within 10 percent of the values predicted by the complete mechanism:

- > The time taken to reach the  $\text{NO}_2$  peak (T)
- > The height of the  $\text{NO}_2$  peak (H)
- > The magnitude of the ozone peak (M).

These three scalars, all of which can be easily quantified, are of interest because the onset of formation of many secondary products in the atmosphere accompanies the peak concentration of  $\text{NO}_2$ , and the intensity of smog is often associated with the ozone and  $\text{NO}_2$  concentrations. Thus, T, H, and M constitute three major indicators of smog formation and severity. The decision that the remaining set of reactions must be capable of predicting these three scalars within 10 percent of the values generated by the total mechanism was arbitrary. However, such a value is less than the uncertainty bounds associated with the experimental chamber data used to evaluate and "tune" the model. Thus, such a choice is reasonable.

Consideration of the sensitivity values associated with each rate constant led to the selection of ten reactions for possible removal from the mechanism. Of these, Roth et al. found that only six could actually be eliminated based on the criteria cited above. These reactions are listed in Table 4.

Table 4

REACTIONS THAT CAN BE ELIMINATED  
FROM THE GENERAL MECHANISM SHOWN IN TABLE 1

<u>Reactants</u>	<u>Reaction</u>
$\text{O} + \text{NO}$	$k_4$
$\text{O} + \text{NO}_2 + \text{M}$	$k_6$
$\text{NO} + \text{HNO}_3$	$k_{12}$
$\text{HNO}_2 + \text{HNO}_3$	$k_{13}$
$\text{RO}_2 + \text{HO}_2$	$k_{38}$
$\text{RO}_2 + \text{RO}_2$	$k_{39}$

As shown in Table 5, the values of T, H, and M after removal of these six reactions are all within 10 percent of their previous values for the three EPA runs that Roth et al. examined. A number of other reactions could have been removed for one or two of the EPA runs, but not for all three. However, their elimination would limit the applicability of the kinetic mechanism to a narrower range of initial concentrations and ratios. Consequently, no other reactions can be dropped from the general mechanism.

Table 5  
VALUES OF T, H, AND M BEFORE  
AND AFTER REMOVAL OF THE REACTIONS IN TABLE 4

EPA Run	Time T (minutes)		Concentration (ppm)			
			Value of H		Value of M	
	Before	After	Before	After	Before	After
329	87	86	0.25	0.25	0.39	0.40
333	285	281	0.75	0.70	0.40	0.41
352	65	70	0.25	0.25	0.50	0.52

#### B. SIMULATION OF A MULTIPARAFFIN/NO<sub>x</sub> SMOG CHAMBER EXPERIMENT

The chemical systems of greatest interest in the control of ambient air pollution are considerably more complicated than the propylene/n-butane/NO<sub>x</sub> mixtures just discussed. In principle, the kinetic mechanism has been formulated to be capable of simulating the behavior of complex mixtures of organics in an irradiated system containing NO<sub>x</sub> and air. The ultimate test of the mechanism in this regard will rest on its ability to predict the chemical transformations occurring in a polluted air mass. But, before the mechanism is applied to a system as complicated as the atmosphere, it should be proven capable of simulating the chemical behavior of a simple mixture of hydrocarbons under well-controlled laboratory conditions.

In this section, we discuss a test of the generality of the mechanism. We used the general kinetic mechanism to simulate a smog chamber experiment in which five different paraffins and  $\text{NO}_x$  were irradiated in air. Although each paraffin was treated separately in this simulation (i.e., the behavior of each paraffin was described by its own differential equation), all five paraffins were assumed to react alike, in accordance with the principles of formulation of the mechanism (Seinfeld et al., 1973).\*

The multiparaffin/ $\text{NO}_x$  experiment was conducted in the same chamber that was used for the propylene and butane experiments discussed in the previous section and in Hecht et al. (1973). No data relating chamber operating characteristics were included with the concentration-time data; we therefore assumed the same values of light intensity, relative humidity, and chamber temperature as were supplied for the propylene and n-butane runs. We further assumed the average dilution rate to be  $4.06 \times 10^{-4} \text{ min}^{-1}$ , which is typical of other runs performed in the NAPCA chamber for which sampling data were available. The concentrations of reactants at the beginning of the experiment were as follows:

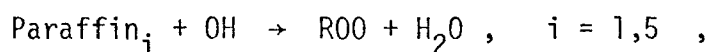
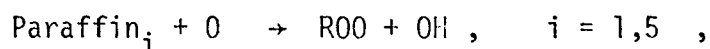
Species	Concentration (ppm)
iso-pentane	0.51
n-pentane	0.69
2-methyl-pentane	0.22
2,4-di-methyl-pentane	0.18
2,2,4-tri-methyl-pentane	0.17
$\text{NO}_2$	0.038
$\text{NO}$	0.458

---

\* In Chapter IX, we present another simulation of this experiment in which we lumped the five individual paraffins into one pseudo-species, or general class.

## 1. Choice of Rate Constants and Reaction Mechanisms

As a reaction framework for the simulation of this experiment, we chose the formulation of the general mechanism in Table 1, except that the reactions for olefins and aromatics (Reactions 22 through 26) were eliminated. We then added reactions for the oxidations of each of the five paraffins by O and OH. Assuming that these reactions proceeded by the same general mechanism, we replaced Reactions 27 and 28 in Table 1 with five pairs of reactions of the following form:



where  $i$  denotes the individual paraffins. The peroxyalkyl radicals produced by these reactions vary in structure, depending upon which hydrogen atoms are abstracted from the hydrocarbons. We assumed, however, that all these radicals react in the same general manner, and we lumped them into the pseudo-species ROO.

Carrying out a simulation of this experiment necessitated specifying the rate constants for the 10 new O and OH oxidation reactions. Herron and Huie (1969) have measured the rate of reaction of O with three of the five paraffins that were used in this chamber experiment: iso-pentane, n-pentane, and 2,2,4-tri-Me-pentane. The rate constants are listed in Table 6. However, we had to estimate the rate constants for the other two O-paraffin reactions. Because iso-pentane and 2-Me-pentane have nearly identical structures (2-Me-pentane has an extra methylene group in its carbon skeleton), we assumed that both compounds react at similar rates with O; we therefore estimated the O-2-Me-pentane rate constant to be  $200 \text{ ppm}^{-1} \text{ min}^{-1}$ . Herron and Huie have also measured the rate of reaction of O with 2,2-di-Me-pentane, a species somewhat similar in structure to 2,4-di-Me-pentane. We assumed that the latter two species react with O at the same rate, and we thus assigned the O-2,4-di-Me-pentane reaction

a rate constant value of  $160 \text{ ppm}^{-1} \text{ min}^{-1}$ . The rate constants of OH-paraffin reactions can be calculated directly using the equations formulated by Greiner (1970a). Values for the OH-paraffin constants calculated in this manner are summarized in Table 6.

## 2. Results and Discussion

We carried out a simulation of this multiparaffin experiment after modifying the mechanism in Table 1 in accordance with the foregoing discussion. (In performing the integration, we did not invoke the steady-state assumption for any species.) Otherwise, the simulation procedure was identical to that described for the propylene and n-butane experiments. The predictions and experimental data are presented graphically in Figures 10 through 12.

The predictions show good qualitative agreement with the experimental data for all species. Although the rates of  $\text{NO}_2$  formation, NO oxidation, aldehyde formation, and PAN formation are all slower than those observed experimentally, the predicted concentrations of  $\text{O}_3$  and the five paraffins agree quite well with the data.

The discrepancies can probably be accounted for in several ways, including the reasons given in Hecht et al. (1973) for the propylene and n-butane simulations. In addition, several considerations pertinent to the simulation of this particular experiment might explain the inaccuracies in the predictions. For example, we made several rather important assumptions concerning chamber operating conditions. If the light intensity, relative humidity, or heterogeneous rate of  $\text{HNO}_2$  formation were greater than we assumed, the predictions for  $\text{NO}_2$ , NO, aldehydes, and PAN would improve and the predictions for other species would deteriorate in relation to the experimental data. Also, we used calculated, rather than experimentally measured, rate constant values for the important OH-paraffin reactions. Although we believe that the technique employed to obtain these values is sound, the rate constants are undoubtedly uncertain by a



Table 6  
RATE CONSTANTS FOR THE O AND OH OXIDATION REACTIONS

Species	Rate Constant for O Oxidation ( $\text{ppm}^{-1} \text{ min}^{-1}$ )	Reference	Rate Constant for OH Oxidation ( $\text{ppm}^{-1} \text{ min}^{-1}$ )	Reference
iso-pentane	190	Herron and Huie (1969)	6,700	Greiner (1970a)
n-pentane	85	Herron and Huie (1969)	6,200	Greiner (1970a)
2-Me-pentane	200	Estimate	8,400	Greiner (1970a)
2,4-di-Me-pentane	160	Estimate	11,200	Greiner (1970a)
2,2,4-tri-Me-pentane	250	Herron and Huie (1969)	7,300	Greiner (1970a)

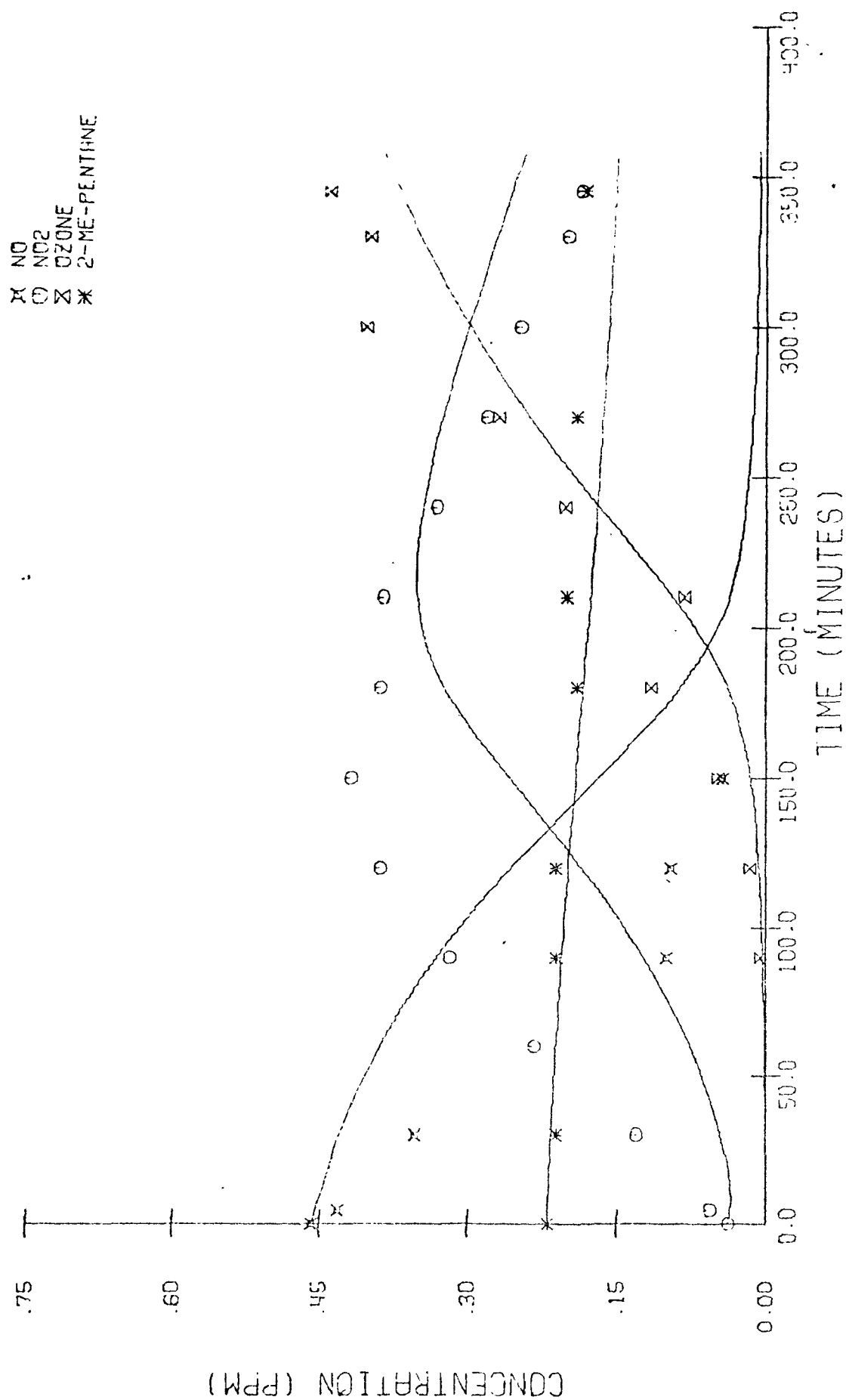


FIGURE 10. SIMULATION OF THE MULTIPARAFFIN/NO<sub>x</sub> RUN--  
PREDICTIONS FOR NO, NO<sub>2</sub>, O<sub>3</sub>, AND 2-METHYL-PENTANE

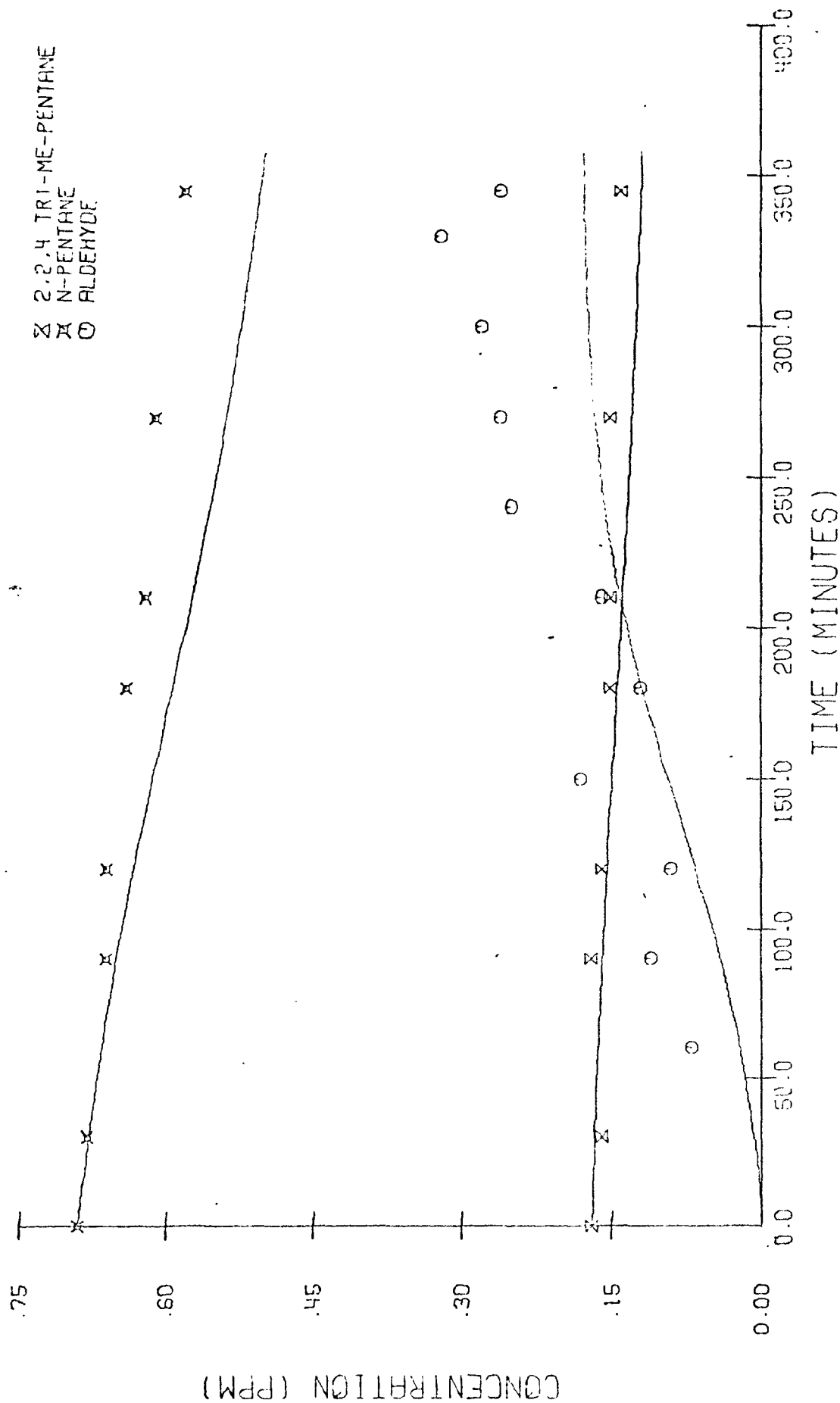


FIGURE 11. SIMULATION OF THE MULTIPARAFFIN/NO<sub>x</sub> RUN--PREDICTIONS FOR 2,2,4-TRI-METHYL-PENTANE, n-PENTANE, AND ALDEHYDE

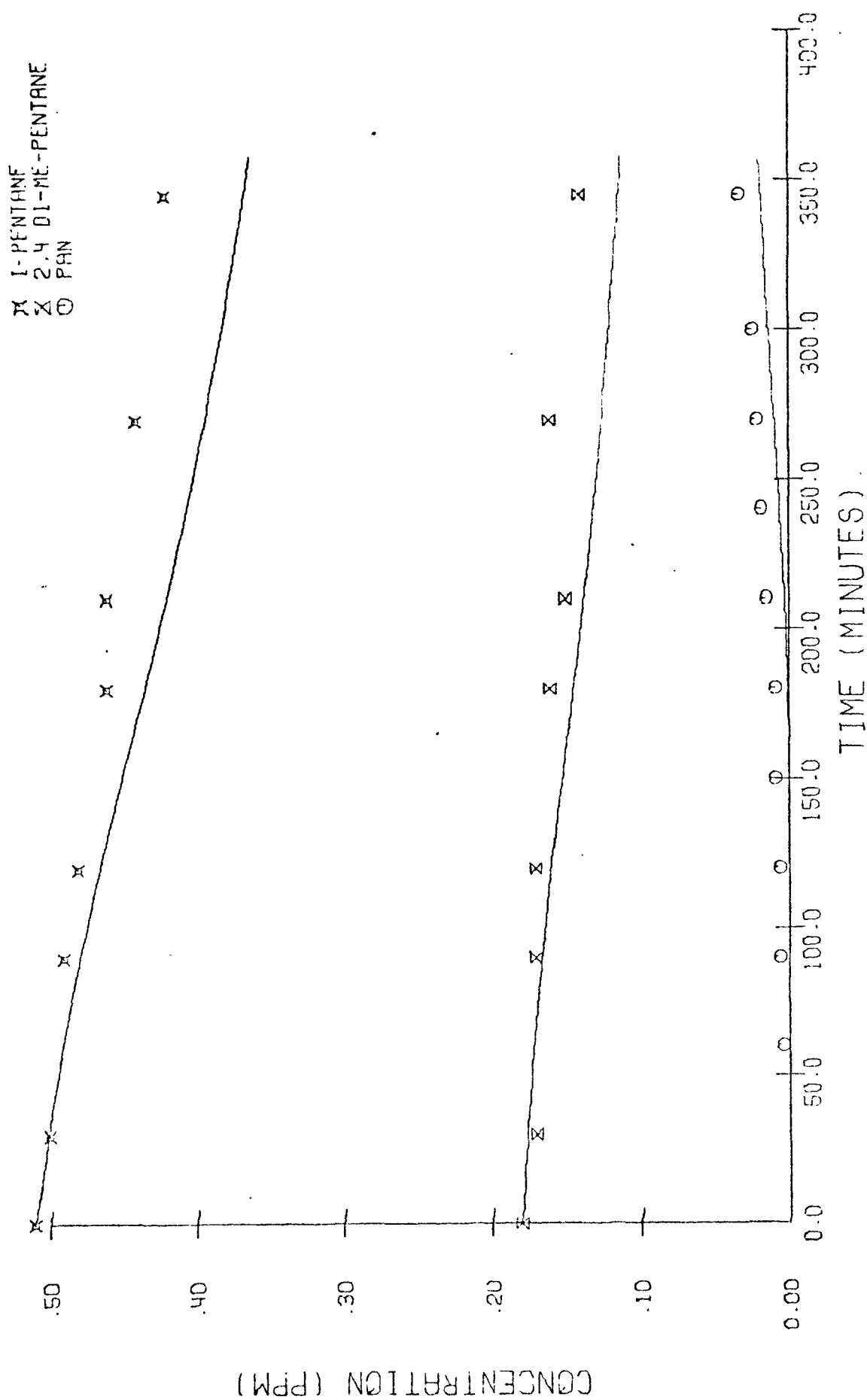


FIGURE 12. SIMULATION OF THE MULTIPARAFFIN RUN--PREDICTIONS FOR ISO-PENTANE, 2,4-DI-METHYL-PENTANE, AND PAN

factor of at least 1.3. Finally, the peroxyalkyl radicals produced in the paraffin oxidation reactions are in many cases considerably larger and more complicated structurally than the radicals produced as a result of propylene and n-butane oxidations. Consequently, some of the free radical reaction chains may not proceed in the manner or at the rate that was assumed in the general mechanism.

Because we tested the mechanism for the multiparaffin case under only one set of initial conditions, it is risky to draw even qualitative conclusions about the merits of the model. The mechanism in Table 1, though formulated and evaluated for paraffins chiefly in relation to n-butane, simulated the chemical transformations occurring in the multiparaffin run surprisingly well. This level of success encourages us about the intrinsic soundness of using a general mechanism to model smog kinetics.

#### C. SIMULATION OF A MULTIOLEFIN/ $\text{NO}_x$ SMOG CHAMBER EXPERIMENT

We undertook the simulation of a multiolefin/ $\text{NO}_x$  smog chamber experiment with the same objectives in mind as those pursued for the multiparaffin run:

- > To examine the generality of the mechanism.
- > To analyze a run with which we could further test our lumping technique (Chapter IX).

This multiolefin experiment had been conducted in the NAPCA chamber at about the same time as the multiparaffin run just discussed. Thus, all of our comments in Section III-B concerning assumptions as to chamber conditions and sampling rates apply to our simulation of this run as well. The concentrations of the six olefins,  $\text{NO}$ , and  $\text{NO}_2$  at the beginning of the run are given on the next page.

Species	Concentration (ppm)
1-butene	0.608
cis-2-butene	0.609
2-methyl-1-butene	0.464
2-methyl-2-butene	0.454
propylene	1.334
ethylene	3.039
NO <sub>2</sub>	0.057
NO	1.013

When we simulated this experiment using the mechanism in Table 1, assigning individual differential equations to each olefin and using the oxidant-olefin rate constants in Table 7 (the choice of these values is discussed shortly), we found that predictions agreed moderately well with the data up to the NO<sub>2</sub> peak, as shown in Figures 13 through 16. After the peak (which occurred 20 minutes after the irradiation was begun), however, the predicted NO<sub>2</sub> concentration decayed rapidly to a value of 0.00007 ppm at 60 minutes. By 100 minutes into the run, the predicted NO<sub>2</sub> concentration was 10<sup>-7</sup> ppm, compared with an observed concentration of 0.09 ppm. Predictions for most other species also agreed poorly with the data. For example, by 100 minutes, O<sub>3</sub> had already peaked and decreased to a predicted concentration level of less than 0.05 ppm. (At that point in the experiment, the O<sub>3</sub> concentration actually stabilized at about 0.55 ppm.) The maximum observed concentration of PAN was one-fifth that predicted. The consumption of the six olefins due to chemical reactions essentially ceased by 100 minutes, since the O<sub>3</sub> had reached a very low level, the NO<sub>2</sub> had been depleted, and the only substantial initiators of free radicals left were the aldehyde and HNO<sub>2</sub> photolysis reactions.

In view of the extremely poor agreement between the predictions and the experimental data, we decided to reexamine those reactions in the general mechanism that became important after the NO<sub>2</sub> peak. As noted in

Table 7  
EXPERIMENTAL VALUES FOR THE SIMULATION OF OXIDANT-OLEFIN REACTIONS

Species	Rate Constant for O Oxidation ( $\text{ppm}^{-1} \text{ min}^{-1}$ )	Reference	Rate Constant for OH Oxidation ( $\text{ppm}^{-1} \text{ min}^{-1}$ )	Reference	Rate Constant for O <sub>3</sub> Oxidation ( $\text{ppm}^{-1} \text{ min}^{-1}$ )	Reference
1-butene	$4.4 \times 10^3$	Cvetanovic (1963)	$6.0 \times 10^4$	Morris and Niki (1971)	$1.3 \times 10^{-2}$	Wei and Cvetanovic (1963)
cis-2-butene	$3.1 \times 10^4$	Elias (1963)	$9.0 \times 10^4$	Morris and Niki (1971)	$4.1 \times 10^{-2}$	Wei and Cvetanovic (1963)
2-Me-1-butene	$1.3 \times 10^4$	Estimate	$7.0 \times 10^4$	Estimate	$1.6 \times 10^{-2}$	Wei and Cvetanovic (1963)
2-Me-2-butene	$6.0 \times 10^4$	Cvetanovic (1963)	$1.3 \times 10^5$	Morris and Niki (1971)	$4.3 \times 10^{-2}$	Wei and Cvetanovic (1963)
ethylene	$7.6 \times 10^2$	Cvetanovic (1963)	$7.5 \times 10^3$	Greiner (1970b)	$3.1 \times 10^{-3}$	Garvin and Hampson (1974)

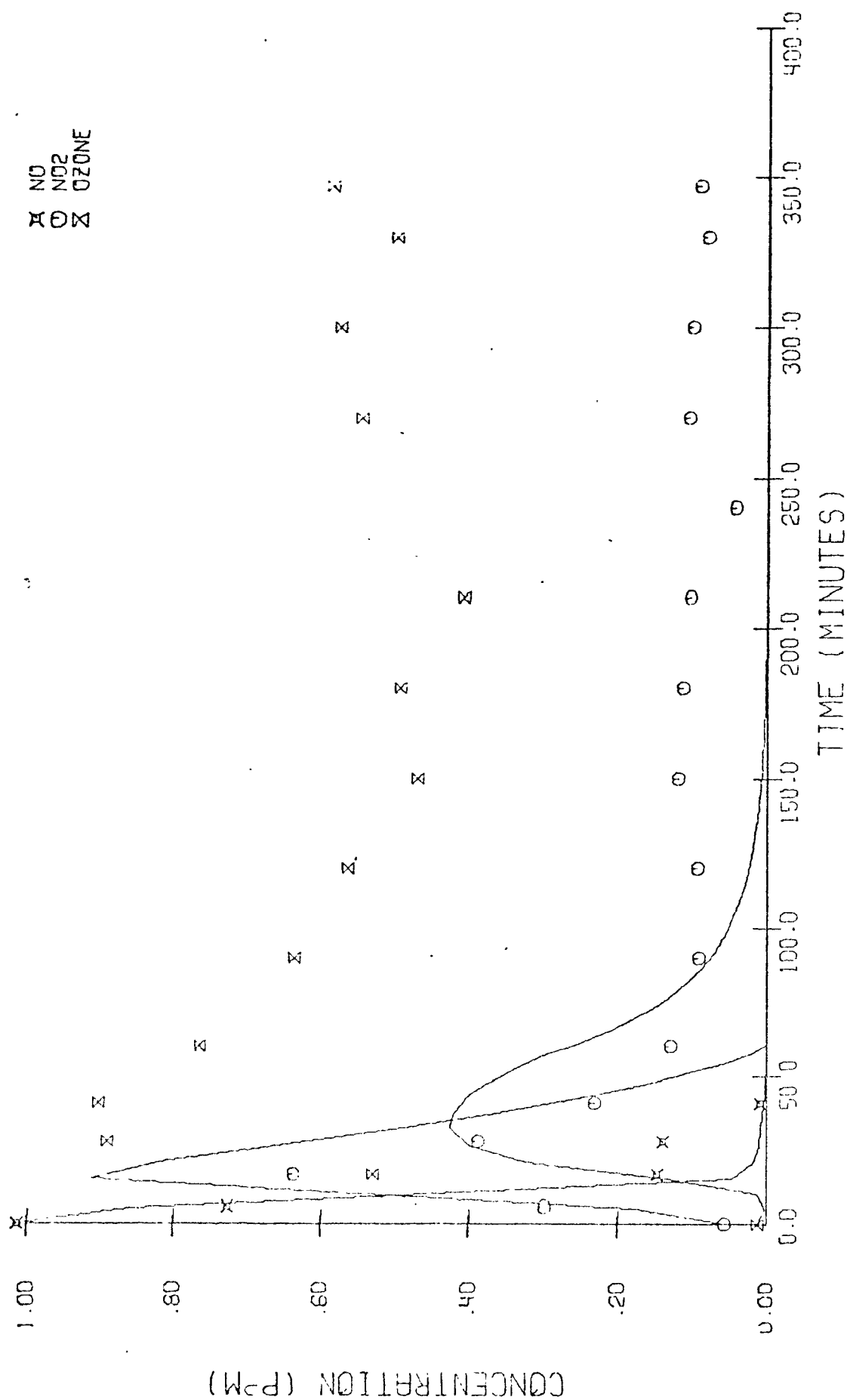


FIGURE 13. SIMULATION OF THE MULTIOLEFIN/NO<sub>x</sub> EXPERIMENT USING THE MECHANISM IN TABLE 1--PREDICTIONS FOR NO, NO<sub>2</sub> AND O<sub>3</sub>



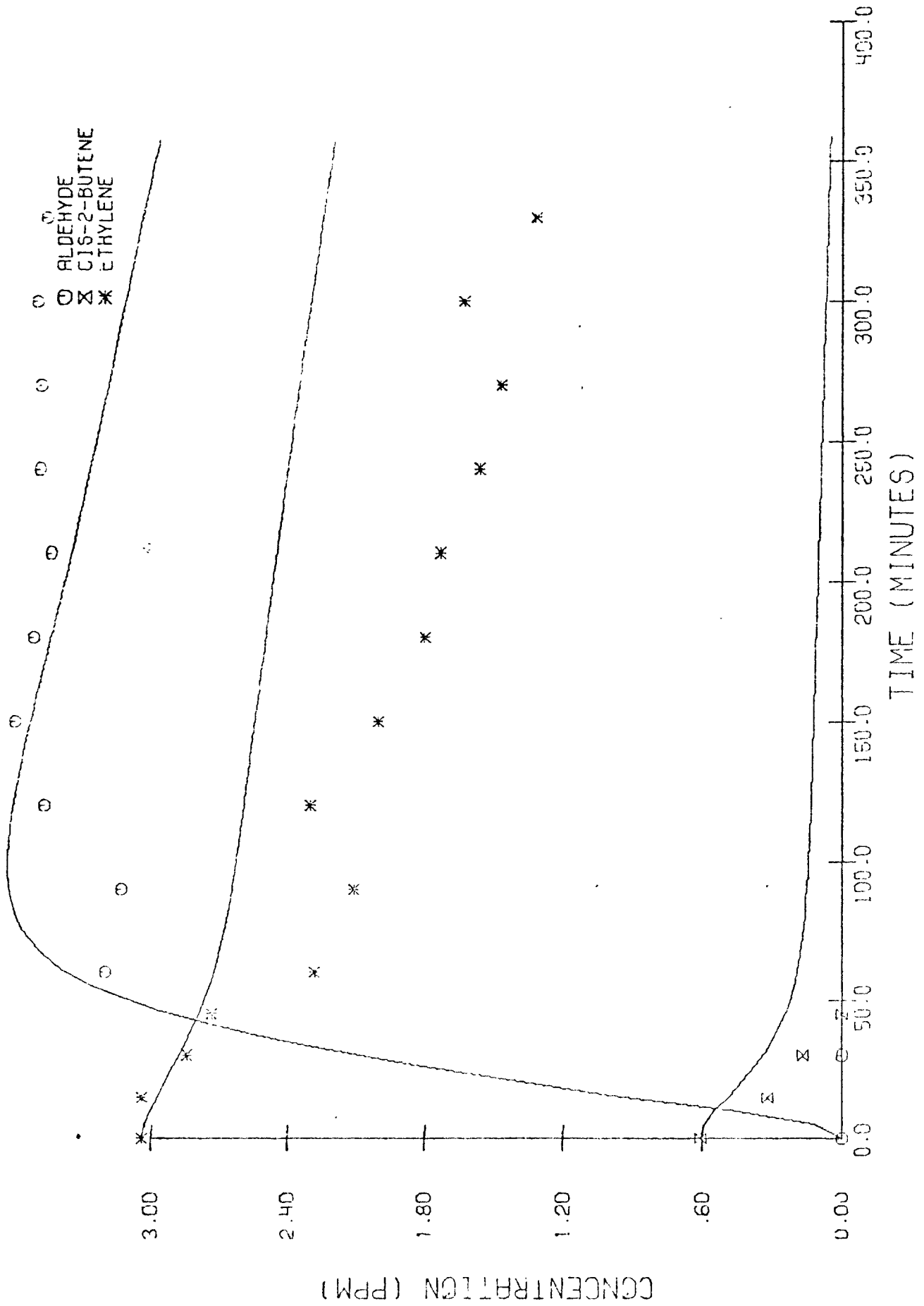


FIGURE 14. SIMULATION OF THE MULTIOLEFIN/NO<sub>x</sub> EXPERIMENT USING THE MECHANISM IN TABLE 1--PREDICTIONS FOR ALDEHYDE, CIS-2-BUTENE, AND ETHYLENE

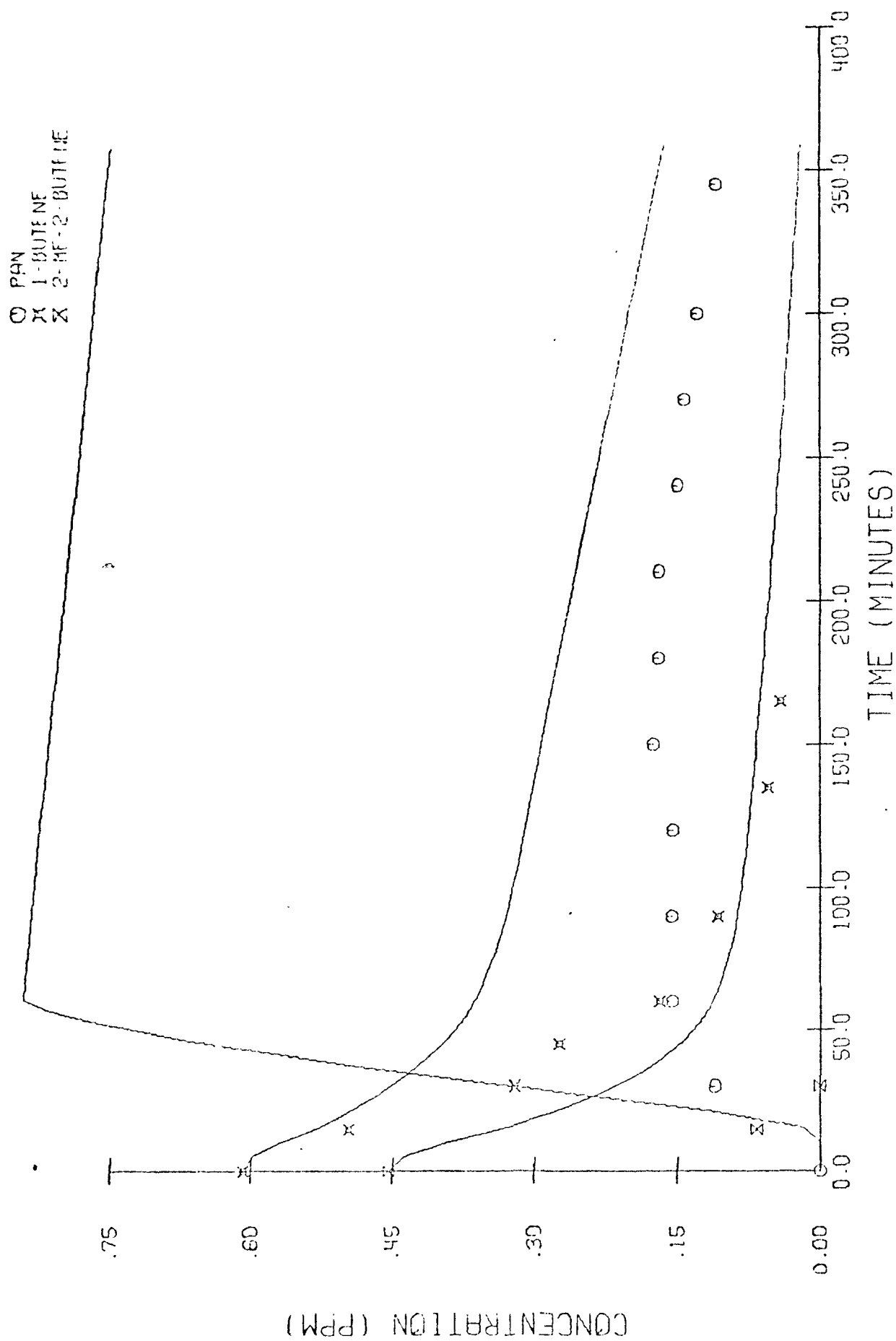


FIGURE 15. SIMULATION OF THE MULTIOLEFIN/NO<sub>x</sub> EXPERIMENT USING THE MECHANISM IN TABLE 1--PREDICTIONS FOR PAN, 1-BUTENE, AND 2-METHYL-2-BUTENE

X 2-ME-1-BUTENE  
 O PROPYLENE

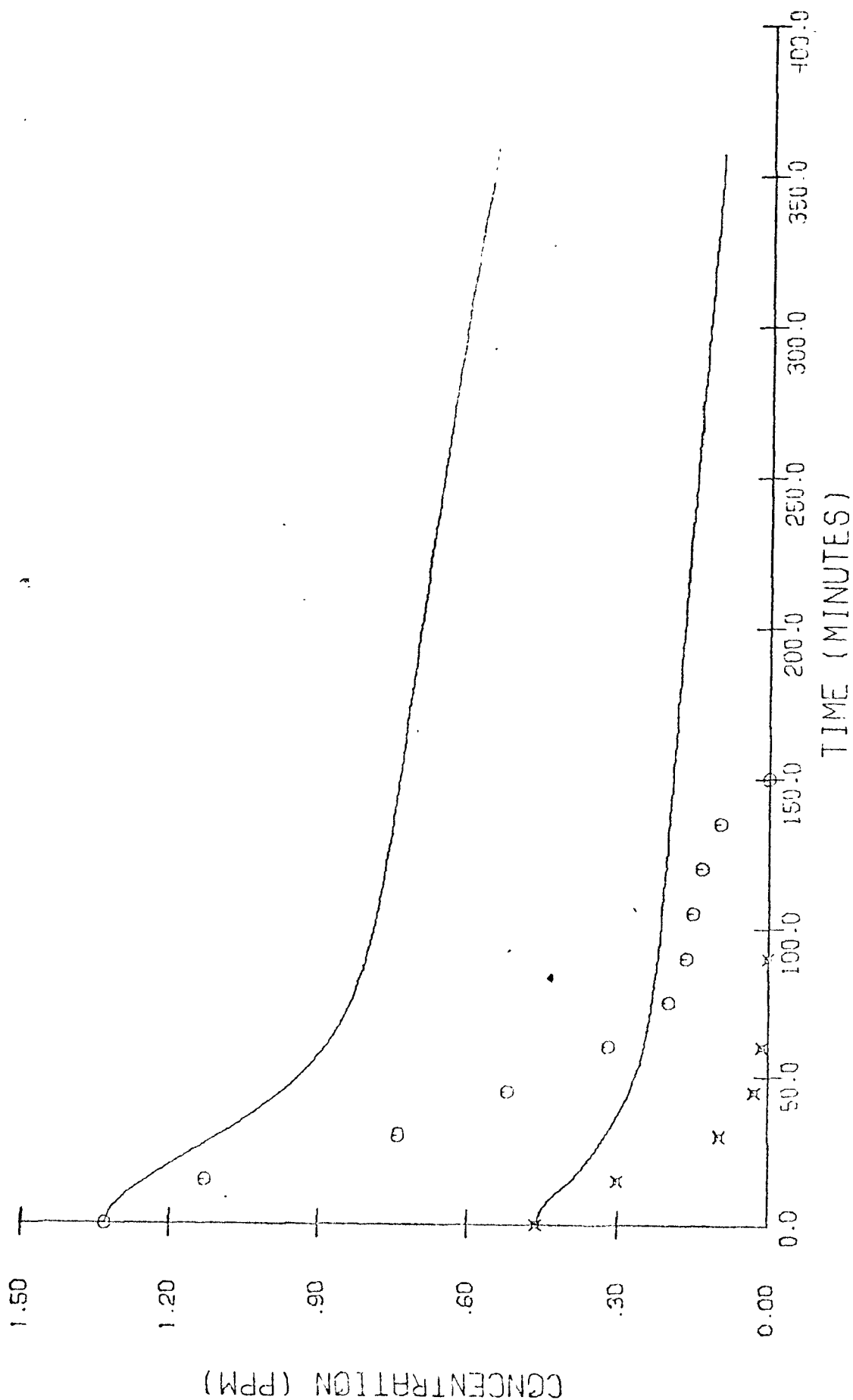


FIGURE 16. SIMULATION OF THE MULTIOLEFIN/NO<sub>x</sub> EXPERIMENT USING THE MECHANISM IN TABLE 1--PREDICTIONS FOR 2-METHYL-1-BUTENE AND PROPYLENE

Chapter IV, the rate constants for many of the most rapid reactions after the peak are uncertain by a factor of 2 or more. In fact, there is no assurance that all of the important reactions are even included in Table 1. Our efforts to improve post- $\text{NO}_2$ -peak predictions of the general mechanism by testing new reactions and varying product distributions in uncertain reactions are delineated in this section.

### 1. Choice of Rate Constants for the Oxidant-Olefin Reactions

We had to specify the rate constants for the reactions of O, OH, and  $\text{O}_3$  with each of the six olefins present at the beginning of the experiments. The rate constants for the reactions of propylene with the three oxidants were required for simulations discussed in Section III-A and are listed in Table 2. Of the other fifteen rate constants, all but two were measured experimentally. The experimental values that we used to simulate this run are listed in Table 7.

The rate constants for the O and OH oxidations of 2-Me-1-butene have not yet been measured. Because 2-Me-1-butene is a branched external olefin, it should be more reactive than the unbranched external olefin, 1-butene (just as 2-Me-2-butene is more reactive than the unbranched olefin, cis-2-butene). However, internal olefins are usually much more reactive than external olefins (Morris and Niki, 1971), and so 2-Me-1-butene should be less reactive than cis-2-butene. Consequently, we estimated that the O and OH rate constants for 2-Me-1-butene fall about one-third of the way between the respective O and OH rate constants for 1-butene and cis-2-butene; e.g.,

$$k_{\text{O}}^{\text{2-Me-1-butene}} = k_{\text{O}}^{\text{1-butene}} + \frac{1}{3} \left( k_{\text{O}}^{\text{cis-2-butene}} - k_{\text{O}}^{\text{1-butene}} \right)$$

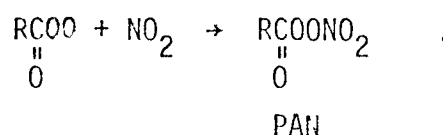
### 2. Changes in the General Mechanism

The results of the simulation of this experiment using the mechanism in Table 1 point out the extreme and antithetical behavior of  $\text{NO}_2$  and PAN.

As already noted, the predicted disappearance rate of  $\text{NO}_2$  and the appearance rate of PAN, a species formed in a direct reaction involving  $\text{NO}_2$  (Reaction 33 in Table 1), were both much greater than that observed in the experiment. Also, the predicted concentration of  $\text{NO}_2$  after its peak was much less than the observed concentration, whereas the predicted PAN concentration was much greater than the experimentally measured PAN value. We therefore suspected that errors in reactions that either (1) produce PAN or its precursors or (2) consume PAN might account for a major portion of the discrepancies in prediction.

a. Reactions That Produce PAN or Its Precursors

PAN is thought to form primarily as a result of a radical-radical reaction involving peroxyacyl radicals (other than  $\text{HCO}_3$ ) and  $\text{NO}_2$ :\*

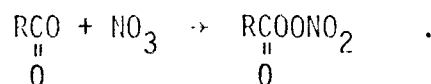


Since the chemistry of  $\text{NO}_2$  is understood fairly well, we focused our attention on reactions producing or consuming  $\text{RCO}_3$  to explain the anomalous PAN predictions.

Reactions Producing  $\text{RCO}_3$ . The principal sources of peroxyacyl radicals in the general mechanism (Table 1) for a system involving olefins are the

---

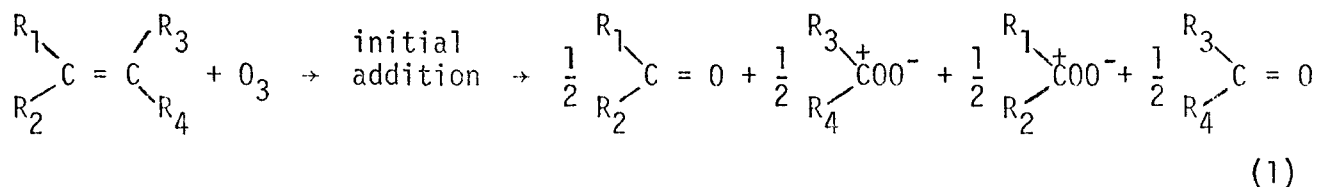
\* Hanst (1971) has suggested that PAN might also--or alternatively--form by the reaction



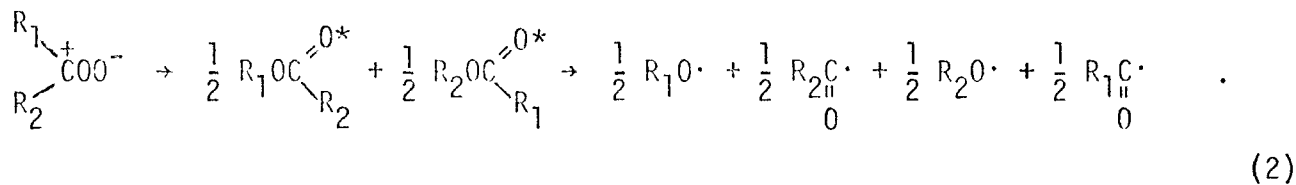
Although neither this reaction nor the  $\text{RCO}_3\text{-NO}_2$  reaction has been observed directly, to our knowledge, we have ruled out the  $\text{RCO}_2\text{-NO}_3$  reaction for conditions typical of irradiated smog chambers and the atmosphere because of the rapid decomposition of acylate radicals to  $\text{R}\cdot$  and  $\text{CO}_2$ .

$O_3$ -olefin reaction (Reaction 23) and the OH oxidation of aldehydes (Reactions 29 and 30). It is common knowledge that the reaction mechanism and elementary products of the  $O_3$ -olefin reaction in the gas phase are extremely uncertain. Chemists, however, feel reasonably certain about the OH-aldehyde elementary mechanism. We treat each of these in turn.

Recently, O'Neal and Blumstein (1973) postulated a "new mechanism" for the  $O_3$ -olefin reaction. The mechanism, in fact, consists of many reaction pathways for the biradical reaction intermediate and was formulated in part on the basis of several  $O_3$ -olefin reaction product studies. It is clear that Reaction 23 in Table 1 is overly simplistic, in view of the large number of reactions pathways that they proposed and defended. On the other hand, one reaction mechanism described by Leighton (1961) approximates many of the important aspects of their mechanism reasonably well. Leighton's mechanism is



followed by

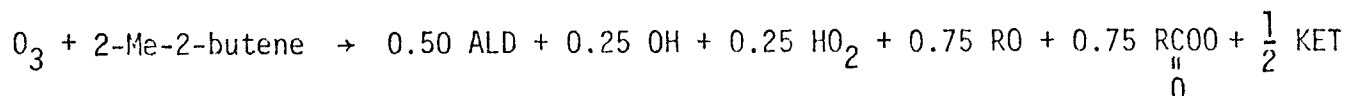
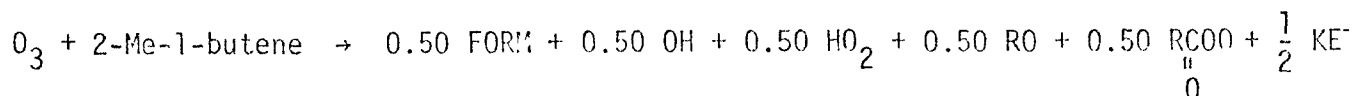
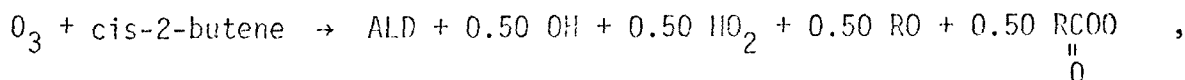
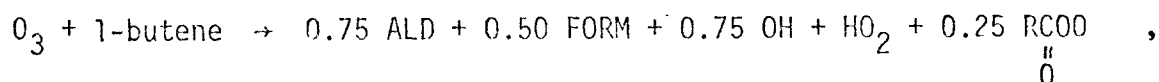


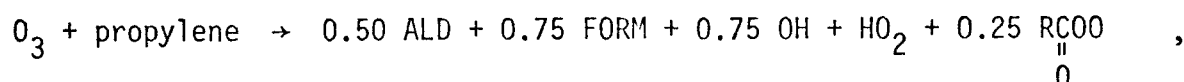
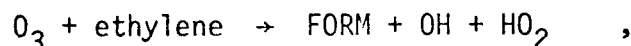
The Leighton mechanism and the O'Neal and Blumstein mechanism agree in the following important respects:

- > Both predict that aldehydes and ketones are formed in the reaction.
- > Both predict that free radicals are formed.
- > Both predict that OH is formed if the olefinic carbon atoms are not completely substituted with carbon chains.

The mechanisms differ chiefly in their level of complexity; the O'Neal and Blumstein mechanism allows a much greater number of reaction pathways.

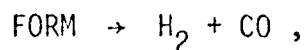
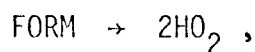
On one hand, Reaction 23 appeared to be inadequate as postulated in Table 1; on the other hand, the O'Neal and Blumstein formulation seemed overly complex (though by no means necessarily improper) for use in the general mechanism. We therefore decided to test the Leighton  $O_3$ -olefin mechanism in the general mechanism on a provisional basis. Reaction 23 in the mechanism was replaced by the following six reactions (one for each olefin in the multiolefin/ $NO_x$  experiment):



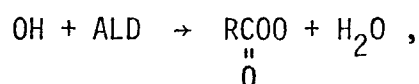
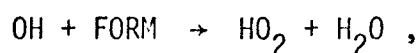


where FORM represents formaldehyde, ALD represents all aldehydes other than formaldehyde, and KET represents ketones.

The other major source of  $\text{RCO}_3$  was the OH oxidation of aldehydes other than formaldehyde (Reaction 30). In our original formulation of the general mechanism, both formaldehyde and higher aldehydes were lumped into the class  $\text{HC}_4$ . Consequently, to indicate the portion of total aldehydes that was not formaldehyde, we introduced a fractional coefficient,  $\beta$ , into the reaction. During the multiolefin/ $\text{NO}_x$  experiment, the concentrations of three aldehydes--formaldehyde, acetaldehyde, and propionaldehyde--were measured; formaldehyde reached a level of over 2 ppm. As a result, the chromatopic acid determination of  $\text{HCHO}$ , which is often imprecise at  $\text{HCHO}$  concentrations less than 0.5 ppm, provided more reliable measurements than are usually possible (see Seinfeld et al., 1973). Thus, before simulating this experiment, we decided to separate the "total aldehyde" class into two classes, formaldehyde and other aldehydes (which in this case consisted of acetaldehyde and propionaldehyde). The coefficient  $\beta$  in Reactions 29 and 30 was eliminated as a result of this change. We also included reaction pathways in the mechanism for the photolysis of both classes of aldehydes to stable products (Calvert et al., 1972). Thus, Reactions 29 and 30 in Table 1 were replaced by

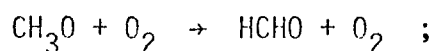




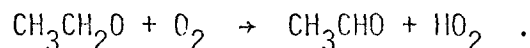


where PROD is a stable product, usually a paraffin (methane when the aldehyde is acetaldehyde).

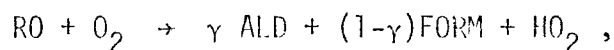
The separation of formaldehyde from the general aldehyde class necessitated one additional change. We were forced to distinguish between methoxy and higher alkoxy radicals, since the former leads to formaldehyde formation, and the latter, to the formation of higher aldehydes:



but, for example,



Thus, Reaction 34 in Table 1 was replaced with the reaction

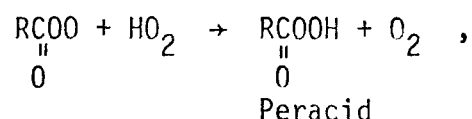


where  $\gamma$  is the fraction of RO that is not  $\text{CH}_3\text{O}$ . For this experiment, we estimated that  $\gamma$  is about 0.25, based on a consideration of the various elementary reactions involving olefins and aldehydes.

The coefficient  $\gamma$  is essentially a direct replacement for  $\beta$ . It, too, could be eliminated if we were to introduce two new free radical species in the general mechanism,  $\text{CH}_3\text{O}$  and  $\text{CH}_3\text{OO}$ . Then, RO would represent all alkoxy radicals other than  $\text{CH}_3\text{O}$ , and  $\text{RO}_2$  would contain all peroxyalkyl radicals other than  $\text{CH}_3\text{OO}$ . If we did this, however, we would also need to specify

the fraction of aldehydes (ALD) that is not acetaldehyde, since the photolysis of acetaldehyde leads to methyl radical formation and the photolysis of higher aldehydes leads to the formation of alkyl radicals other than methyl. When the chemistry is generalized in this manner, one parametric coefficient must be introduced into the mechanism to close the reaction sequence.

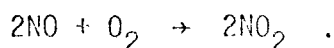
A Reaction Consuming  $\text{RCO}_3$ . Finally, we added one radical chain termination reaction to the mechanism to control the concentration of  $\text{RCO}_3$  in the absence of both NO and  $\text{NO}_2$  (Reactions 32 and 33). This reaction is



for which we assigned a rate constant of  $100 \text{ ppm}^{-1} \text{ min}^{-1}$  by analogy to Reaction 38.

b. Reactions That Consume PAN

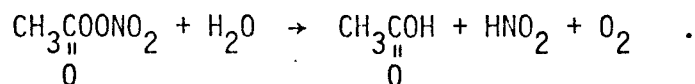
PAN is known to be unstable. In 1969 Stephens reported that PAN decomposes on the walls of a reactor, yielding a variety of products, including  $\text{CH}_3\text{ONO}_2$ ,  $\text{CO}_2$ , and  $\text{CH}_3\text{COOH}$ . Laboratory explosions involving droplets of PAN have also occurred. A reaction between PAN and NO studied by Schuck et al. (1972) involves a mechanism that is apparently complex and that has not yet been established. The reaction is, however, about  $10^3$  times faster than the very slow reaction



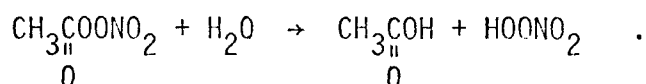
Since PAN absorbs light very weakly at wavelengths greater than  $2800\text{\AA}$  (Stephens, 1969), its photodissociation in the atmosphere can be ruled out.

The reported decomposition of PAN on the reactor walls could conceivably be evidence of a slow PAN hydrolysis reaction. Thus, we hypothesized a

direct reaction between PAN and water leading to the formation of acetic acid, nitrous acid, and  $O_2$ :



Based on the tables in Benson (1968), we calculated that this reaction is exothermic by 7 kcal/mole, and we assigned the reaction a rate constant of  $2 \times 10^{-6} \text{ ppm}^{-1} \text{ min}^{-1}$ . This value seems reasonable in relation to the rate of the  $\text{H}_2\text{O}_5\text{-H}_2\text{O}$  reaction (Reaction 11 in Table 1). One might expect an alternate formulation of the PAN- $\text{H}_2\text{O}$  reaction leading to pernitric acid formation to be even more exothermic:



However, we have not yet pursued this possibility in depth.

### 3. Results and Discussion

The modifications and additions to the general mechanism and the revised reactions and rate constants are presented in Table 8. Using the mechanism and rate constants in this table, we carried out a simulation of the multiolefin run. The results are depicted graphically in Figures 17 through 20.

As shown in these figures, the agreement between predictions and data-- up to the time of the  $\text{NO}_2$  peak--using the mechanism in Table 1 is preserved using the new formulation of the mechanism. After the peak, however, the  $\text{NO}_2$  disappearance rate predicted by the new reaction scheme agrees more closely with the observations. The predicted ozone asymptote agrees very well with the data, although the mechanism fails to predict the  $\text{O}_3$  peak even qualitatively. The peak in the  $\text{O}_3$  concentration-time profile may have been due to  $\text{NO}_2$  interferences in the experimental  $\text{O}_3$  measurements (see Seinfeld et al., 1973). However, this hydrocarbon/ $\text{NO}_x$  system is extremely reactive. It is not unreasonable to expect that  $\text{O}_3$  would accumulate rapidly

Table 8

REVISED GENERAL MECHANISM USED TO SIMULATE  
THE MULTIOLEFIN/NO<sub>x</sub> EXPERIMENT

Number	Reaction	Rate Constant*
1	$\text{NO}_2 + h\nu \rightarrow \text{NO} + \text{O}$	$2.23 \times 10^{-1} \text{ min}^{-1}$
2	$\text{O} + \text{O}_2 + \text{M} \rightarrow \text{O}_3 + \text{M}$	$2.00 \times 10^{-5} \text{ ppm}^{-2} \text{ min}^{-1}$
3	$\text{NO} + \text{O}_3 \rightarrow \text{NO}_2 + \text{O}_2$	$2.08 \times 10^1$
4	$\text{O} + \text{NO} + \text{M} \rightarrow \text{NO}_2 + \text{M}$	$3.50 \times 10^3$
5	$\text{O} + \text{NO}_2 \rightarrow \text{NO} + \text{O}_2$	$1.38 \times 10^4$
6	$\text{O} + \text{NO}_2 + \text{M} \rightarrow \text{NO}_3 + \text{M}$	$2.20 \times 10^3$
7	$\text{NO}_2 + \text{O}_3 \rightarrow \text{NO}_3 + \text{O}_2$	$4.65 \times 10^{-2}$
8	$\text{NO}_3 + \text{NO} \rightarrow 2\text{NO}_2$	$1.50 \times 10^4$
9	$\text{NO}_3 + \text{NO}_2 \rightarrow \text{N}_2\text{O}_5$	$4.50 \times 10^3$
10	$\text{N}_2\text{O}_5 \rightarrow \text{NO}_2 + \text{NO}_3$	$2.70 \times 10^1 \text{ min}^{-1}$
11	$\text{N}_2\text{O}_5 + \text{H}_2\text{O} \rightarrow 2\text{HNO}_3$	$1.00 \times 10^{-5}$
12	$\text{NO} + \text{HNO}_3 \rightarrow \text{HNO}_2 + \text{NO}_2$	$2.50 \times 10^{-4}$
13	$\text{HNO}_2 + \text{HNO}_3 \rightarrow \text{H}_2\text{O} + 2\text{NO}_2$	$2.00 \times 10^{-1}$
14	$\text{NO} + \text{HO}_2 + \text{H}_2\text{O} \rightarrow 2\text{HNO}_2$	$2.10 \times 10^{-6} \text{ ppm}^{-2} \text{ min}^{-1}$
15	$2\text{HNO}_2 \rightarrow \text{NO} + \text{NO}_2 + \text{H}_2\text{O}$	4.50
16	$\text{HNO}_2 + h\nu \rightarrow \text{OH} + \text{NO}$	$1.30 \times 10^{-2} \text{ min}^{-1}$
17	$\text{OH} + \text{NO}_2 \rightarrow \text{HNO}_3$	$1.50 \times 10^4$
18	$\text{OH} + \text{NO} \rightarrow \text{HNO}_2$	$1.20 \times 10^4$
19	$\text{HO}_2 + \text{NO} \rightarrow \text{OH} + \text{NO}_2$	$7.00 \times 10^2$
20	$\text{HO}_2 + \text{HO}_2 \rightarrow \text{H}_2\text{O}_2 + \text{O}_2$	$5.30 \times 10^3$
21	$\text{H}_2\text{O}_2 + h\nu \rightarrow 2\text{OH}$	$1.06 \times 10^{-3} \text{ min}^{-1}$
22	$\text{HC11} + \text{O} \rightarrow \text{ROO} + 0.50 \text{RCOO} + 0.50 \text{HO}_2$	$4.70 \times 10^3$
	$\text{O}$	
23	$\text{HC12} + \text{O} \rightarrow \text{ROO} + \text{RCOO}$	$3.10 \times 10^4$
	$\text{O}$	

Table 8 (Continued)

Number	Reaction	Rate Constant*
24	$\text{HC13} + \text{O} \rightarrow \text{ROO} + 0.50 \underset{\text{O}}{\text{RCOO}} + 0.50 \text{HO}_2$	$1.30 \times 10^4$
25	$\text{HC14} + \text{O} \rightarrow \text{ROO} + \underset{\text{O}}{\text{RCOO}}$	$6.00 \times 10^4$
26	$\text{HC15} + \text{O} \rightarrow \text{ROO} + \text{HO}_2$	$7.60 \times 10^2$
27	$\text{HC16} + \text{O} \rightarrow \text{ROO} + 0.50 \underset{\text{O}}{\text{RCOO}} + 0.50 \text{HO}_2$	$6.80 \times 10^3$
28	$\text{HC11} + \text{O}_3 \rightarrow 0.75 \text{ALD} + 0.50 \text{HCHO} + 0.75 \text{OH} + \text{HO}_2 + 0.25 \underset{\text{O}}{\text{RCOO}}$	$1.30 \times 10^{-2}$
29	$\text{HC12} + \text{O}_3 \rightarrow \text{ALD} + 0.50 \text{OH} + 0.50 \text{HO}_2 + 0.50 \text{RO} + 0.50 \underset{\text{O}}{\text{RCOO}}$	$4.10 \times 10^{-2}$
30	$\text{HC13} + \text{O}_3 \rightarrow 0.50 \text{HCHO} + 0.50 \text{OH} + 0.50 \text{HO}_2 + 0.50 \text{RO} + 0.50 \underset{\text{O}}{\text{RCOO}}$	$1.60 \times 10^{-2}$
31	$\text{HC14} + \text{O}_3 \rightarrow 0.50 \text{ALD} + 0.25 \text{OH} + 0.25 \text{HO}_2 + 0.75 \text{RO} + 0.75 \underset{\text{O}}{\text{RCOO}}$	$4.30 \times 10^{-2}$
32	$\text{HC15} + \text{O}_3 \rightarrow \text{HCHO} + \text{OH} + \text{HO}_2$	$3.10 \times 10^{-3}$
33	$\text{HC16} + \text{O}_3 \rightarrow 0.50 \text{ALD} + 0.75 \text{HCHO} + 0.75 \text{OH} + \text{HO}_2 + 0.25 \underset{\text{O}}{\text{RCOO}}$	$1.60 \times 10^{-2}$
34	$\text{HC11} + \text{OH} \rightarrow \text{ROO} + \text{HCHO}$	$6.00 \times 10^4$
35	$\text{HC12} + \text{OH} \rightarrow \text{ROO} + \text{HCHO}$	$9.00 \times 10^4$
36	$\text{HC13} + \text{OH} \rightarrow \text{ROO} + \text{HCHO}$	$7.00 \times 10^4$
37	$\text{HC14} + \text{OH} \rightarrow \text{ROO} + \text{HCHO}$	$1.30 \times 10^5$
38	$\text{HC15} + \text{OH} \rightarrow \text{ROO} + \text{HCHO}$	$7.50 \times 10^3$
39	$\text{HC16} + \text{OH} \rightarrow \text{ROO} + \text{HCHO}$	$2.50 \times 10^4$
40	$\text{HCHO} + h\nu \rightarrow 2\text{HO}_2$	$2.50 \times 10^{-3} \text{ min}^{-1}$
41	$\text{HCHO} + h\nu \rightarrow \text{H}_2 + \text{CO}$	$2.50 \times 10^{-3} \text{ min}^{-1}$
42	$\text{ALD} + h\nu \rightarrow \text{RO}_2 + \text{HO}_2$	$2.50 \times 10^{-3} \text{ min}^{-1}$
43	$\text{ALD} + h\nu \rightarrow \text{Alkane} + \text{H}_2$	$2.50 \times 10^{-3} \text{ min}^{-1}$
44	$\text{OH} + \text{HCHO} \rightarrow \text{HO}_2 + \text{H}_2\text{O}$	$2.30 \times 10^4$
45	$\text{OH} + \text{ALD} \rightarrow \underset{\text{O}}{\text{RCOO}} + \text{H}_2\text{O}$	$2.30 \times 10^4$

Table 8 (Concluded)

Number	Reaction	Rate Constant*
46	$\text{ROO} + \text{NO} \rightarrow \text{RO} + \text{NO}_2$	$9.10 \times 10^2$
47	$\text{RCOO} + \text{NO} \xrightarrow{\text{O}_2} \text{ROO} + \text{NO}_2 + \text{CO}_2$ $\text{O}$	$9.10 \times 10^2$
48	$\text{RCOO} + \text{NO}_2 \rightarrow \text{RCOONO}_2$ $\text{O}$	$1.00 \times 10^2$
49	$\text{RCOONO}_2 + \text{H}_2\text{O} \rightarrow \text{Acid} + \text{HNO}_2 + \text{O}_2$ $\text{O}$	$2.00 \times 10^{-6}$
50	$\text{RO} + \text{O}_2 \rightarrow \text{HO}_2 + 0.75 \text{ HCHO} + 0.25 \text{ ALD}$	$2.40 \times 10^{-2}$
51	$\text{RO} + \text{NO} \rightarrow \text{RONO}$	$2.50 \times 10^2$
52	$\text{RO} + \text{NO}_2 \rightarrow \text{RONO}_2$	$4.90 \times 10^2$
53	$\text{HO}_2 + \text{ROO} \rightarrow \text{RO} + \text{OH} + \text{O}_2$	$1.00 \times 10^2$
54	$\text{RCOO} + \text{HO}_2 \rightarrow \text{Peracid} + \text{O}_2$ $\text{O}$	$1.00 \times 10^2$
55	$2\text{ROO} \rightarrow 2\text{RO} + \text{O}_2$	$1.00 \times 10^2$

HC11 = 1-butene.

HC12 = cis-2-butene.

HC13 = 2-Me-1-butene.

HC14 = 2-Me-2-butene.

HC15 = ethylene.

HC16 = propylene.

\* In units of  $\text{ppm}^{-1} \text{ min}^{-1}$  unless otherwise indicated.

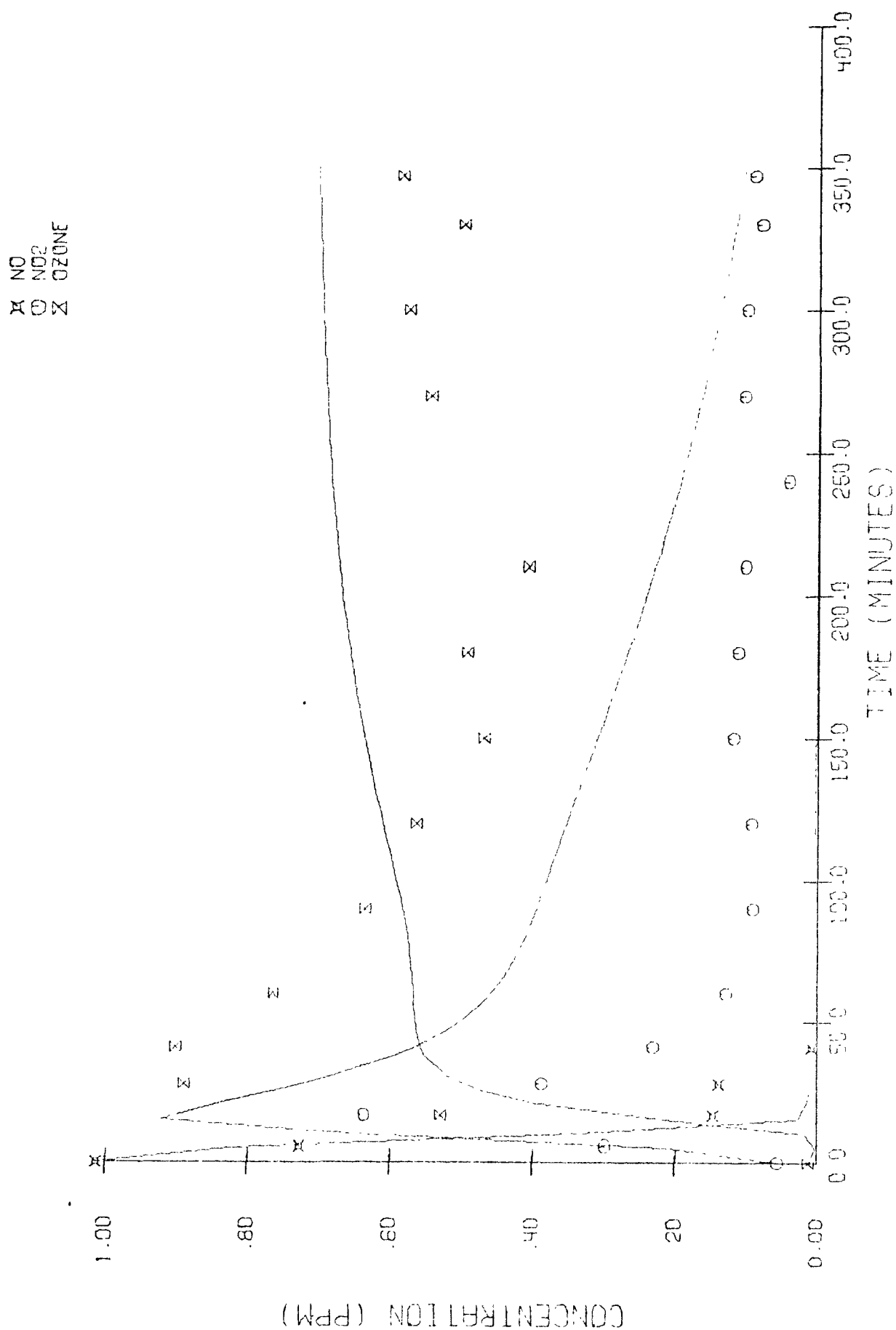


FIGURE 17. SIMULATION OF THE MULTIOLEFIN/NO<sub>x</sub> EXPERIMENT USING THE REVISED MECHANISM (TABLE 8)--PREDICTIONS FOR NO, NO<sub>2</sub>, AND O<sub>3</sub>

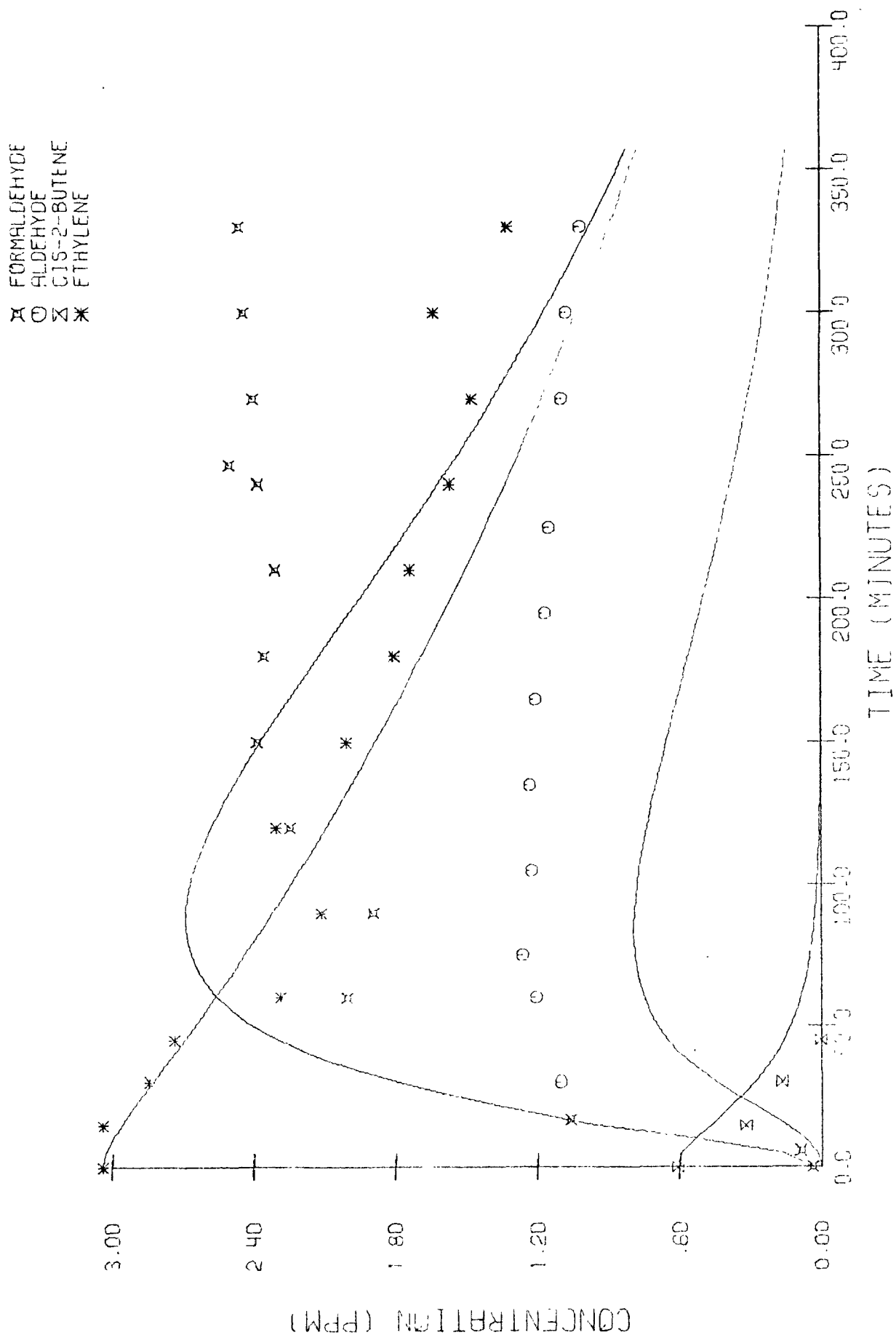


FIGURE 18. SIMULATION OF THE MULTIOLEFIN/NO<sub>x</sub> EXPERIMENT USING THE REVISED MECHANISM (TABLE 8)--PREDICTIONS FOR FORMALDEHYDE, ALDEHYDE, CIS-2-BUTENE, AND ETHYLENE



O PAN  
 X 1-BUTENE  
 Z 2-ME-2-BUTENE

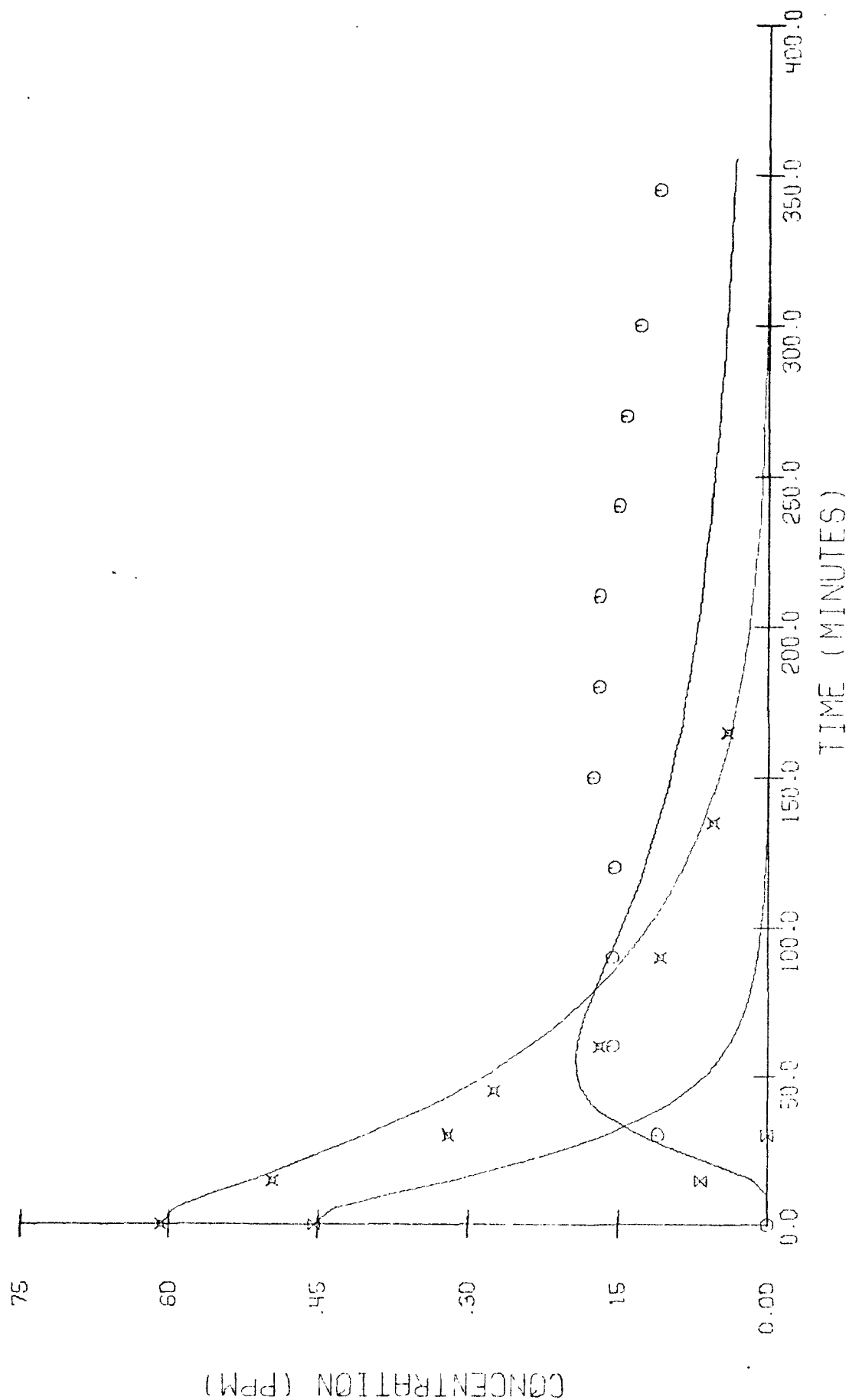


FIGURE 19. SIMULATION OF THE MULTIOLEFIN/NO<sub>x</sub> EXPERIMENT USING THE REVISED MECHANISM (TABLE 8)--PREDICTIONS FOR PAN, 1-BUTENE, AND 2-METHYL-2-BUTENE

X 2-ME-1-BUTENE  
 O PROPYLENE

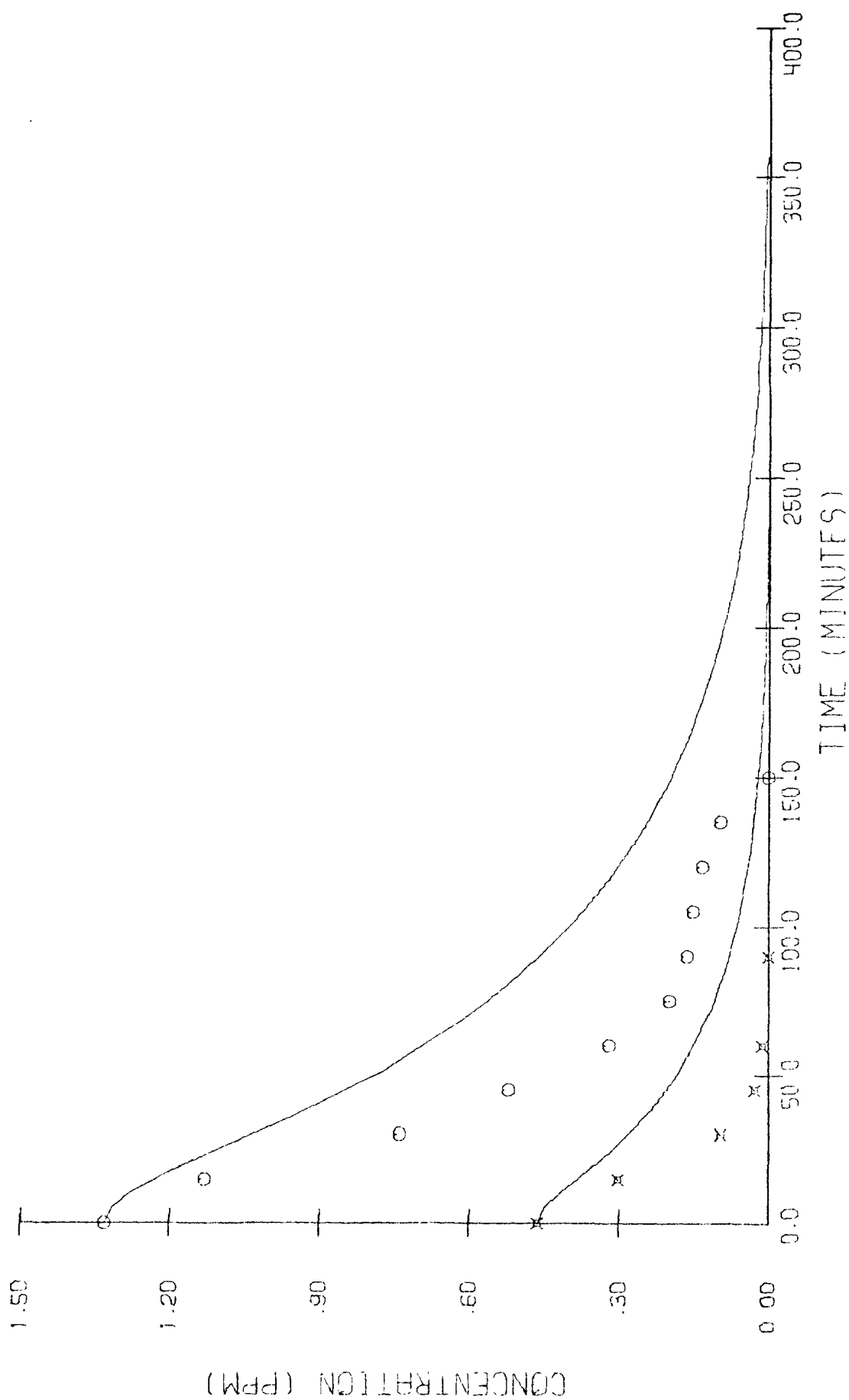


FIGURE 20. SIMULATION OF THE MULTIOLEFIN/NO<sub>x</sub> EXPERIMENT USING THE REVISED MECHANISM  
 (TABLE 8)--PREDICTIONS FOR 2-METHYL-1-BUTENE AND PROPYLENE

with  $\text{NO}_2$  and then be consumed by the  $\text{O}_3\text{-NO}_2$  and  $\text{O}_3\text{-olefin}$  reactions. Formaldehyde measurements agree reasonably well with observations through much of the run, but discrepancies become increasingly more serious after 200 minutes of the run. The predictions of the concentrations of other aldehydes are low throughout the simulation. PAN predictions, which were five times greater than the observations when the Table 1 mechanism was used, are in much better agreement with the data here, although the predicted concentration is too low after about 150 minutes. Finally, the predictions for all the olefins are vastly improved compared with those obtained using the mechanism in Table 1.

We made several changes in the mechanism to simulate this particular experiment. Although the results are encouraging, this exercise, by itself, does little to substantiate the veracity of these modifications. The improvement in predictions can be attributed chiefly to the expanded treatment of the  $\text{O}_3\text{-olefin}$  reactions and to the introduction of the  $\text{PAN-H}_2\text{O}$  reaction. Unfortunately, both of these reactions are speculative. The latter, in particular, has never been studied explicitly in a laboratory, though we understand that the rate constant for the reaction is to be determined soon at the University of California, Riverside.

Perhaps the only conclusion we can draw from this work is that the formulation of the general mechanism in Table 1 is inadequate for the simulation of post- $\text{NO}_2$  peak chemistry. The improved agreement between predictions and experimental data using the reactions and mechanisms postulated here does not necessarily prove that they are the correct explanations for the experimental observations. However, the change in agreement between predictions and data was dramatic enough to make us feel that the mechanism of the  $\text{O}_3\text{-olefin}$  reaction and the rate constant and mechanism of the  $\text{PAN-H}_2\text{O}$  reaction merit further detailed experimental scrutiny.

As noted earlier, this set of data was the last that we simulated during the contract year. The modified mechanism predicts this one multi-olefin/ $\text{NO}_x$  experiment quite well and will be developed further next year during the analysis of the UCR propylene/ $\text{NO}_x$  experiments.



#### IV SENSITIVITY AND UNCERTAINTY OF REACTIONS IN THE GENERAL MECHANISM

The evaluation studies presented in Chapter III are chiefly a test of the accuracy of the specific set of reactions and rate constants employed in the general mechanism. We realize, of course, that other important reactions may have been omitted from the mechanism and that elementary mechanisms proposed for some reactions may be incorrect. However, the value of every rate constant in the mechanism is uncertain to some degree. If a newly measured or redetermined rate constant were to differ significantly from the value used in our simulations, the predictions and, consequently, the accuracy of the kinetic mechanism would be altered greatly. Therefore, before the general mechanism is used for decision-making, it is important to quantify the extent to which uncertainties in values of the rate constants influence the prediction of photochemical smog formation. Toward this end, we calculated the sensitivity (defined as  $\partial p / \partial k_i$ , the rate of change in the predictions of the model with changes in the value of the  $i$ -th rate constant) of every rate constant in the general mechanism.

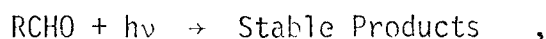
A second factor, however, must be taken into account in judging the effect of this sensitivity. Suppose that every rate constant were known with absolute accuracy. Then, it would make little difference if predictions were extremely "sensitive" to variations of the rate constant(s), since the possibility of a change in the rate constants would never arise. As we stated above, and as we discuss in depth later in this chapter, every rate constant in the general mechanism is uncertain to some degree. The magnitudes of the individual uncertainties influence our interpretation or weighting of the sensitivity value calculated for each constant. We therefore combined the calculated sensitivity measures with estimates of the uncertainty bound of each rate constant to create a new index that reflects the importance of obtaining more accurate measurements of rate constants to reduce the uncertainties in the model predictions. From the ranking of

the reactions according to this index, we were able to identify (1) reactions for which accurate measurements of the associated rate constants are needed and (2) insensitive reactions that can possibly be eliminated from the mechanism without a significant loss of accuracy.

#### A. THE MECHANISM EMPLOYED

When we carried out the sensitivity calculations, we used a slightly modified version of the kinetic mechanism presented in Tables 1 and 2. The changes had been implemented to augment the agreement between predictions and experimental data for EPA Run 329:  $[\text{NO}_2]_0 = 0.06$  ppm,  $[\text{NO}]_0 = 0.29$  ppm,  $[\text{C}_3\text{H}_6]_0 = 0.24$  ppm, and  $[\text{H}_2\text{O}]_0 = 10,000$  ppm. We were particularly interested in this experiment because the initial concentrations were at values typical of polluted atmospheres and because ozone accumulated to an asymptotic level during the experiment.

Although the mechanism used for the sensitivity analysis (see Table 9) closely resembles the kinetic mechanism presented in Tables 1 and 2, some minor differences are worth noting. In earlier simulations, we had shown that Reactions 12 and 13 could be eliminated from the general mechanism (Table 1) without affecting predictions. Also, since no CO, paraffins, or aromatics were present in EPA Run 329, Reactions 19 and 25 through 28 were not needed to carry out the simulation. However, the photolysis reaction of aldehydes leading to stable products,



had not been included in Table 1. Since we thought this reaction was of moderate importance (Calvert et al., 1972), we included it in the modified version of the mechanism.

Several rate constants were also changed within their bounds of uncertainty to improve the predictions for EPA Run 329. The reactions so affected, the values of the rate constants in Table 2, and the values of

Table 9  
THE KINETIC MECHANISM USED FOR THE SENSITIVITY ANALYSIS

Number	Reaction	Rate Constant*	Uncertainty Factor
1	$\text{NO}_2 + h\nu \rightarrow \text{NO} + \text{O}$	$2.7 \times 10^{-1+}$	1.4
2	$\text{O} + \text{O}_2 \xrightarrow{\text{M}} \text{O}_3$	$3.3 \times 10^{6s}$	1.2**
3	$\text{O}_3 + \text{NO} \rightarrow \text{NO}_2 + \text{O}_2$	$2.1 \times 10^1$	1.3**
4	$\text{O}_3 + \text{NO}_2 \rightarrow \text{NO}_3 + \text{O}_2$	$4.6 \times 10^{-2}$	1.3**
5	$\text{NO}_3 + \text{NO} \rightarrow 2\text{NO}_2$	$1.5 \times 10^4$	5.0**
6	$\text{NO}_2 + \text{NO}_3 \xrightarrow{\text{H}_2\text{O}} 2\text{HNO}_3$	4.5++	2.5**
7	$\text{O} + \text{NO} \xrightarrow{\text{M}} \text{NO}_2$	$2.5 \times 10^{3++}$	1.2**
8	$\text{O} + \text{NO}_2 \rightarrow \text{NO} + \text{O}_2$	$1.4 \times 10^4$	1.2**
9	$\text{O} + \text{NO}_2 \xrightarrow{\text{M}} \text{NO}_3$	$3.0 \times 10^{3++}$	1.6**
10	$\text{NO} + \text{NO}_2 \xrightarrow{\text{H}_2\text{O}} 2\text{HNO}_2$	$1.5 \times 10^{-2++}$	10.0
11	$\text{HNO}_2 + \text{HNO}_2 \rightarrow \text{NO} + \text{NO}_2 + \text{H}_2\text{O}$	1.1	10.0
12	$\text{HNO}_2 + h\nu \rightarrow \text{OH} + \text{NO}$	$1.3 \times 10^{-2+}$	3.0
13	$\text{OH} + \text{NO}_2 \rightarrow \text{HNO}_3$	$6.0 \times 10^3$	2.0**
14	$\text{OH} + \text{NO} \rightarrow \text{HNO}_2$	$4.8 \times 10^3$	2.0**
15	$\text{HO}_2 + \text{NO} \rightarrow \text{OH} + \text{NO}_2$	$7.0 \times 10^2$	3.2**
16	$\text{HOOH} + h\nu \rightarrow 2\text{OH}$	$1.5 \times 10^{-3+}$	3.0
17	$\text{OLEF} + \text{O} \rightarrow \text{RO}_2 + 0.5\text{HO}_2 + 0.5\text{RCO}_3$	$6.8 \times 10^3$	1.2**
18	$\text{OLEF} + \text{OH} \rightarrow \text{RCHO} + \text{RO}_2$	$2.5 \times 10^4$	1.2
19	$\text{OLEF} + \text{O}_3 \rightarrow \text{RCHO} + \text{RCO}_3 + \text{OH}$	$1.6 \times 10^{-2}$	1.5

Table 9 (Concluded)

Number	Reaction	Rate Constant*	Uncertainty Factor
20	$\text{RCHO} + h\nu \rightarrow \text{Stable Products}$	$2.5 \times 10^{-3+}$	3.0
21	$\text{RCHO} + h\nu \rightarrow 0.5\text{RO}_2 + 1.5\text{HO}_2$	$2.5 \times 10^{-3+}$	3.0
22	$\text{RCHO} + \text{OH} \rightarrow 0.5\text{RCO}_3 + 0.5\text{HO}_2$	$2.3 \times 10^4$	1.3**
23	$\text{RO}_2 + \text{NO} \rightarrow \text{RO} + \text{NO}_2$	$3.0 \times 10^3$	5.0
24	$\text{RCO}_3 + \text{NO} \rightarrow \text{RO}_2 + \text{NO}_2$	$1.5 \times 10^3$	5.0
25	$\text{RCO}_3 + \text{NO}_2 \rightarrow \text{PAN}$	$5.0 \times 10^2$	5.0
26	$\text{RO} \xrightarrow{\text{O}_2} \text{RCHO} + \text{HO}_2$	$5.0 \times 10^{3§}$	5.0
27	$\text{RO} + \text{NO}_2 \rightarrow \text{RONO}_2$	$4.9 \times 10^2$	5.0
28	$\text{RO} + \text{NO} \rightarrow \text{RONO}$	$2.5 \times 10^2$	5.0
29	$\text{HO}_2 + \text{HO}_2 \rightarrow \text{H}_2\text{O}_2 + \text{O}_2$	$5.3 \times 10^3$	2.0**
30	$\text{RO}_2 + \text{HO}_2 \rightarrow \text{RO} + \text{OH} + \text{O}_2$	$1.0 \times 10^2$	4.0
31	$\text{RO}_2 + \text{RO}_2 \rightarrow 2\text{RO} + \text{O}_2$	$1.0 \times 10^2$	10.0

\* Second-order rate constants (in units of  $\text{ppm}^{-1} \text{min}^{-1}$ ) unless otherwise indicated.

+ First-order reaction (in units of  $\text{min}^{-1}$ ).

§ Pseudo-first-order rate constant value.

\*\* Garvin and Hampson (1974).

†† Pseudo-second-order rate constant value.



the rate constants used in the improved prediction of EPA Run 325 are tabulated below:

Reaction	Rate Constant in Table 2 (ppm <sup>-1</sup> min <sup>-1</sup> )	Rate Constant Used for the Special Simulation of EPA Run 329 (ppm <sup>-1</sup> min <sup>-1</sup> )
$O + O_2 \xrightarrow{M} O_3$	$2.0 \times 10^{1*}$	$1.65 \times 10^{1*}$
$O + NO \xrightarrow{M} NO_2$	$3.5 \times 10^{3*}$	$2.5 \times 10^{3*}$
$O + NO_2 \xrightarrow{M} NO_3$	$2.2 \times 10^{3*}$	$3.0 \times 10^{3*}$
$HNO_2 + HNO_2 \rightarrow NO + NO_2 + H_2O$	4.5	1.1
$OH + NO_2 \rightarrow HNO_3$	$1.5 \times 10^4$	$6.0 \times 10^3$
$OH + NO \rightarrow HNO_2$	$1.2 \times 10^4$	$4.8 \times 10^3$
$RO_2 + NO \rightarrow RO + NO_2$	$9.1 \times 10^2$	$3.0 \times 10^3$
$RCO_3 + NO \rightarrow RO_2 + NO_2$	$9.1 \times 10^2$	$1.5 \times 10^3$
$RCO_3 + NO_2 \rightarrow PAN$	$1.0 \times 10^2$	$5.0 \times 10^1$

There are several reasons why we did not feel compelled to use the mechanism and rate constants in Tables 1 and 2 for the sensitivity calculations. First, we carried out the sensitivity analysis using a single set of initial reactant concentrations. Although this automatically limited the scope, or generality, of our results, the information that we obtained was sufficient to answer the questions posed at the beginning of this project:

---

\* Pseudo-second-order rate constants.

- (1) Which rate constants should be determined with greatest accuracy and precision to reduce uncertainty in predictions of smog formation?
- (2) Which reactions can we possibly eliminate from the mechanism without a significant loss of accuracy?

Because we were examining the sensitivity of the mechanism under only one set of initial conditions, we wanted the predictions to be as good as possible for that case. If the predictions were not accurate to begin with, the sensitivity results have little value.

Even aside from these considerations, there are many uncertainties in the kinetic mechanism regarding reactions and rate constants. Thus, although we tested the mechanism in Tables 1 and 2 over a range of initial conditions and observed moderate accuracy in prediction, it is difficult to state definitely that the mechanism in Tables 1 and 2 is intrinsically more accurate (or inaccurate) than that given in Table 9. As shown in Figure 21, the kinetic mechanism in Table 9 simulates EPA Run 329 with very good accuracy.

In summary, the two mechanisms differ, but most of the changes are minor. We realize, of course, that slightly different rankings of reactions according to sensitivity might result using Tables 1 and 2 for the calculations. However, the general groupings of sensitive and insensitive reactions for EPA Run 329 observed using Table 9 would almost certainly be similar to those that would be obtained using Tables 1 and 2 [cf. the sensitivity analysis of the mechanism in Tables 1 and 2 discussed in Roth et al. (1974)]

## B. SENSITIVITY ANALYSIS

Central to the performance of a sensitivity analysis of a mathematical model is the meaningful quantification of changes that perturbations of input parameters cause in predictions of the model. The sensitivity,  $S_i$ , of the  $i$ -th parameter,  $k_i$ , can be defined as

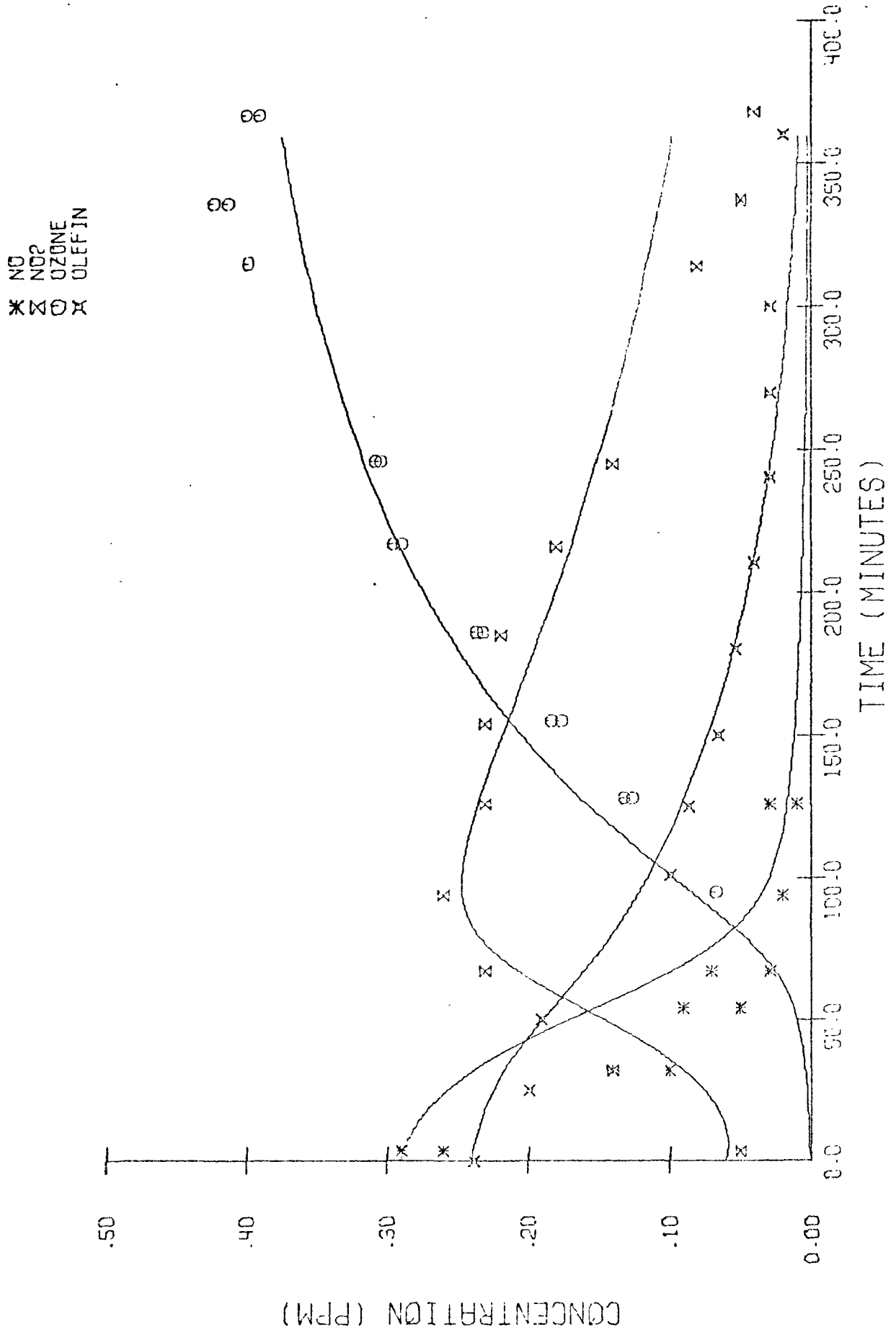


FIGURE 21. BASE CASE FOR THE SENSITIVITY STUDY--RUN EPA 329

$$S_i = \frac{\partial p}{\partial k_i} \quad , \quad (3)$$

the rate of change of the predictions of the mechanism,  $p$ , with changes in the parameter. Obviously, the calculated values of  $S_i$  depend on the model (mechanism) that is being tested, the initial conditions, and the base values (which may not necessarily be the true values) of the rate parameters  $k_i$ .

### 1. Criterion of Sensitivity

The definition of sensitivity in Eq. (3) is somewhat stricter than that needed to reach our objectives, which were stated in Questions 1 and 2 in Section IV-A. For example, at every time step, integration of the kinetic mechanism generates the concentrations of 19 different chemical species. Yet, we are most interested in the concentration-versus-time behavior of just four of these--NO, NO<sub>2</sub>, O<sub>3</sub>, and propylene--the species for which the experimental measurements are most accurate. Thus, in calculating sensitivity in this study, we characterized the change in prediction,  $\Delta p$ , as the change in predicted concentration of each of those four species.

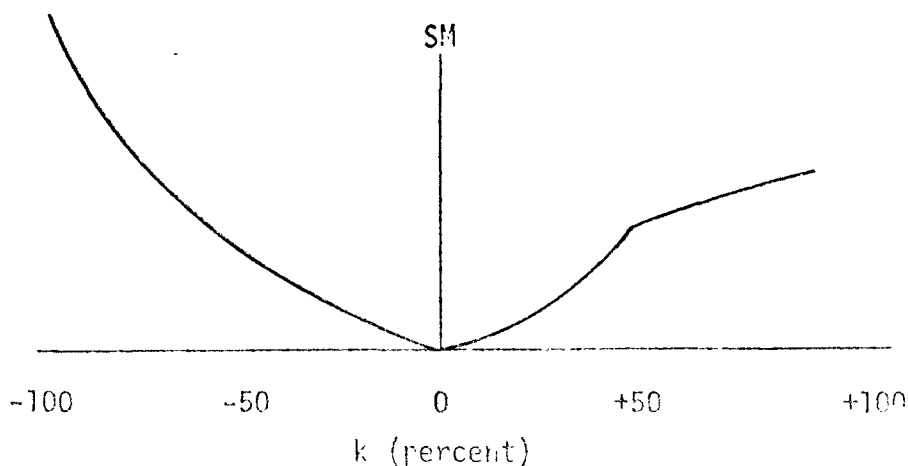
Although strict adherence to Eq. (3) would require the use of a very small perturbation of each rate constant, the large uncertainties of many rate constants made that choice seem unrealistic for this investigation. For example, many of the rate constants are poorly characterized, having associated uncertainties of a factor of 5 or greater.\* Even the best known of the rate constants have uncertainty factors of 1.2. To facilitate comparison and ranking of the sensitivities of the constants, we wished to vary all parameters in turn by the same fixed percentage. An inspection of the uncertainty factors in Table 9 suggested that 1.5 was a representative uncertainty factor--roughly  $\pm 50$  percent. Therefore, we elected to use that percentage as the magnitude of perturbation for the sensitivity calculations. Because the precision bounds of the rate constant values for individual

---

\* The manner in which the uncertainty estimates were made is discussed in Section IV-C.

reaction rate constants vary greatly, however, the choice of the "range of perturbation" must be regarded as arbitrary. This factor of 1.5, or 50 percent, is significant only because it marks the approximate division between the very uncertain and the less uncertain parameters (see Table 9).

One would, of course, expect the magnitude of the change in prediction,  $\Delta p$ , to depend on the degree of perturbation of the parameter (e.g., 10 percent versus 50 percent). However, the values of the sensitivity measures are not, in general, identical, even for plus and minus perturbations in a given parameter, because the equations governing the kinetics are nonlinear. For example, if we were to carry out sensitivity calculations for a single parameter,  $k$ , varying it continuously from its nominal value to  $k+100$  percent and from  $k$  to  $k-100$  percent, we might find that the sensitivity measure (SM) changes in the following manner:



(If predictions of the model were insensitive to the value of this parameter, the rise along the ordinate with perturbations in  $k$  would be slight.) Carrying out such a detailed analysis of the sensitivity of each parameter would be prohibitively expensive. Thus, our analysis was limited to determining two points on that curve-- $+50$  and  $-50$  percent. Since the calculated sensitivity measures for positive and negative perturbations were in reasonably

good agreement, we decided to average the two values for the ranking of rate constants by sensitivity.

Equation (3) makes no reference to time. But, in simulating chemical transformations with the kinetic mechanism, the concentrations of reactants, intermediates, and products constantly change; these changes are reflected in the rates of the various reactions and the sensitivities of the rate constants. Since we are primarily interested in identifying the sensitivities (or insensitivities) of the kinetic mechanism for the overall prediction of smog, a mean value of  $S_i$  over the period of integration would be adequate for our needs. Because the mechanism has been used primarily in the simulation of six-hour smog chamber experiments, 360 minutes appeared to be an appropriate period over which to determine the mean sensitivity. We realize that the use of mean value sensitivity criteria in the analysis of nonlinear systems can sometimes be misleading, inasmuch as momentary periods of extreme sensitivity of a parameter might be masked or obscured by the time-averaging process. However, in view of our application of the calculated sensitivity data, we believe that the use of mean values is justified. This does not rule out the utility of examining sensitivity as a function of time in the future. Furthermore, in the subsequent discussion of the possible elimination of insensitive reactions, we emphasize the need for additional detailed testing of the reactions over a range of initial conditions and bounds of uncertainty of the rate constant.

## 2. Procedure

The sensitivity analysis was carried out in the following manner. Concentration-time profiles for propylene, NO, NO<sub>2</sub>, and O<sub>3</sub> were obtained by integrating the governing rate equations with each rate constant at its "standard" value (Table 9). One of the rate constants was then increased by 50 percent of this value while all other rate constants were held fixed. The equations were then integrated for this new rate-constant setting. The concentration-time profiles obtained for each of the four species at this setting were compared with the respective profiles obtained

when all rate constants were at their standard value (Table 9). The area of the absolute differences between these profiles was then calculated. The standard value for the rate constant was decreased by 50 percent and the process was repeated. The areas determined in this manner for each species at the two rate-constant settings were averaged. This average was then divided by the area under the curve obtained for the respective species when all rate constants were at their standard values. This number was multiplied by 100 to yield the normalized percentage change in the average area resulting from the perturbation of this rate constant by +50 and -50 percent. Finally, the percentage changes obtained for each of the four species were averaged to yield the sensitivity of this rate constant. This procedure was repeated for each of the 31 rate constants.

In summary, the criterion of sensitivity used in this study is given by

$$S_i = \frac{1}{4} \sum_{j=1}^4 \frac{100}{D_j} \int_{t=0}^{t=360} \frac{1}{2} \left[ |C_j(k_i, t) - C_j(k_i + 50\% k_i, t)| + |C_j(k_i, t) - C_j(k_i - 50\% k_i, t)| \right] dt, \quad (4)$$

where the variables and indices are defined as follows:

- $S_i$  the sensitivity of the  $i$ -th rate constant
- $D_j$  area under the concentration-time profile for the  $j$ -th species
- $C_j$  concentration of the  $j$ -th chemical species
- $k_i$  value of the  $i$ -th rate constant
- $j$  species index ( $\text{NO}_2$ ,  $\text{NO}$ ,  $\text{O}_3$ , and propylene)

i reaction or rate constant number

t time.

### 3. Results

If the time history of a chemical species was greatly altered when a given rate constant was perturbed, the value calculated according to Eq. (4) for the sensitivity was small.

The results of the sensitivity study are given in Table 10. As this table shows, the following rate constants display the greatest overall sensitivity:

- $k_1$  the photolysis of  $\text{NO}_2$
- $k_3$  the oxidation of NO by  $\text{O}_3$
- $k_{10}$  the formation of  $\text{HNO}_2$  from NO,  $\text{NO}_2$ , and  $\text{H}_2\text{O}$
- $k_{12}$  the photolysis of  $\text{HNO}_2$
- $k_{13}$  the reaction of OH with  $\text{NO}_2$
- $k_{14}$  the reaction of OH with NO
- $k_{15}$  the oxidation of NO by  $\text{HO}_2$
- $k_{18}$  the oxidation of olefins by OH
- $k_{19}$  the oxidation of olefins by  $\text{O}_3$
- $k_{21}$  the photolysis of aldehydes to radicals.



Table 10  
SENSITIVITY OF THE REACTIONS

Rank	Reaction	Sensitivity
1	OLEF + OH	27.9
2	RCHO + $h\nu \rightarrow$ Radicals	22.0
3	$\text{NO}_2 + h\nu$	13.8
4	$\text{O}_3 + \text{NO}$	12.6
5	$\text{OH} + \text{NO}_2$	11.1
6	$\text{OH} + \text{NO}$	9.1
7	$\text{HNO}_2 + h\nu$	8.5
8	OLEF + $\text{O}_3$	7.4
9	$\text{HO}_2 + \text{NO}$	7.2
10	$\text{NO} + \text{NO}_2 + \text{H}_2\text{O}$	6.4
11	RCHO + OH	4.8
12	$\text{RCO}_3 + \text{NO}_2$	4.5
13	$\text{RCO}_3 + \text{NO}$	4.4
14	$\text{HO}_2 + \text{HO}_2$	3.2
15	$\text{RO} + \text{O}_2$	2.4
16	$\text{O} + \text{O}_2$	2.4
17	OLEF + O	2.0
18	$\text{HNO}_2 + \text{HNO}_2$	1.9
19	RCHO + $h\nu \rightarrow$ Products	1.8
20	$\text{RO} + \text{NO}_2$	1.1
21	$\text{RO} + \text{NO}$	0.8
22	$\text{NO}_2 + \text{O}$	0.6
23	$\text{NO}_2 + \text{O}_3$	0.5
24	$\text{NO}_3 + \text{NO}$	0.4
25	$\text{HOOH} + h\nu$	0.3
26	$\text{NO}_2 + \text{NO}_3$	0.3
27	$\text{RO}_2 + \text{NO}$	< 0.1
28	$\text{RO}_2 + \text{HO}_2$	< 0.1
29	$\text{NO}_2 + \text{O} + \text{M}$	< 0.1
30	$\text{RO}_2 + \text{RO}_2$	< 0.1
31	$\text{O} + \text{NO}$	< 0.1

### C. THE IMPLICATIONS OF COMBINED SENSITIVITY AND UNCERTAINTY DATA

The sensitivity results have additional meaning when assessed in conjunction with the uncertainties of the rate constants used in this study. If a rate constant is well known, little uncertainty is introduced into the predictions, even though this rate constant may rank high on the sensitivity scale. The same holds true if a rate constant is highly uncertain but its sensitivity is negligible. Therefore, meaningful improvement in the kinetic mechanism will be achieved if accurate values are determined for those rate constants whose combined sensitivities and uncertainties are high. To identify these major sources of uncertainty in the model predictions, we formulated the following ad hoc index:

$$S*U = \text{Sensitivity} \times \text{Uncertainty} \quad .$$

Values selected for the uncertainty of each rate constant are listed in Table 9. The uncertainty is expressed in terms of a multiplicative factor. Thus, the "true" value of  $k_3$  might be within the range  $1.3 \times k_3$  to  $(1/1.3) \times k_3$ . Many of the uncertainty estimates, especially for the inorganic reactions, are those of the National Bureau of Standards (NBS), as referenced in Garvin and Hampson (1974). These estimates were determined in most cases through a critical evaluation of experimental methods. The remaining values are our subjective estimates or those of Golden, Hendry, and Mendenhall of Stanford Research Institute; Garvin and Hampson of the NBS, and Dodge of EPA.

#### 1. Rate Constants That Should Be Determined With Great Accuracy

The values of the  $S*U$  index calculated for each rate constant are given in Table 11. Because of the subjective nature of many of the uncertainty estimates, their relative order in this table has greater meaning than their actual numerical rankings. Particular attention should be directed toward those clusters of reactions ranking very high or very low in the table. The reactions that rank highest include the following:

- $k_{10}$  the formation of  $\text{HNO}_2$  from  $\text{NO}$ ,  $\text{NO}_2$ , and  $\text{H}_2\text{O}$
- $k_{12}$  the photolysis of  $\text{HNO}_2$
- $k_{13}$  the reaction of  $\text{OH}$  with  $\text{NO}_2$
- $k_{15}$  the oxidation of  $\text{NO}$  by  $\text{HO}_2$
- $k_{18}$  the oxidation of olefins by  $\text{OH}$
- $k_{21}$  the photolysis of aldehydes to radicals
- $k_{24}$  the oxidation of  $\text{NO}$  by  $\text{RCO}_3$
- $k_{25}$  the formation of PAN from  $\text{RCO}_3$  and  $\text{NO}_2$ .

The uncertainty in predictions of the kinetic mechanism will be reduced significantly if more reliable values for these rate constants are determined.

This list includes rate constants that must be measured in situ (i.e., in smog chambers) as well as rate constants most easily measured in independent laboratory experiments. Carefully executed chamber experiments are a key ingredient in a successful kinetic mechanism verification program. It is generally recognized that, for the data to be of optimum value, the experiment should be monitored accurately, and the chamber should be maintained at constant conditions of temperature, humidity, light intensity, wall activity, and the like. For some time, investigators have realized the importance of determining  $k_1$ , the photolysis rate of  $\text{HNO}_2$ . Yet, the results of this study indicate that because of their combined sensitivities and uncertainties, the rate constants chosen for the photolysis of nitrous acid ( $k_{10}$ ) and aldehydes ( $k_{21}$ ) to radicals introduce even more unreliability into the predicted concentration-time profiles. Unless our nominal values for these two rate constants are gross overestimates, we feel that the photolytic dissociation rates for aldehydes and nitrous acid must also be measured in future chamber experiments.

Table 11  
COMBINED SENSITIVITY AND UNCERTAINTY  
OF THE REACTIONS

<u>Rank</u>	<u>Reaction</u>	<u>S*U Index</u>
1	$\text{RCHO} + h\nu \rightarrow \text{Radicals}$	66.0
2	$\text{NO} + \text{NO}_2 + \text{H}_2\text{O}$	64.0
3	$\text{OLEF} + \text{OH}$	33.5
4	$\text{HNO}_2 + h\nu$	25.5
5	$\text{HO}_2 + \text{NO}$	23.0
6	$\text{RCO}_3 + \text{NO}_2$	22.5
7	$\text{OH} + \text{NO}_2$	22.2
8	$\text{RCO}_3 + \text{NO}$	22.0
9	$\text{NO}_2 + h\nu$	19.3
10	$\text{HNO}_2 + \text{HNO}_2$	19.0
11	$\text{OH} + \text{NO}$	18.2
12	$\text{O}_3 + \text{NO}$	16.4
13	$\text{RO} + \text{O}_2$	12.0
14	$\text{OLEF} + \text{O}_3$	11.1
15	$\text{HO}_2 + \text{HO}_2$	6.4
16	$\text{RCHO} + \text{OH}$	6.2
17	$\text{RO} + \text{NO}_2$	5.5
18	$\text{RCHO} + h\nu \rightarrow \text{Products}$	5.4
19	$\text{RO} + \text{NO}$	4.0
20	$\text{O} + \text{O}_2$	2.9
21	$\text{OLEF} + \text{O}$	2.4
22	$\text{NO}_3 + \text{NO}$	2.0
23	$\text{HOOH} + h\nu$	0.9
24	$\text{NO}_2 + \text{NO}_3$	0.8
25	$\text{NO}_2 + \text{O}$	0.7
26	$\text{NO}_2 + \text{O}_3$	0.6
27	$\text{RO}_2 + \text{NO}$	< 0.1
28	$\text{RO}_2 + \text{HO}_2$	< 0.1
29	$\text{NO}_2 + \text{O} + \text{M}$	< 0.1
30	$\text{RO}_2 + \text{RO}_2$	< 0.1
31	$\text{O} + \text{NO}$	< 0.1

Other rate measurements that should be carried out involve OH, HO<sub>2</sub>, and HNO<sub>2</sub>. The smog formation process is sustained to a significant degree by reactions involving the interconversion of OH and HO<sub>2</sub> radicals. The formation reaction of HNO<sub>2</sub> from NO, NO<sub>2</sub>, and H<sub>2</sub>O (Reaction 10) may contribute significantly to the accumulation rate and maximum concentration of nitrous acid in smog. Since OH is a photolysis product of HNO<sub>2</sub>, Reaction 10 may, in fact, participate indirectly in the initiation of ambient smog formation. The termination of OH chains through a reaction with NO<sub>2</sub> (k<sub>13</sub>) and the OH-olefin chain transfer reaction (k<sub>18</sub>) strongly influence the OH concentration and, hence, the rate at which the overall chemical transformations occur in olefin/NO<sub>x</sub> smog chamber experiments. In addition, the accumulation of O<sub>3</sub> as a result of disruption of the O<sub>3</sub>-NO-NO<sub>2</sub> equilibrium (Reactions 1 through 3) is attributable chiefly to the oxidation of NO by HO<sub>2</sub> (Reaction 15). We strongly recommend that these rate constants be reevaluated.

The "high sensitivity" list also includes two reactions for which no experimental determinations of the rate constants have yet been made. Should our estimated values be low, these rate constants may be more important than the sensitivity analysis indicates. Thus, we also recommend that initial rate determinations for the RCO<sub>3</sub> + NO (k<sub>24</sub>) and RCO<sub>3</sub> + NO<sub>2</sub> (k<sub>25</sub>) reactions be carried out.

## 2. Reactions That Can Possibly Be Eliminated from the General Mechanism

In addition to the "critical" parameters in the model whose values must be determined with certainty, the model contains some parameters that are almost insensitive. These are parameters for which large variations in magnitude result in small changes in the predictions. By identifying those reactions that contribute minimally to the total predicted response, the sensitivity analysis forms the basis for eliminating reactions from the mechanism, subject to further limited individual testing of each reaction over a range of initial conditions and bounds of uncertainty. The elimination of insignificant reactions results not only in a clearer perception of the fundamental process by which smog forms, but

also in a reduction in the amount of computer time necessary to carry out a simulation.

Reactions with  $S*U$  values of less than 1.0 are quite insensitive, their rate constants are known with certainty, or both. Thus, this study indicates that reactions exhibiting both low sensitivity and low  $S*U$  indices should be tested individually over a range of initial reactant concentrations and rate constant uncertainty bounds to evaluate the effect that their elimination would have on predictions. As noted earlier, we have shown that reactions ranking 28 through 31 can be eliminated from the general mechanism without a significant loss of accuracy.

#### D. CONCLUDING COMMENTS

The results of the sensitivity analysis depend on the initial concentrations of reactants chosen for the test. If the calculations were repeated with half the initial hydrocarbon and twice the initial  $NO_x$  used in the present study, we would expect the ordering of rate constants to be somewhat different than that shown in Tables 10 and 11. However, based on our experience in applying the general mechanism over a wide range of initial conditions and in carrying out a similar sensitivity calculation for another reactant system (n-butane-propylene- $NO_x$ ) [Roth et al. (1974)], our feeling is that the rankings in the two tables represent the approximate order of parameter sensitivity fairly well.

The sensitivity values calculated in this study can be used quantitatively to facilitate model evaluation. They can also be used to establish weighting factors for regression analyses or linear programming studies that optimize the agreement between predictions and experimental data by perturbing rate constants within their bounds of uncertainty. The ordering of the rate constants in Table 11 can also be used as a guide to kineticists in choosing reactions for future study. Kineticists might contribute most directly and meaningfully to the understanding of air pollution by investigating the rates of those reactions that have been shown to introduce significant uncertainty into the predictions of the kinetic mechanism.

## V ANALYSIS OF UCR DATA

Under EPA sponsorship, the Statewide Air Pollution Research Center (SAPRC) at the University of California, Riverside (UCR), is presently carrying out an extensive series of experiments in the UCR evacuable smog chamber. The intended use of these data is primarily for kinetic mechanism evaluation, although UCR is also engaged in an effort to detect and quantify the presence of "novel" (speculated but heretofore unmeasured) chemical species. Special care is being taken in the program to assess quantitatively the magnitude of chamber parameters.

Although the determination of chamber operating properties is an ongoing process, a particularly extensive characterization was undertaken in the first phase of the UCR project. A number of experiments were carried out to measure the photolysis rate of  $\text{NO}_2$ , the spatial distribution of light, the time required for an initial charge of reactants to distribute homogeneously within the chamber, the decomposition rate of ozone on the walls of the chamber, and the like. The details of these experiments are being transmitted to EPA by the SAPRC periodically. We deal with the results here on a provisional basis and only to the extent needed to substantiate our choices of chamber parameters for the simulation of UCR photochemistry runs.

Because of the extent of the chamber characterization effort undertaken, the results of the first photochemistry (propylene/ $\text{NO}_x$ ) experiments suitable for mechanism evaluation were not available for use until the last working month of this project. The short amount of time that was available for mechanism development before the end of this year's work, along with the scheduling of the majority of photochemistry experiments next (project calendar) year, have led us to defer detailed discussion of these first experiments until next year. In lieu of presenting a version of the

mechanism tentatively revised in accordance with the results of the propylene/ $\text{NO}_x$  experiments, we chose to simulate the runs using the mechanism presented in Tables 1 and 2. Because no changes other than those necessary to describe physical and chemical parameters of the UCR chamber have been introduced into the general kinetic mechanism, these simulations can be viewed as a test of the accuracy of the model in making predictions.

#### A. CHARACTERISTICS OF THE CHAMBER SYSTEM THAT AFFECT THE CHEMICAL KINETICS

As we stressed in Chapter I, it is extremely important to account for physical and chemical characteristics of smog chamber systems when using chamber data for mechanism evaluation. In this section, we summarize the bases for all chamber parameter values that we must specify in carrying out simulations of the experimental runs.

##### 1. Light Intensity

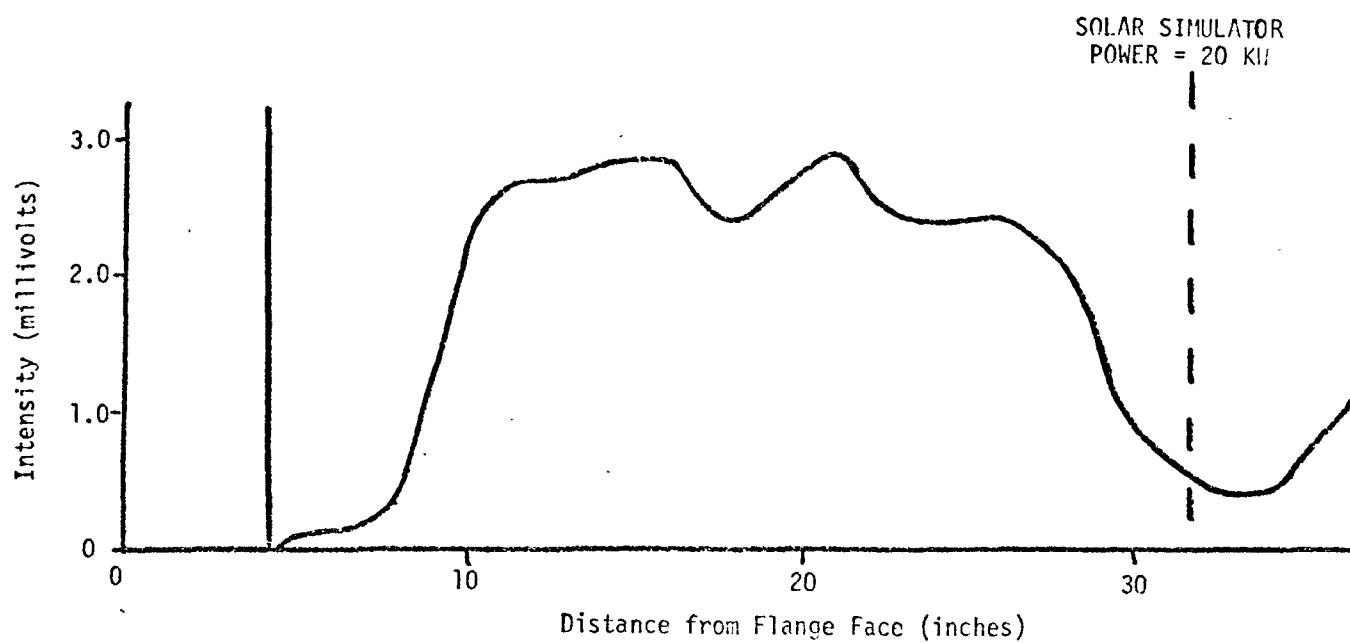
###### a. Spectral Light Distribution

The evacuable chamber is irradiated by a "solar simulator" (Beauchene et al., 1973) positioned at one end of the cylindrical reactor. The spectral emission pattern of the lamp and the transmission characteristics of the quartz windows and special filters enable the spectral light distribution within the chamber to simulate sunlight at sea level.

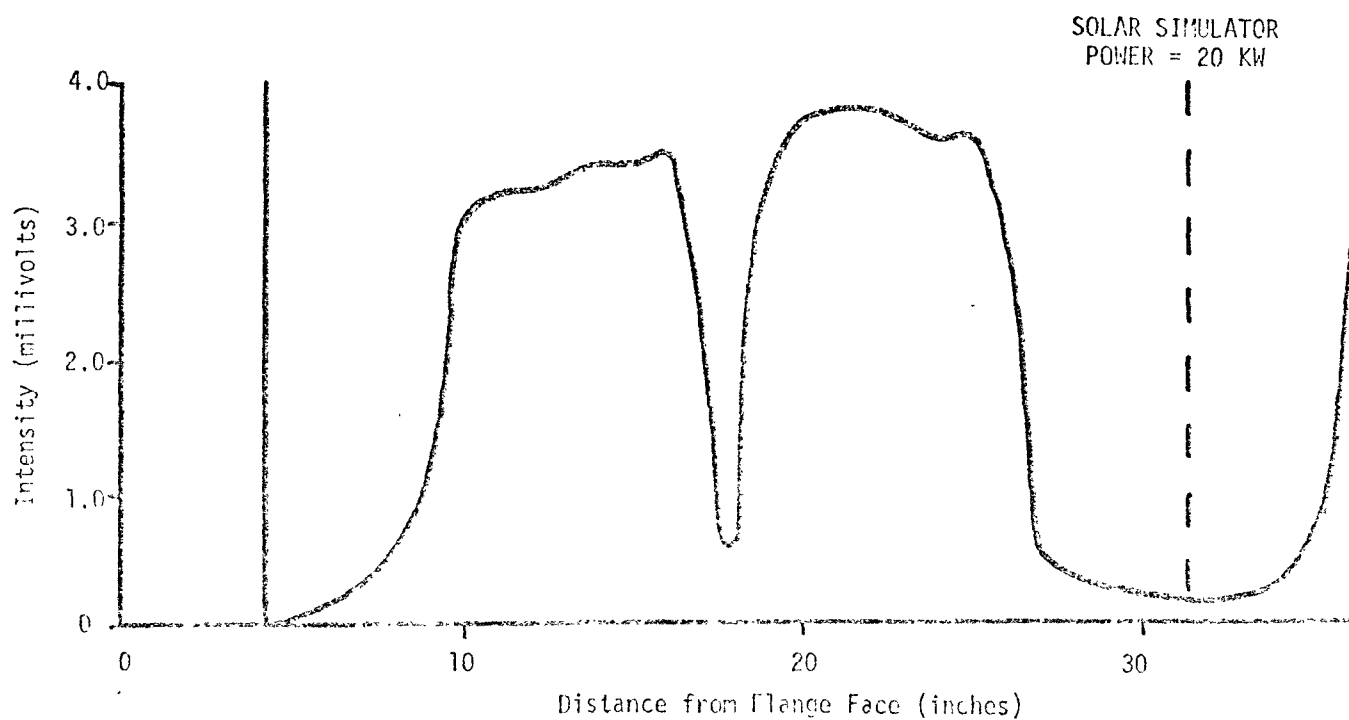
###### b. Spatial Light Distribution

The solar simulator was specially designed for the chamber to minimize spatial light inhomogeneities. However, an annular region of the chamber near the walls was deliberately designed not to be irradiated so as to minimize the heating of the walls and the rates of surface reactions. Also, a focusing mirror in the lamp and the lattice securing the quartz windows block the light and thereby reduce its intensity in certain portions of the chamber. Consequently, the spatial distribution of the light across various sections of the chamber is somewhat irregular (see Figure 22).





(a) Port Near Back of Chamber



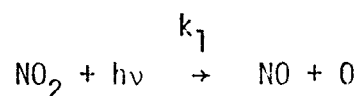
(b) Port Near Simulator

FIGURE 22. SPATIAL DISTRIBUTION OF LIGHT WITHIN THE EVACUABLE CHAMBER WITHOUT A REFLECTOR

Approximately 85 percent of the chamber volume is irradiated at full light intensity, and 15 percent of the chamber (including the wall boundary layer) is weakly illuminated.

Under these conditions, the following question arises: In carrying out a mathematical simulation of the chemistry occurring in this chamber, should spatial variations in the light intensity be treated explicitly, or can an "average" light intensity value be used without a significant loss of accuracy? The answer to this question depends on the rates of the photolytic reactions and the time required for the reactants in the weakly irradiated portions of the chamber to mix into the bulk gas.

For example, consider the change in the average concentration of  $\text{NO}_2$  with time in the chamber that is due only to the photolysis reaction



in two extreme cases: (1) instantaneous mixing between the boundary layer (weakly irradiated portion) and bulk gas and (2) no mixing between the two volumes. For the purposes of this calculation, we also assume that 85 percent of the volume is exposed to the full value of  $k_1$ , and 15 percent, to  $k_1 = 0$ . The concentration of  $\text{NO}_2$  as a function of time for Case 1 is given by

$$C(t) = C_0 e^{-0.85 k_1 t} \quad . \quad (5)$$

For Case 2, the situation in which no mixing between the irradiated and nonirradiated volumes occurs, the average concentration of  $\text{NO}_2$  in the chamber is given by

$$C(t) = 0.15 C_0 + 0.85 C_0 e^{-k_1 t} \quad . \quad (6)$$

At  $t = 0$ , these expressions predict that the  $\text{NO}_2$  concentration is identical for both cases, as one would expect. As time passes, however, the predicted  $\text{NO}_2$  concentration in the "well-mixed" case decreases much more rapidly than it does in the "no-transfer" case. The ratio of the predicted  $\text{NO}_2$  concentration in the latter case to that in the former case is

$$R = \frac{\text{Concentration no transfer}}{\text{Concentration well mixed}} = \frac{0.15 + 0.85 e^{-k_1 t}}{e^{-0.85 k_1 t}} \quad (7)$$

Assuming that  $k_1 = 0.2$  (a typical value for this chamber), the ratio increases rapidly with time, as shown by the tabulation below:

<u>T</u> (minutes)	<u>R</u>
0	1
1	1.003
5	1.08
10	1.45
25	11.12

If, for example, the gas in the boundary layer actually takes five minutes, on the average, to exchange with or mix into the bulk gas, and if we assume that the mixing is instantaneous, the actual  $\text{NO}_2$  concentration would be 8 percent higher than we would predict with an otherwise correct model.

In fact, an experiment carried out in the evacuable chamber indicates that, at a distance of one-half radius from the center of the chamber, the characteristic mixing time is one minute or less. The use of an average photolysis rate constant for  $\text{NO}_2$  determined experimentally in the manner

described by Holmes et al. (1973) (photolysis of  $\text{NO}_2$  in  $\text{N}_2$ ) would, therefore, be in error by only 0.3 percent according to Eq. (7).

We are presently using spatially averaged photolysis rate constants in our simulations of UCR chamber data. However, we recognize the need for the characteristic mixing times to be determined in the boundary layer and at the center of the chamber before such usage can be considered "well justified."

c. Photolysis Rate of  $\text{NO}_2$

To determine the photolysis rate of  $\text{NO}_2$  experimentally, UCR uses the method described by Holmes et al. (1973). For the photochemistry experiments simulated in Section V-B, the value of  $k_1$  was  $0.223 \text{ min}^{-1}$ . However, the intensity of the solar simulator has been found to diminish slowly with time. Consequently, UCR redetermines  $k_1$  often, and the value of  $k_1$  presented here should not be applied indiscriminately for the simulation of future experimental data.

d. Photolysis Rates of Other Photoabsorbers

Doyle and Winer (1974) have made preliminary estimates of the photodissociation rates of other photoabsorbing species present during organic/ $\text{NO}_x$  smog chamber experiments. The pertinent reactions and rate constants\* are as follows:

Reaction	Rate Constant ( $\text{min}^{-1}$ )
$\text{HNO}_2 + h\nu \rightarrow \text{OH} + \text{NO}$	0.0138
$\text{HCHO} + h\nu \rightarrow \text{H} + \text{CHO}$	0.0010
$\text{HCHO} + h\nu \rightarrow \text{H}_2 + \text{CO}$	0.0013
$\text{CH}_3\text{CHO} + h\nu \rightarrow \text{CH}_3 + \text{CHO}$	0.0011
$\text{CH}_3\text{CHO} + h\nu \rightarrow \text{CH}_4 + \text{CO}$	0.0003

\* The values were calculated for a light intensity at which  $k_1 = 0.223 \text{ min}^{-1}$ .

We used these provisional values in our simulations of evacuable chamber experiments.

## 2. Homogeneity of Reactants

Experiments have shown that approximately 20 minutes are required for a reactant charge introduced in one end of the chamber to distribute uniformly throughout the volume. Consequently, a period of 30 minutes or more is generally allowed between charging of the chamber and initiation of the photolysis. Homogeneity is checked before every photochemistry experiment by continuous monitoring of the NO concentration at a single location within the chamber.

## 3. Temperature

The temperature within the chamber is controlled through adjustments of a heating/cooling circulation system on the chamber walls. The temperatures of both the walls and the gas being withdrawn for analysis are determined once every 15 minutes. In general, the temperature during a photochemistry experiment is maintained within  $\pm 3^{\circ}\text{F}$  of the mean value (usually  $84^{\circ}\text{F}$ ). For the simulations presented in Section V-B, we assumed that the temperature remained constant throughout the experiment. In view of the small temperature variations and the substantial uncertainties as to the activation energies of the reactions in the general mechanism, we feel that this assumption was justified.

## 4. Water Concentration

The relative humidity within the chamber is determined every 15 minutes using a Brady Array. The water concentration can then be calculated directly from the temperature, relative humidity, and saturation water vapor pressure at the given temperature and total chamber pressure (1 atmosphere). Concentration-time profiles of  $\text{H}_2\text{O}$  for two of the evacuable chamber (EC) runs (EC-11 and EC-16) simulated are shown in Figures 23 and 24. Typically, the total variation of water concentration was about 10 percent of the

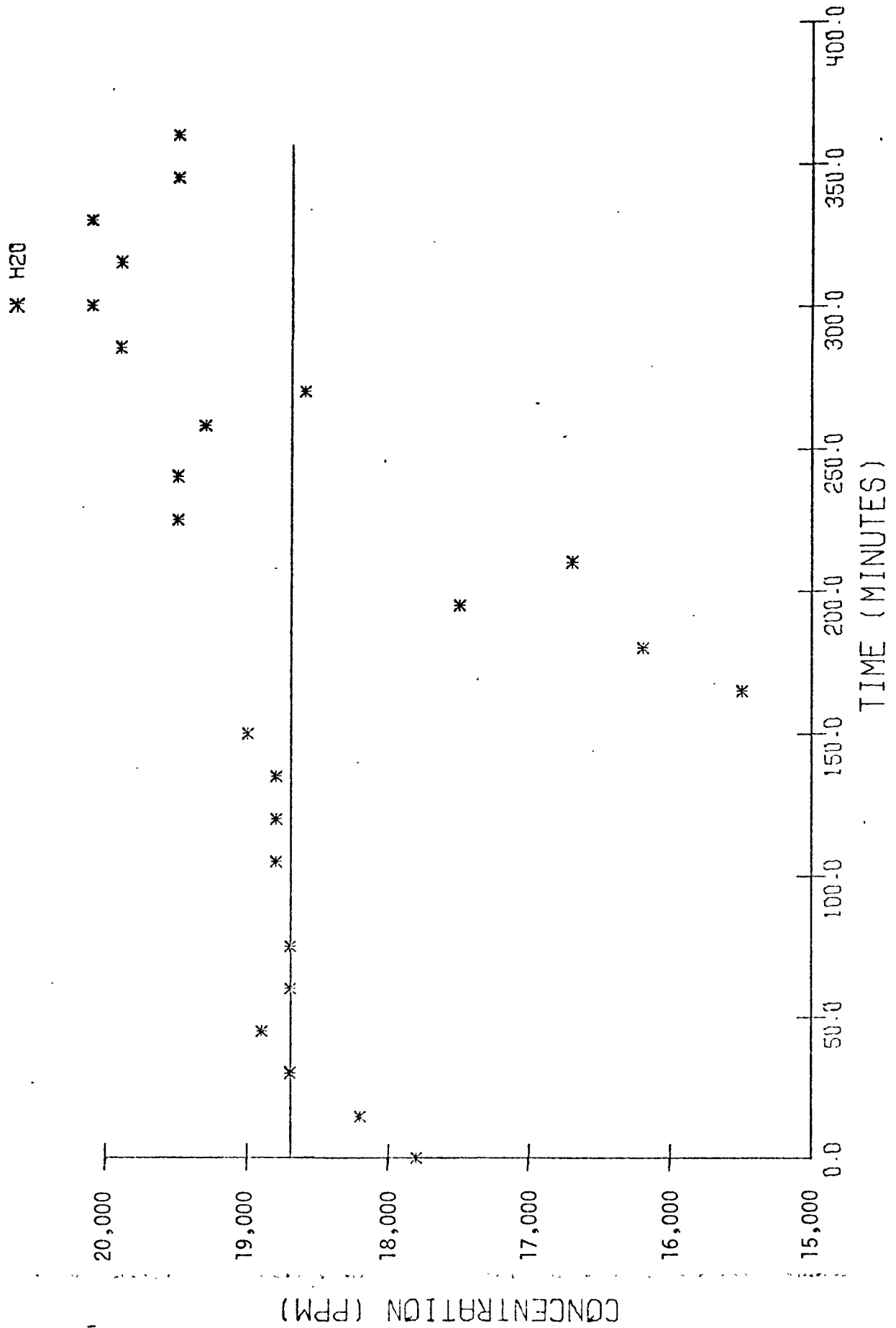


FIGURE 23. WATER CONCENTRATION AS A FUNCTION OF TIME FOR RUN EC-11,  
AND CONSTANT VALUE (SOLID LINE) USED FOR SIMULATING THIS  
EXPERIMENT

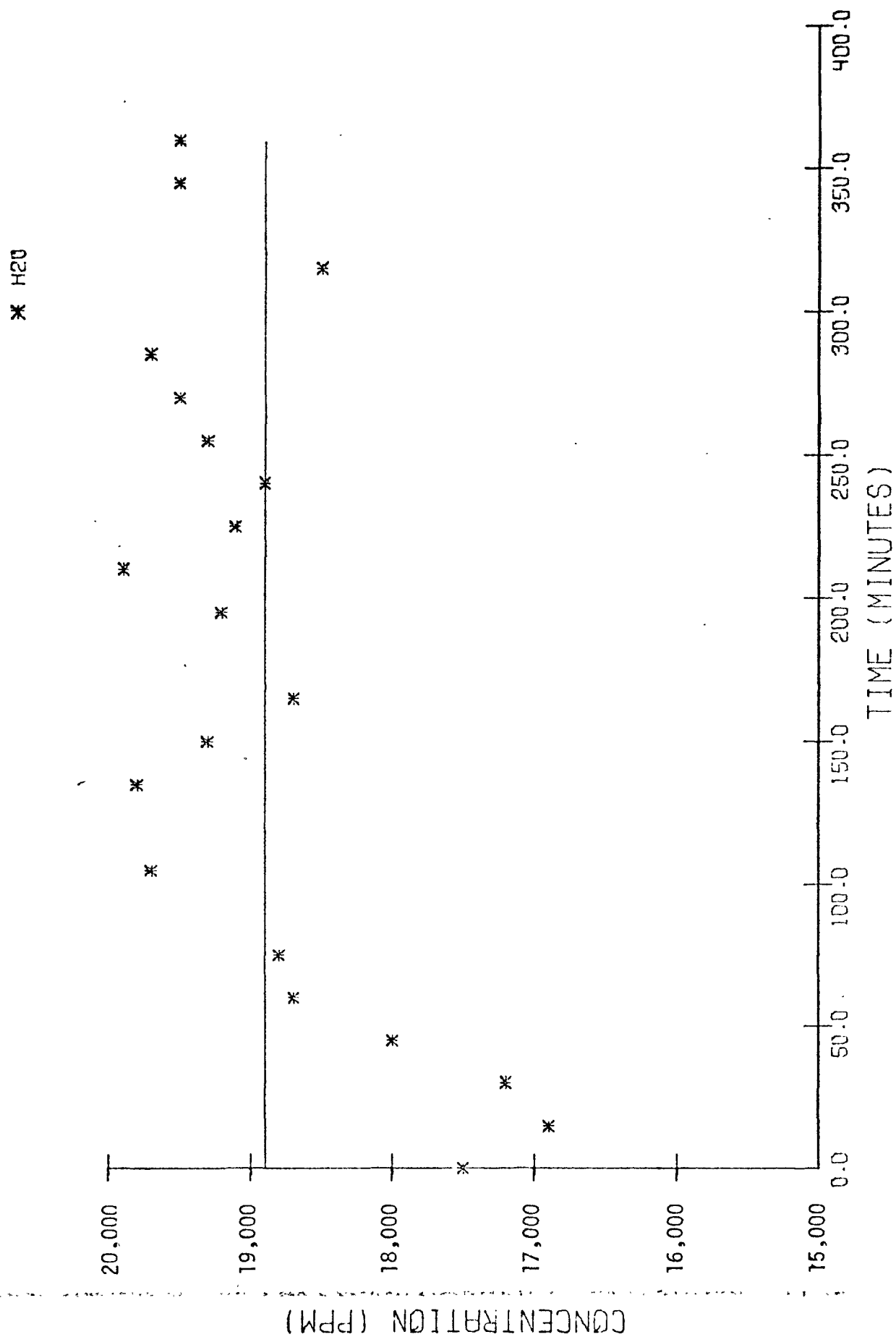


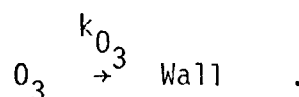
FIGURE 24. WATER CONCENTRATION AS A FUNCTION OF TIME FOR RUN EC-16, AND CONSTANT VALUE (SOLID LINE) USED FOR SIMULATING THIS EXPERIMENT

mean concentration. In Run EC-16, the variation was as large as 18 percent but was exhibited in a manner suggesting a short-time-measurement anomaly.

In simulating the photochemistry experiments, we assumed that the water concentration is constant and is equal to the average value observed during an experiment. We realize that under these assumptions the rates of reactions involving water may be understated or overstated at times. However, the rate constants of reactions occurring in smog are, for the most part, significantly more than 10 percent uncertain. Furthermore, to our knowledge, the role of water in the overall smog formation process is experimentally unquantified. We recommend that a series of organic/ $\text{NO}_x$ /air experiments be carried out at various water concentrations to determine what effect, if any, water has on the rate of formation and the observed distribution of products. If such experiments were to show that large variations in the water concentration affect the process only minimally, the use of a constant average value in our simulation would be substantiated.

## 5. Wall Effects

Scientists have shown that the surface-to-volume ratio and surface materials of a smog chamber influence the overall chemical process observed (cf. Seinfeld et al., 1973). The detailed nature and magnitude of the effects of surfaces on the kinetics, however, are poorly understood. The only wall reaction that has been considered extensively is the heterogeneous decomposition of  $\text{O}_3$  [see references in Seinfeld et al. (1973)] which can be represented as



### a. Heterogeneous Loss of Ozone

Scientists at UCR carried out several ozone decay experiments during the first phase of the project to determine  $k_{\text{O}_3}$ . The chamber preparation



for a " $k_{O_3}$  experiment" was the same as that made for a photochemistry experiment.<sup>3</sup> First, the reactor was pumped to a few microns of mercury pressure. Air containing about 1 ppm of  $O_3$  was then rapidly introduced into the chamber, and a total pressure of 1 atmosphere was achieved through the addition of pure air. Subsequently, the time required for one-half of the ozone to be consumed in the dark was determined. The half-life was found to be about 8.35 hours.

If we assume that the loss of  $O_3$  during a decay experiment is attributable entirely to the reaction on the walls, the rate of  $O_3$  decay is given by

$$\frac{dO_3}{dt} = -k_{O_3}[O_3]$$

The half-life of  $O_3$  is related to the  $O_3$  decay constant as

$$k_{O_3} = \frac{0.693}{t_{1/2}}$$

from which we calculate that  $k_{O_3} = 0.0014 \text{ min}^{-1}$ . This value indicates, for example, that the rate of  $O_3$  loss to the walls will exceed the rate of loss due to reaction with propylene, should the concentration of  $C_3H_6$  in the reactor be less than 0.08 ppm. (Two of the eight experiments in the propylene experimental block considered in Section V-B have an initial  $C_3H_6$  concentration of 0.1 ppm.) Thus, the rate of  $O_3$  decay in the UCR chamber is significant, and the  $O_3$  wall loss reaction must be included in our simulations.

Ozone decay experiments were also performed under irradiated, rather than dark, conditions, and the  $O_3$  half-life was found to be about 4.25 hours. We believe that this decrease in the  $O_3$  half-life from that observed in a dark chamber is due to a series of chemical reactions involving  $O_3$ ,  $O(^1D)$ ,  $H_2O$ , free radicals, and light, rather than any intrinsic change in the activity of the walls when the solar simulator is in operation.

(Recall that the solar simulator has been focused so that it does not shine directly on the cylindrical surfaces.)

We carried out a mathematical simulation of the August 15, 1973 light decay experiment, which was similar in all ways, except for the presence of light, to the dark decay experiments used to calculate  $k_{O_3}$  above. We assumed that the 12 reactions in Table 12--in addition to the wall reaction--participated in the total  $O_3$  decay process.

The  $O_3$  photolysis rates were based on the results of Demerjian et al. (1974), who calculated the photolysis rates of  $NO_2$ ,  $O_3$ , and many other species for sunlight with  $z = 45^\circ$ . Under those conditions, they calculated that the photolysis constant for  $NO_2$  was  $0.48 \text{ min}^{-1}$ . Since the rate of that reaction in the UCR chamber is  $0.223 \text{ min}^{-1}$ , we scaled Demerjian's  $O_3$  photolysis constants by  $0.223/0.48$ . We further assumed that the rate of  $H_2O_2$  photolysis was  $1/250$  of the rate of  $NO_2$  photolysis. This rate constant is quite uncertain; we found that this reaction can be eliminated from the mechanism without seriously affecting the reactions, and so the choice of this rate constant is not critical. The rate constants of the other reactions are based on the recommended values of Garvin and Hampson (1974) and Demerjian et al. (1974).

Integrating this mechanism and using the initial conditions for the experiment ( $[O_3]_0 = 1.15 \text{ ppm}$ ,  $[H_2O] = 2.0 \times 10^4 \text{ ppm}$ ,  $[O_2] = 2.0 \times 10^5 \text{ ppm}$ , and  $[I] = 1.0 \times 10^6 \text{ ppm}$ ) resulted in a predicted  $O_3$  half-life of 4.48 hours. The observed half-life for this particular experiment was  $4.35 \pm 0.09$  hours.

The results of this exercise are consistent with the following tentative conclusions. First, the "true"  $O_3$  wall decay constant appears to be that measured in the dark, rather than the illuminated, decay experiments. Second, the  $O_3$  photolysis reactions, which initiate reactions such as  $O(^1D) + H_2O$ , are an important sink for  $O_3$  and should be considered in future smog chamber simulations. In the simulations discussed subsequently, we use the value of  $k_{O_3}$  determined in the dark. The sequence of reactions initiated by the photolysis of  $O_3$  will be included in the next formulation of the kinetic mechanism.

Table 12  
REACTIONS PARTICIPATING IN THE TOTAL OZONE DECAY PROCESS

Number	Reaction	Rate Constant*
1	$O_3 \rightarrow \text{Wall}$	$1.38 \times 10^{-3} \text{ min}^{-1}$
2	$O_3 + h\nu \rightarrow O(^1D) + O_2$	$1.58 \times 10^{-3} \text{ min}^{-1}$
3	$O_3 + h\nu \rightarrow O(^3P) + O_2$	$9.76 \times 10^{-3} \text{ min}^{-1}$
4	$O(^1D) + M \rightarrow O(^3P) + M$	$8.70 \times 10^4$
5	$O(^3P) + O_2 + M \rightarrow O_3 + M$	$2.00 \times 10^{-5} \text{ ppm}^{-2} \text{ min}^{-1}$
6	$O(^1D) + O_3 \rightarrow 2O_2$	$9.80 \times 10^4$
7	$O(^1D) + H_2O \rightarrow 2OH$	$5.25 \times 10^5$
8	$OH + O_3 \rightarrow HO_2 + O_2$	$8.60 \times 10^1$
9	$HO_2 + O_3 \rightarrow OH + 2O_2$	2.40
10	$HO_2 + HO_2 \rightarrow H_2O_2 + O_2$	$8.40 \times 10^3$
11	$H_2O_2 + h\nu \rightarrow 2OH$	$8.90 \times 10^{-4} \text{ min}^{-1}$
12	$OH + OH + H_2O \rightarrow H_2O_2 + H_2O$	$3.25 \times 10^{-1} \text{ ppm}^{-2} \text{ min}^{-1}$
13	$OH + OH + M \rightarrow H_2O_2 + M$	$6.50 \times 10^{-2} \text{ ppm}^{-2} \text{ min}^{-1}$

\* In units of  $\text{ppm}^{-1} \text{ min}^{-1}$  unless otherwise indicated.

b. Wall Off-Gassing

After several consecutive photochemistry experiments had been conducted in the evacuable chamber, a study was made of the rate of wall off-gassing. The reactor was evacuated, refilled with nitrogen, and irradiated for 5.5 hours. The maximum concentrations of the species monitored were as follows:

<u>Species</u>	<u>Maximum Concentration (ppm)</u>
HCHO	None detected (less than 0.02)
CH <sub>3</sub> CHO	0.002
acetone	0.012
methylethylketone	0.0014
NO	0.005
NO <sub>2</sub>	0.004
O <sub>3</sub>	0.028

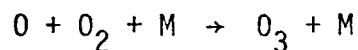
The concentrations of the two aldehydes are of little concern, since the formaldehyde and acetaldehyde concentrations observed in virtually every experiment in the propylene photochemistry block exceeded the measured background values by a factor of 10 or more because of off-gassing. Although the acetone and MEK concentrations are a sizable fraction of the values observed during the photochemistry experiments, neither of these species is particularly reactive, especially at these concentrations.

The background NO<sub>2</sub> level due to off-gassing is much lower than that observed in most propylene photochemistry experiments and probably need not be considered further.

The measured NO concentration is more disturbing. In most of the propylene-NO<sub>x</sub> experiments discussed in the following section, the NO (after the NO<sub>2</sub> peak) stabilized at about 0.005 to 0.009 ppm--well within the range of off-gassing levels observed in the irradiated chamber. Since the exact

rate of NO off-gassing depends on the chamber operating history (e.g., was the previous experiment conducted at high initial NO levels?), it is extremely difficult to account for this effect properly. Thus, we do not now include a source term in the kinetic simulations for NO due to wall emissions.

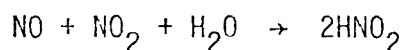
A very small amount of  $O_3$  was measured during the off-gassing experiment. Because the investigation was conducted in a pure  $N_2$ , rather than an air, atmosphere, ozone formation due to the reaction



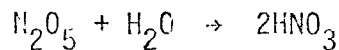
may have been suppressed. Consequently, the  $O_3$  produced as a result of reactions involving off-gassed organics and  $NO_x$  may be understated. At present, we make no correction for this wall-related effect because its true magnitude is still unclear.

#### c. Other Effects

Reactions such as



and



are thought to proceed more rapidly on surfaces than in the gas phase. And PAN, like  $O_3$ , may decompose on the walls. The PAN reaction, however, is the only additional wall effect to be studied at present.

## 6. Analytical Methods and Dilution Due to Sampling

### a. Instrumentation

The accuracy, precision, and range of applicability of the analytical techniques and instrumentation used in measuring the chamber conditions and the concentrations of reactants and products are summarized in Table 13. All of the chemical measurement techniques have been discussed extensively in the literature, and synopses of the methods are presented in Seinfeld et al. (1973). Instruments and techniques employed for the physical measurements will be discussed in a forthcoming UCR report; we note here only that instruments are recalibrated frequently to ensure accurate, precise measurements.

### b. Sampling and Dilution

Four chemical analyzers operate continuously throughout each experiment: Dasibi 1003 for ozone, Mast for oxidant, Teco for NO and NO<sub>x</sub>, and Beckman 6000 for CO. An additional continuous instrument, the Bendix, is used occasionally to determine NO and NO<sub>x</sub>. Samples for two other analyses--organics using a gas chromatograph (GC), and formaldehyde (HCHO) using the chromotopic acid method--are taken on a discrete (usually periodic) basis. Together, these instruments abstract about 15 percent of the original chamber volume during a six-hour experiment.

The timing of sample withdrawals for the GC and HCHO analyzers is as follows. Five samples for GC measurements are taken at the beginning of a run. Thereafter, one sample is withdrawn every 15 minutes for propylene, one every 30 minutes for PAN, and three additional every hour for all organic species other than HCHO; all GC samples are 200 cc. The duration of HCHO sampling symmetrically spans the recorded time.\* Thus, if, for example, the log shows a 30 liter HCHO sample at 1230, sampling was begun at 1215 and was terminated at 1245.

---

\* Except at  $t = 0$ , when the sample is taken in the 30 minutes prior to the irradiation.

Table 13

## PHYSICAL AND CHEMICAL PARAMETERS MEASURED

Parameter	Range	Method	Precision	Accuracy
Total HC	0-10 ppm	Gas chromatograph	±0.5% full scale or 0.05 ppm, whichever is greater	Limited by calibration standard; typically ±1%
Individual HCs	0.5-1 ppb 1-2 ppb >2 ppb	Gas chromatograph Gas chromatograph Gas chromatograph	±15% ±10% ±5%	Limited by calibration standard; typically ±5%
Ozone	0-20 ppm	Dasibi O <sub>3</sub> analyzer	±1% full scale	±3%
Total oxidant	0-1 ppm	Master analyzer	±0.05 ppm	±0.05 ppm
NO	0-5 ppm	Chemiluminescent analyzer	±2% full scale By difference	±5%
NO <sub>2</sub>	0-5 ppm		±2% full scale	By difference ±5%
NO <sub>x</sub>	0-5 ppm			±5%
PAN	0-100 ppm	Gas chromatograph	±5%	±5%
Formaldehyde	>20 ppb	Chromotropic acid	±5%	±10%
Acetaldehyde	>100 ppb 1-6 ppb >6 ppb	Long path infrared Gas chromatograph Gas chromatograph	±20% ±10% ±5%	Limited by calibration standard Limited by calibration standard Typically ±5%
CO	0-10 ppm	Gas chromatograph	±0.5% full scale or 0.1 ppm, whichever is greater	Limited by calibration standard; typically ±2%

Table 13 (Concluded)

Parameter	Range	Method	Precision	Accuracy
Hydrogen peroxide	100 ppb	Long path infrared	±10%	±10%
Nitrous acid	15 ppb	Long path infrared	±10%	±10%
Nitric acid	15 ppb	Long path infrared	±10%	±10%
Chamber operating pressure	700-800 torr	Validyne gauge	±5%	±10%
Temperature at chamber walls	-40 to +100°C	Thermocouple	±0.5°C	±0.5°C
Light intensity	0-1 solar constant	Radiometer	To be determined	To be determined
Relative humidity	0-100%	Brady Array	±2% relative humidity	±2%



Because the GC and HCHO samples are taken at varying time intervals, rather than continuously, the dilution rate fluctuates somewhat. The GC sampling rate is small (less than 2 liters/hour) in comparison with the continuous (typically 120 liters/hour) and HCHO (30 liters/hour) sampling rates; the assumption of continuous sampling for GC introduces less than 1 percent average error in the instantaneous dilution rate. The HCHO sampling cycle is normally 30 minutes on followed by 30 minutes off. Although the instantaneous sampling rate for HCHO swings  $\pm 25$  percent about the average HCHO sampling rate, we assumed that the sample for the HCHO measurement is withdrawn at a continuous average rate. The total sample loss due to HCHO analysis is small enough that no appreciable error results from this assumption. The dilution constants for each UCR photochemistry experiment considered in this report are listed with the initial conditions in the following section.

As samples are withdrawn from the chamber, an equal volume of replacement air is introduced to maintain the chamber pressure at 1 atmosphere. The replacement gas is room air that passes through a canister containing activated charcoal and Purafil for removal of hydrocarbons and  $\text{NO}_x$ , respectively. Experiments have shown that the system is capable of reducing background NO in the air to 0.005 ppm, acetaldehyde to 0.001 ppm, acetone to 0.005 ppm, methylethylketone to less than 0.001 ppm, and CO to about 2.0 ppm. The background levels on any given day depend somewhat on the pollutant concentrations in the outside air. Our concern with these background levels is essentially that stated in our discussion of off-gassing. Fortunately, however, most of the air from the clean air system is introduced before an irradiation is undertaken; so the concentration of any reactants present in the background air are accounted for when the initial conditions of the chamber ( $t = 0$ ) are determined.

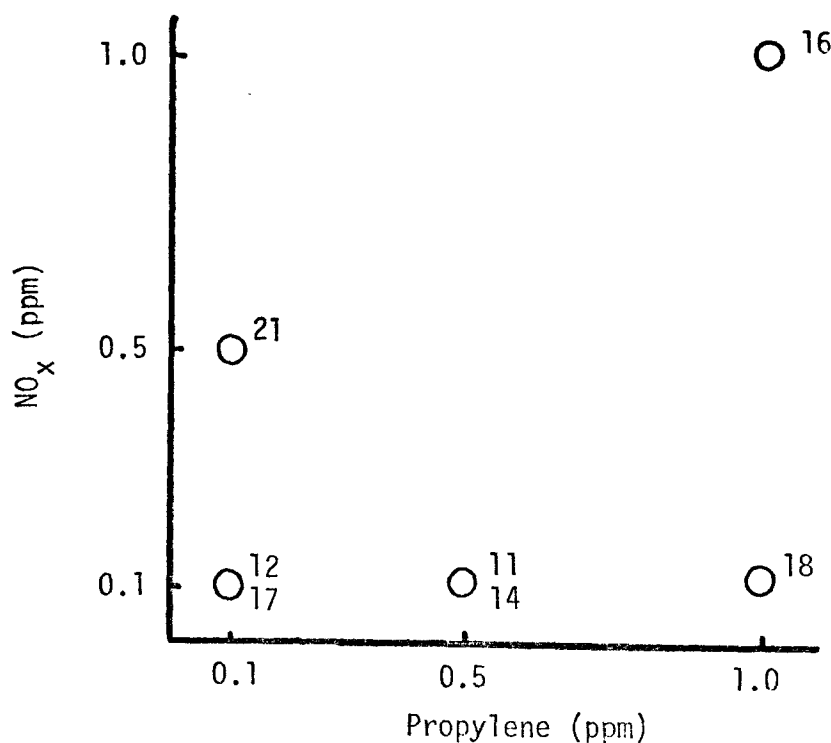
#### B. SIMULATION OF UCR PROPYLENE/ $\text{NO}_x$ EXPERIMENTS USING THE GENERAL MECHANISM

The data generated in the UCR evacuable chamber provide a reference against which the predictions of the general mechanism can be measured. Because the mechanism cannot predict the concentration-time histories of many chemical species accurately over a wide range of initial reactant

ratios, we seek clues to specific weak points in the mechanism by thoroughly examining disagreements between data and predictions. In fact, our efforts to reduce the discrepancies between predictions and data often result in the introduction of new reactions into the mechanism and in the variation of certain rate constants within their uncertainty bounds.

As a prelude to the utilization of the UCR data for the further development of the general mechanism, we carried out simulations of the first seven UCR propylene/ $\text{NO}_x$  photochemistry experiments. These simulations essentially use the formulation of the general mechanism presented in Tables 1 and 2, which was tested extensively in relation to NAPCA propylene/, n-butane/, and propylene/n-butane/ $\text{NO}_x$  data. Only those reactions and rate constants explicitly affected by characteristics of the UCR chamber were altered. Specifically, the rates of photolysis of  $\text{NO}_2$ ,  $\text{HNO}_2$ , and aldehydes were changed in line with the discussion in Section V-A; and the reaction for  $\text{O}_3$  decay on the walls, using the constant determined in the darkened UCR chamber, was included in the mechanism. No attempt was made to improve the agreement between predictions and the UCR data (that, of course, is the goal of next year's project). Consequently, these simulations can be viewed as a test of the mechanism in Tables 1 and 2.

The initial conditions for the seven experiments, which are the first of about fifty scheduled to be conducted in the evacuable chamber as part of the EPA-UCR chamber program, are listed in Table 14. Since two pairs of experiments are essentially replicate runs (which differ enough that they cannot be compared directly), the seven experiments fill only five positions in the following propylene/ $\text{NO}_x$  factorial block:



Predictions of the general kinetic mechanism and the experimental results for the seven EC runs are presented graphically in Figures 25 through 38.

In some cases, severe discrepancies occur between the predictions and the experimental observations. The time of the predicted  $\text{NO}_2$  peak is, for the most part, late compared with the data, and the predicted  $\text{O}_3$  level and rate of propylene oxidation are less than those observed for every run. The predicted aldehyde maxima are in good agreement with the data for some of the experiments but are low for the others. Finally, the quality of the PAN predictions varies, but, in general, the predictions are low for runs with  $[\text{propylene}]_0 \approx 0.1$  ppm and high for all of the other runs.

Many possible explanations can account for these discrepancies. First, we suspect that the kinetic mechanism in Tables 1 and 2 may be "chamber dependent." By this we mean that values of uncertain rate constants may have unknowingly been chosen to compensate for effects attributable to the NAPCA chamber system not explicitly included in the kinetic mechanism. As a result,

while we thought we were modeling just the gas phase chemistry in the NAPCA chamber, we may, in fact, have been tuning the reaction set in relation to gas phase reactions and chamber effects. Second, the set of reactions in Table 1 may be incomplete. In discussing the  $O_3$  wall decay constant, we presented evidence to suggest that a reaction sequence involving the photolysis of  $O_3$  and the oxidation of water by  $O(^1D)$  may be important in the UCR chamber. Other reactions may also be omitted from or misrepresented in the general mechanism, as noted below:

- > The reactions of the OH-olefin adduct are poorly understood and may be oversimplified in Table 1.
- > Formic acid is observed as a product in the UCR chamber but is not predicted by the mechanism. Does it result from an  $O_3$ -olefin reaction, from formaldehyde oxidation, or from other sources?
- > PAN may react with  $H_2O$  or other species found in a smog chamber. No such reactions have been included in the general mechanism.

Finally, many of the rate constants may be in error. Garvin and Hampson (1974) have recently evaluated the rate constant values of many of the reactions in the general mechanism. Most of the values in Table 2 are close or identical to their recommended values. However, the rate constants in Table 2 of the two radical chain termination reactions,  $OH + NO_2$  and  $OH + NO$ , are high (compared with the values of Garvin and Hampson) by a factor of greater than 2. Other rate constant values not yet evaluated by NBS may also be in serious error.

In the next phase of this project, we will pursue these and other possibilities. Many kinetics laboratories that were being used primarily for the study of stratospheric reactions until recently are now being used increasingly for the study of smog-related reactions. Consequently, we expect that our knowledge of the elementary kinetics will continue to improve substantially in the foreseeable future. We believe that the UCR evacuable chamber is one of the best characterized in the country and that it is well suited for the experimental study of complicated organic/ $NO_x$ /air reactant systems.

Table 14  
INITIAL CONDITIONS FOR EXPERIMENTS IN THE PROPYLENE/NO<sub>x</sub> BLOCK

EC Run No.	Figure No.	Initial Concentration (ppm)					Dilution Rate (min <sup>-1</sup> × 10 <sup>-4</sup> )
		NO <sub>2</sub>	NO	O <sub>3</sub>	OLEF	ALD	H <sub>2</sub> O (× 10 <sup>-4</sup> )
11	25-26	0.017	0.096	0.004	0.447	0.002	1.87
12	27-28	0.01	0.088	0	0.082	0.001	2.1
14	29-30	0.01	0.087	0	0.504	0.01	2.34
16	31-32	0.13	0.935	0	1.036	0.022	2.19
17	33-34	0.012	0.088	0	0.103	0.002	2.21
18	35-36	0.012	0.088	0	0.972	0.003	2.16
21	37-38	0.055	0.465	0	0.104	0.011	2.22
							4.05
							2.6
							3.8
							4.1
							2.9
							2.6
							3.8

X NO  
 \* NO2  
 X PAN

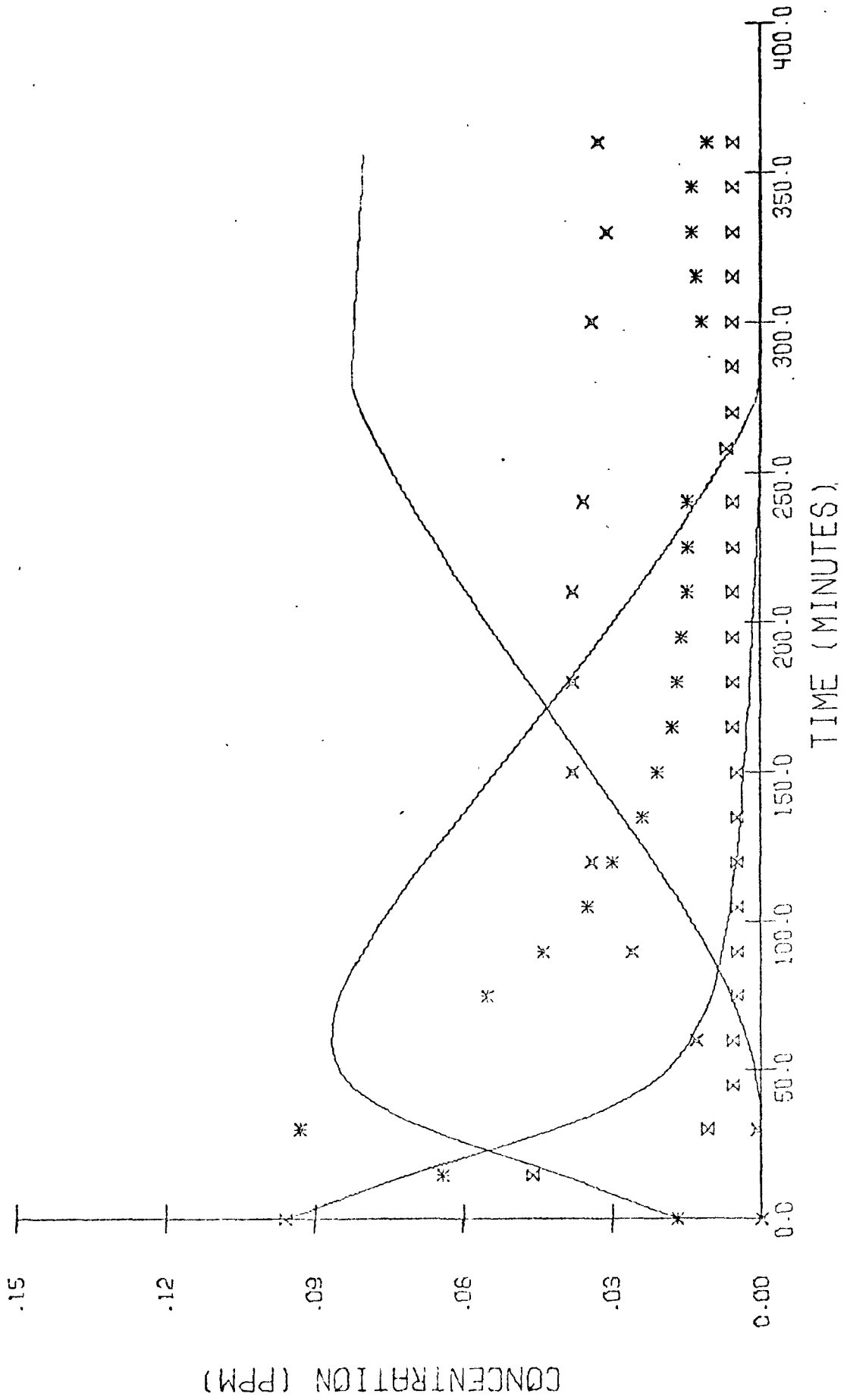


FIGURE 25. SIMULATION OF RUN EC-11 USING THE MECHANISM IN TABLE 1--  
PREDICTIONS FOR NO, NO<sub>2</sub>, AND PAN

\* OLEFIN  
 x ALDEHYDE  
 x O<sub>3</sub>

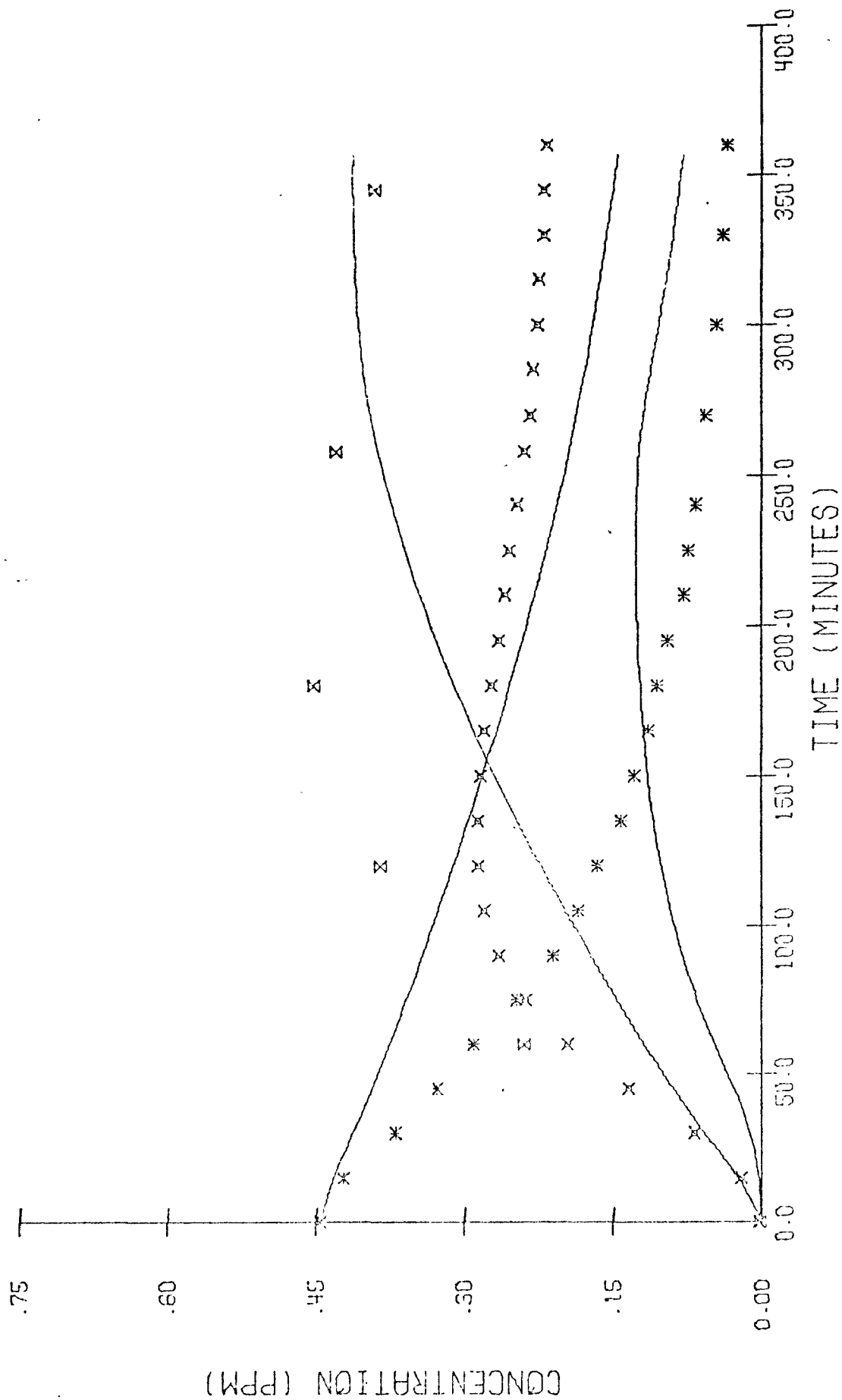


FIGURE 26. SIMULATION OF RUN EC-11 USING THE MECHANISM IN TABLE 1--  
PREDICTIONS FOR OLEFIN, ALDEHYDE, AND O<sub>3</sub>

X NO  
 \* NO2  
 X PAN

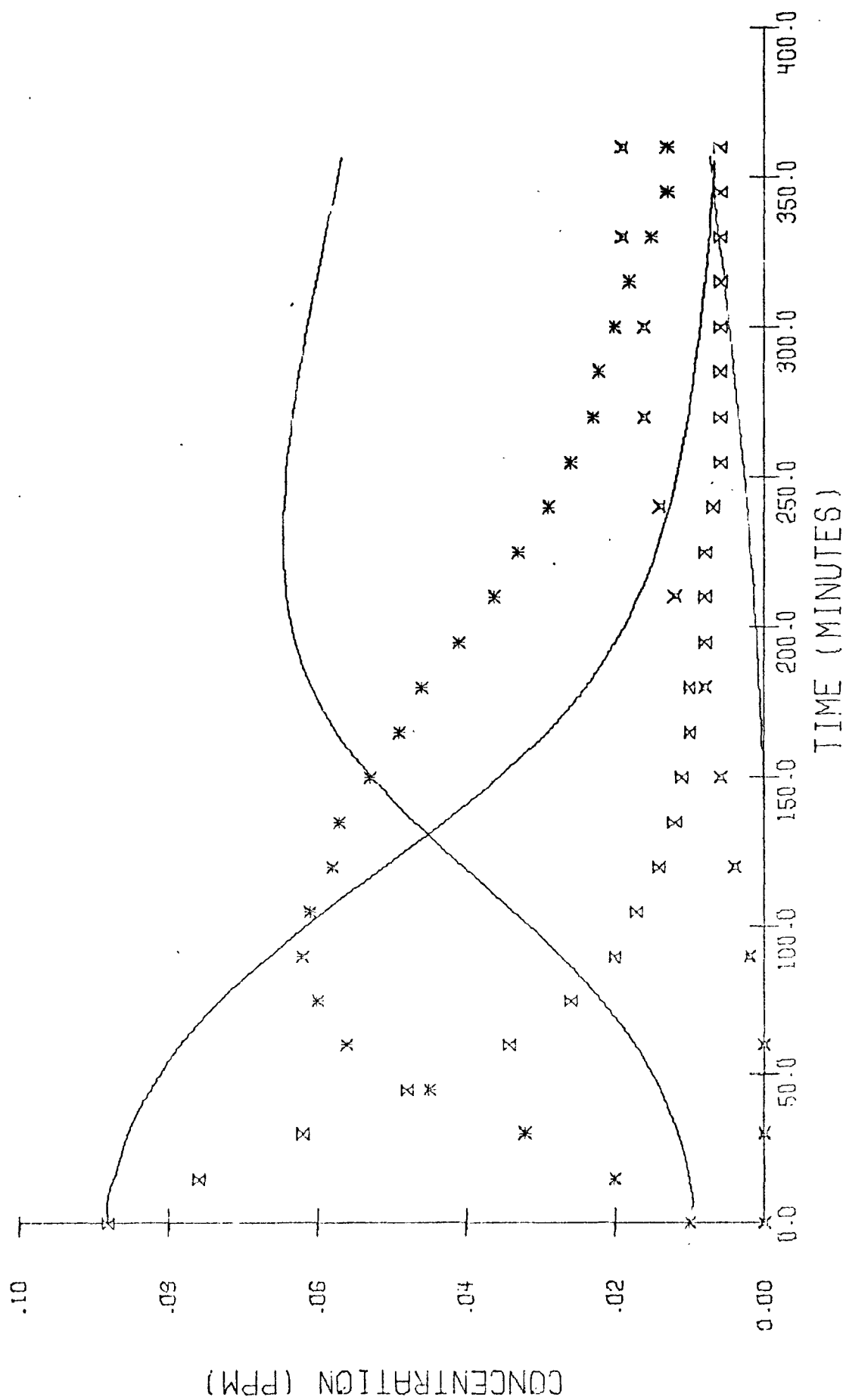


FIGURE 27. SIMULATION OF RUN EC-12 USING THE MECHANISM IN TABLE 1---  
PREDICTIONS FOR NO, NO<sub>2</sub>, AND PAN



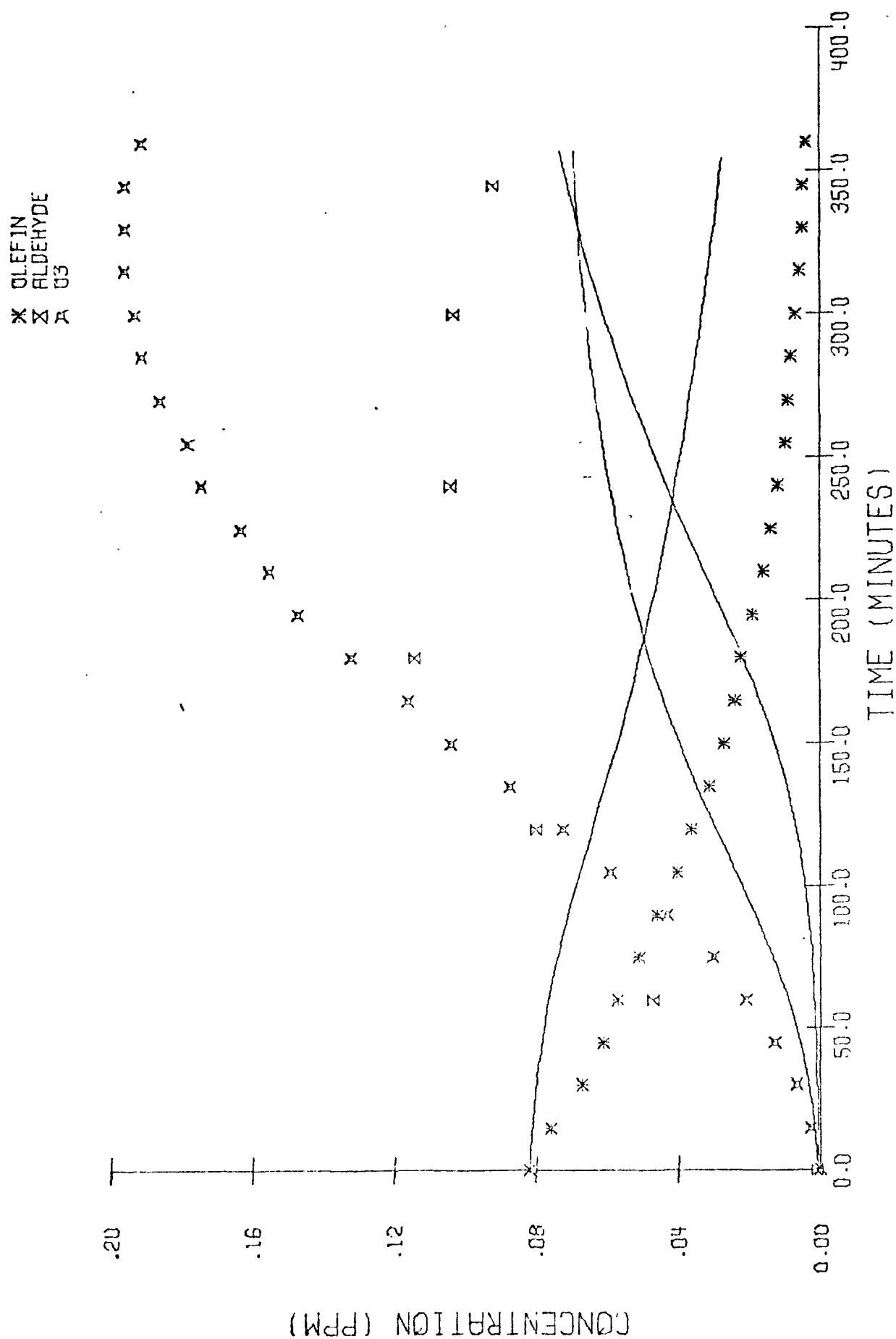


FIGURE 28. SIMULATION OF RUN EC-12 USING THE MECHANISM IN TABLE 1--  
PREDICTIONS FOR OLEFIN, ALDEHYDE, AND O<sub>3</sub>

X NO  
 \* NO  
 X PAN

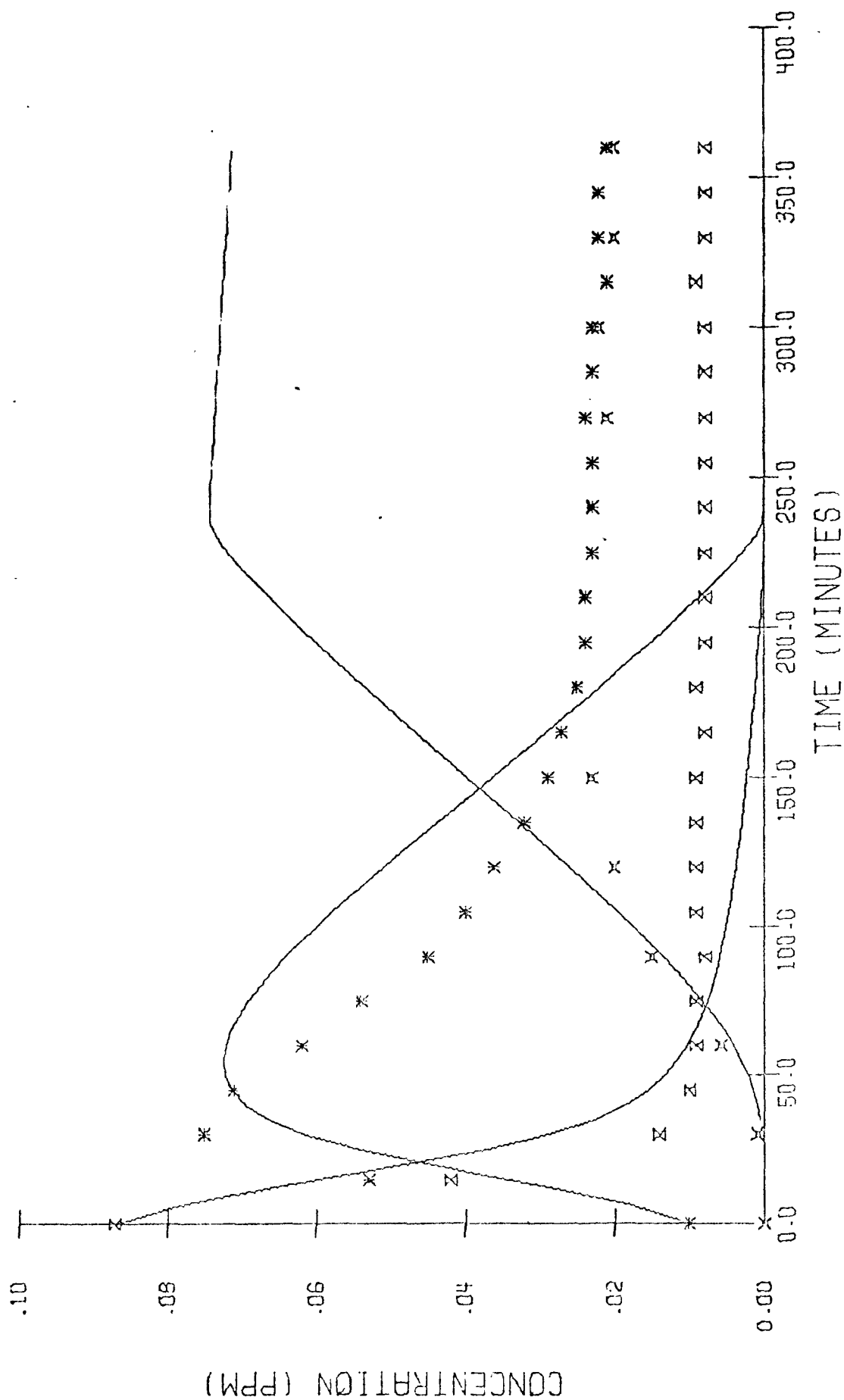


FIGURE 29. SIMULATION OF RUN EC-14 USING THE MECHANISM IN TABLE 1--  
 PREDICTIONS FOR NO, NO<sub>2</sub>, AND PAN

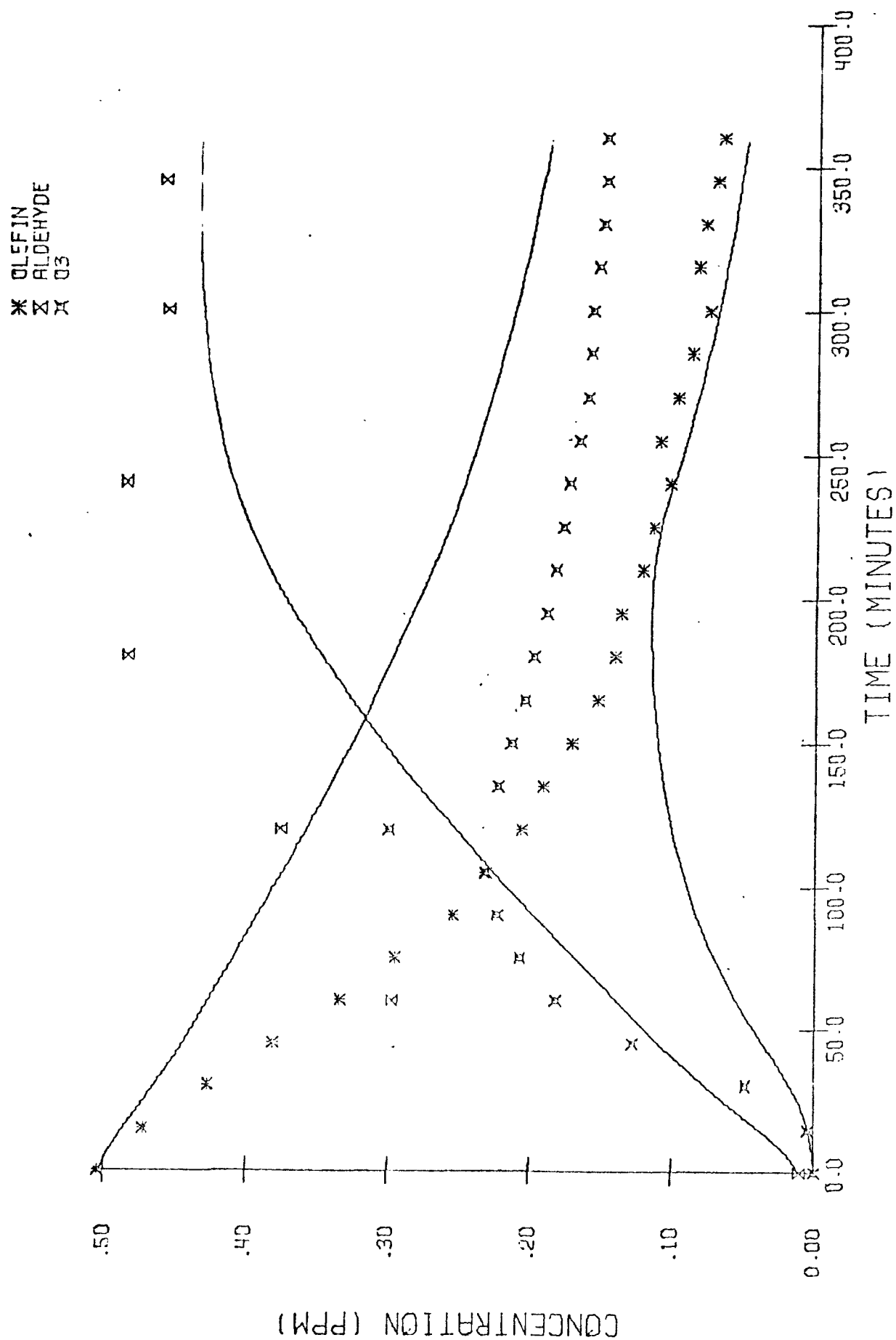


FIGURE 30. SIMULATION OF RUN EC-14 USING THE MECHANISM IN TABLE 1--  
PREDICTIONS FOR OLEFIN, ALDEHYDE, AND O<sub>3</sub>

X NO  
 \* NO2  
 X PAN

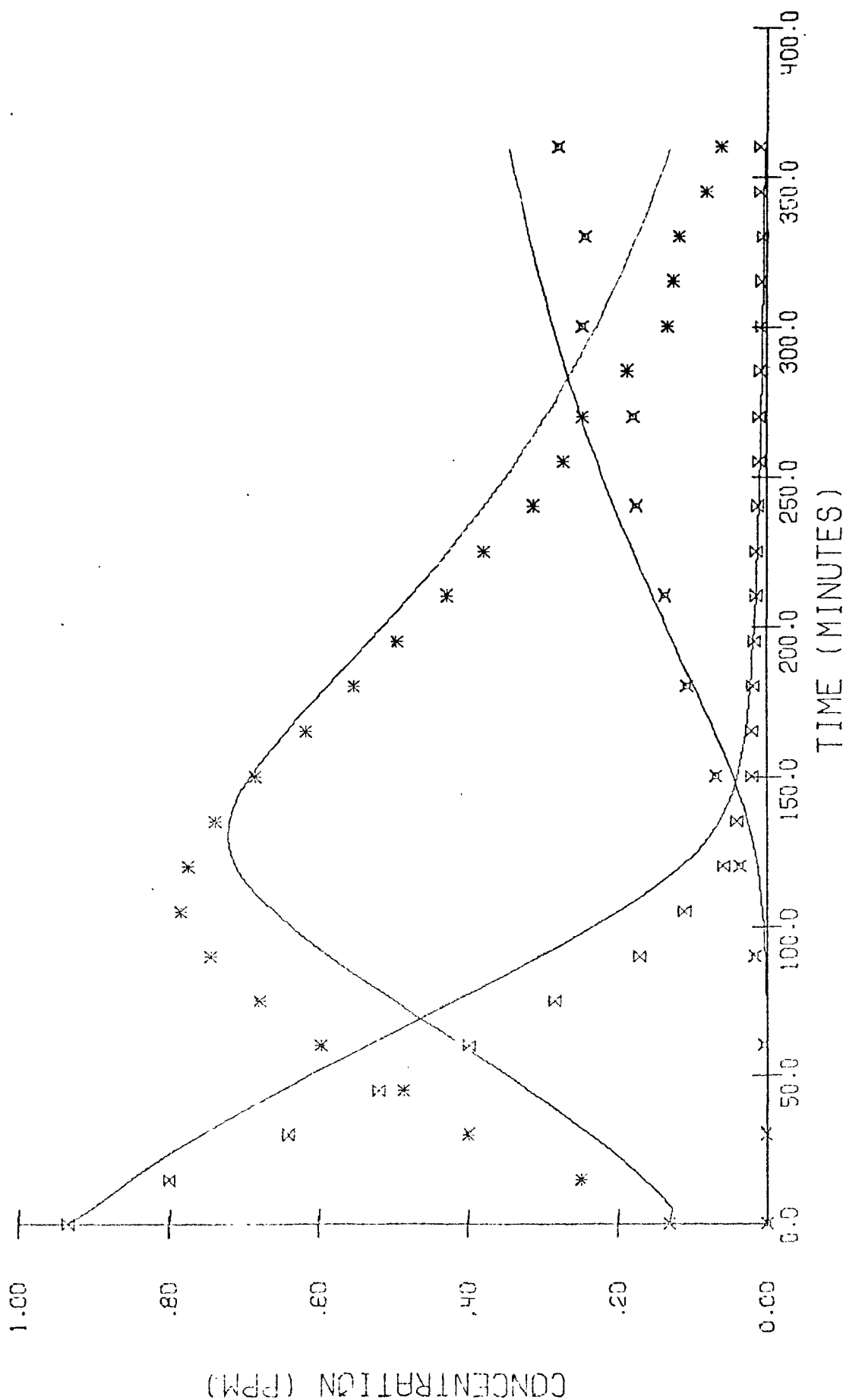


FIGURE 31. SIMULATION OF RUN EC-16 USING THE MECHANISM IN TABLE 1---  
PREDICTIONS FOR NO, NO<sub>2</sub>, AND PAN

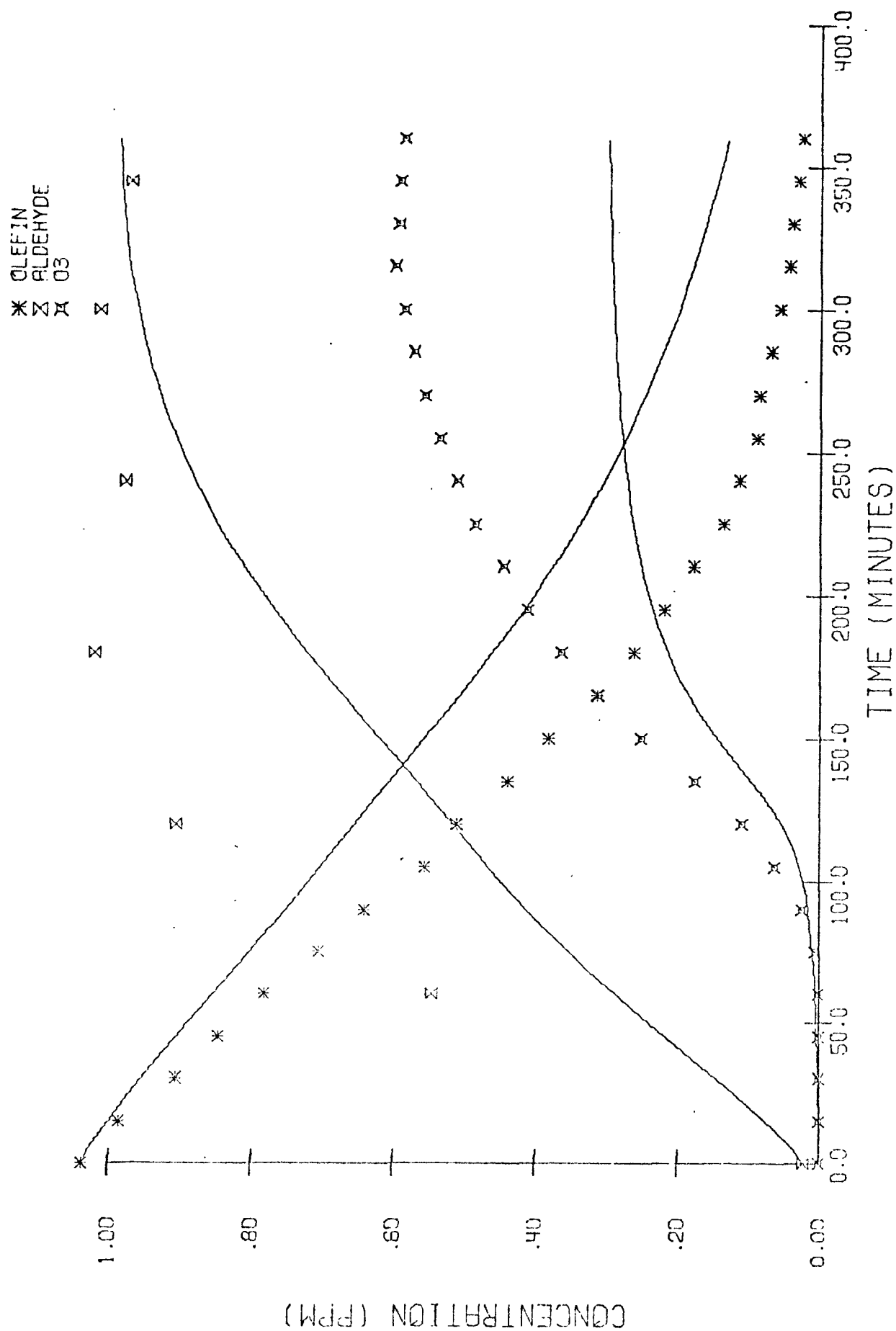


FIGURE 32. SIMULATION OF RUN EC-16 USING THE MECHANISM IN TABLE 1--  
PREDICTIONS FOR OLEFIN, ALDEHYDE, AND O<sub>3</sub>

X NO  
 \* NO<sub>2</sub>  
 Δ PAN

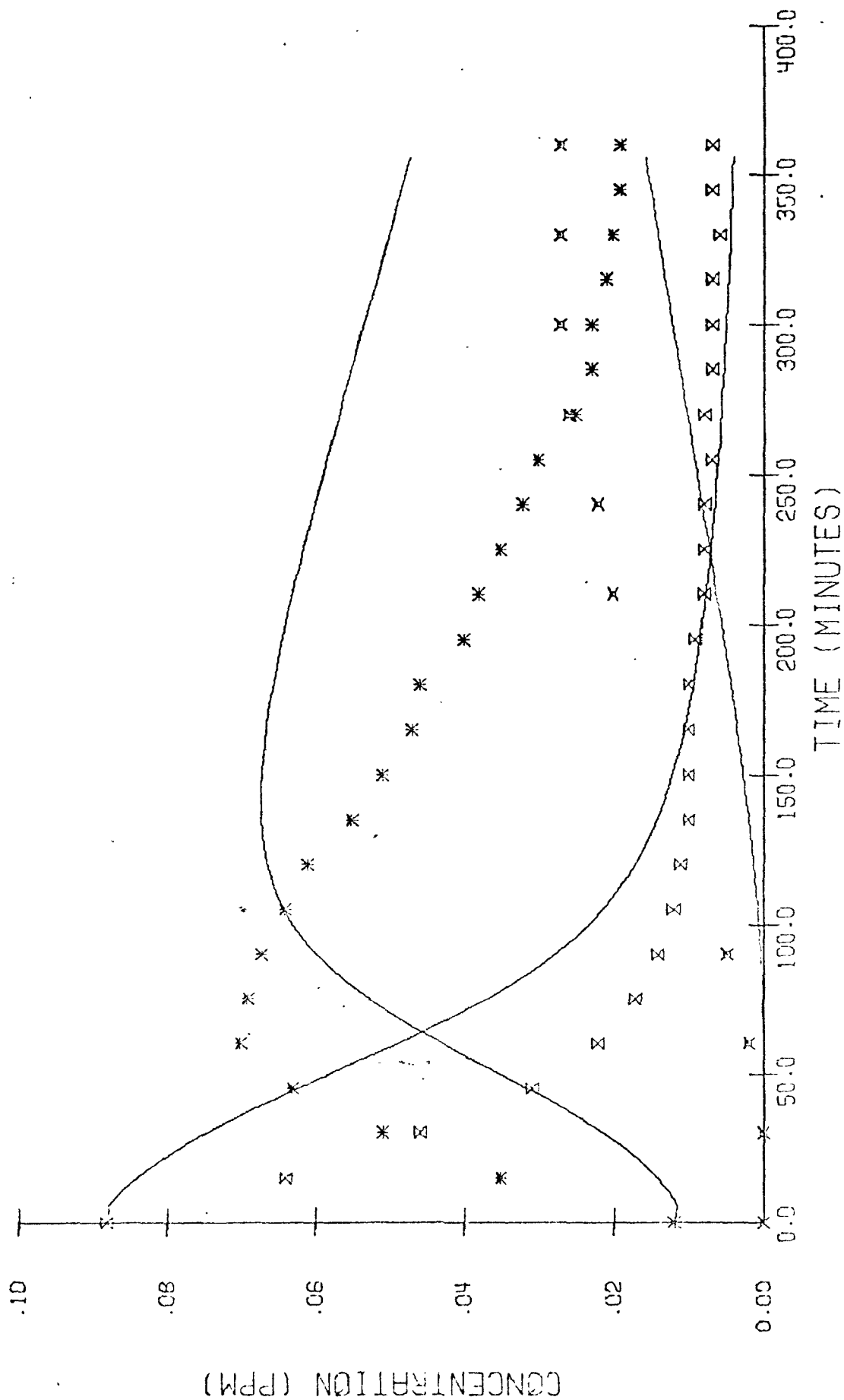


FIGURE 33. SIMULATION OF RUN EC-17 USING THE MECHANISM IN TABLE 1--  
PREDICTIONS FOR NO, NO<sub>2</sub>, AND PAN

\* OLEFIN  
 x ALDEHYDE  
 x O<sub>3</sub>

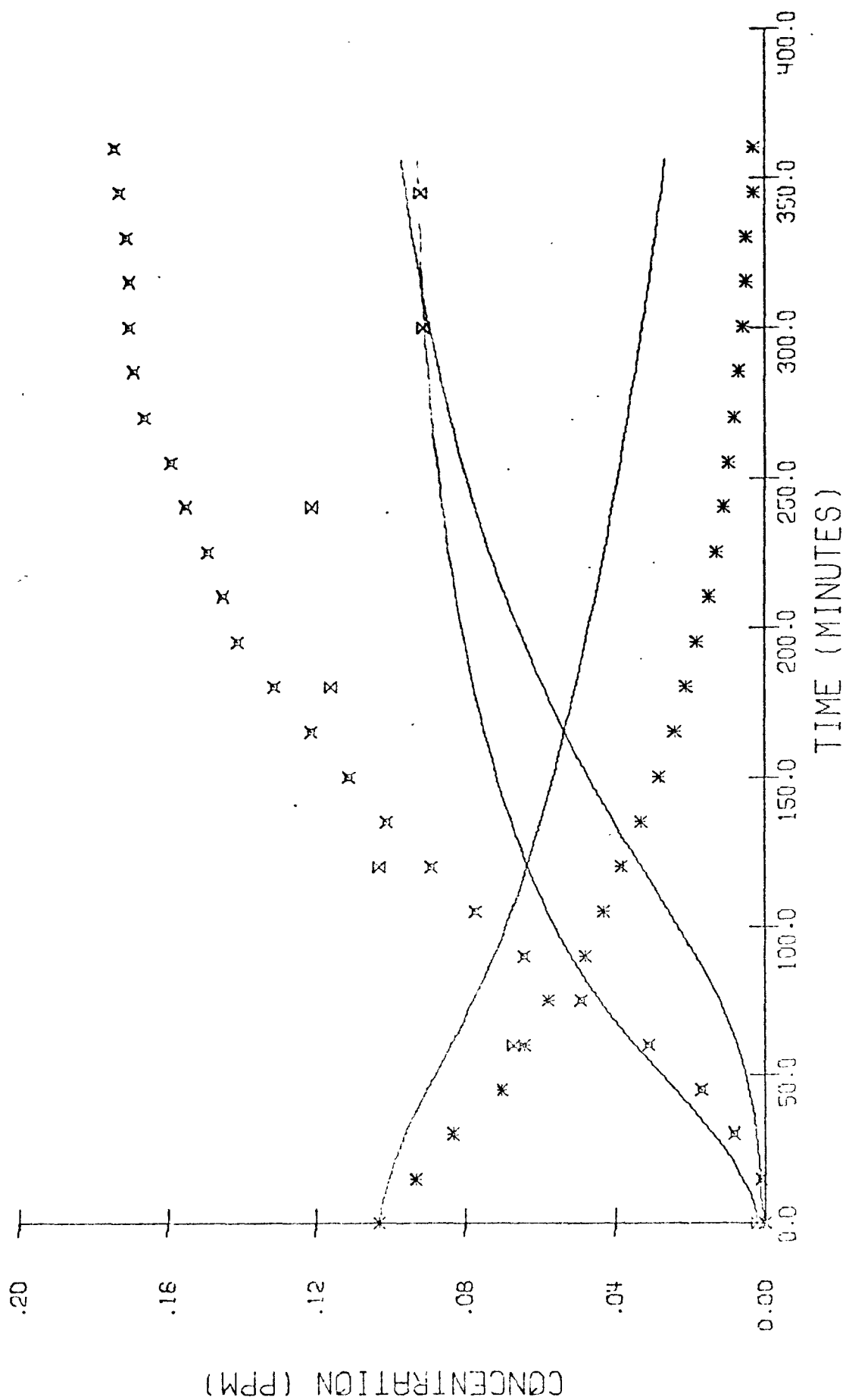


FIGURE 34. SIMULATION OF RUN EC-17 USING THE MECHANISM IN TABLE 1--  
 PREDICTIONS FOR OLEFIN, ALDEHYDE, AND O<sub>3</sub>

X NO  
 \* NO<sub>2</sub>  
 H PHN

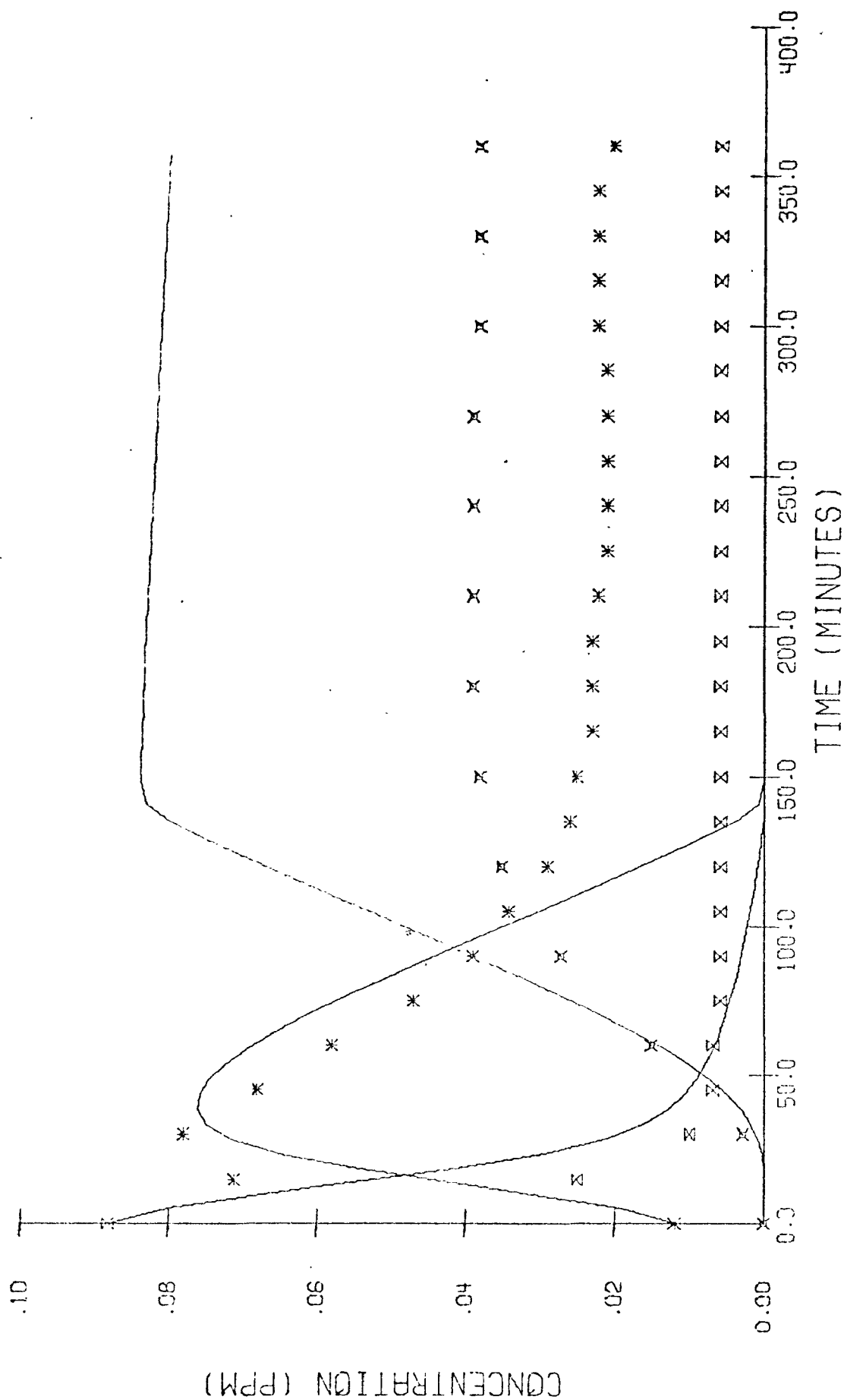


FIGURE 35. SIMULATION OF RUN EC-18 USING THE MECHANISM IN TABLE 1--  
PREDICTIONS FOR NO, NO<sub>2</sub>, AND PHN



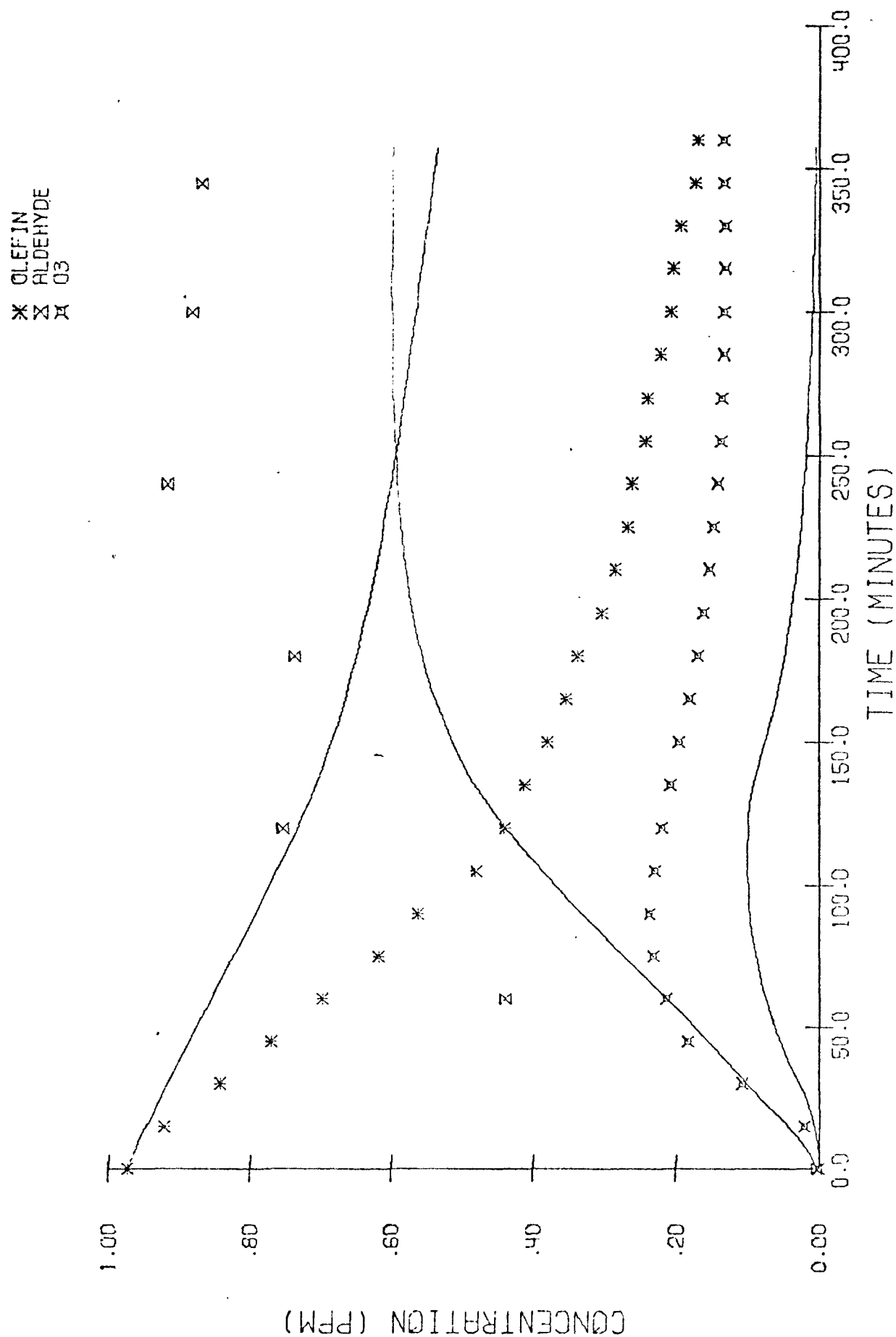


FIGURE 36. SIMULATION OF RUN EC-18 USING THE MECHANISM IN TABLE 1--  
PREDICTIONS FOR OLEFIN, ALDEHYDE, AND O<sub>3</sub>

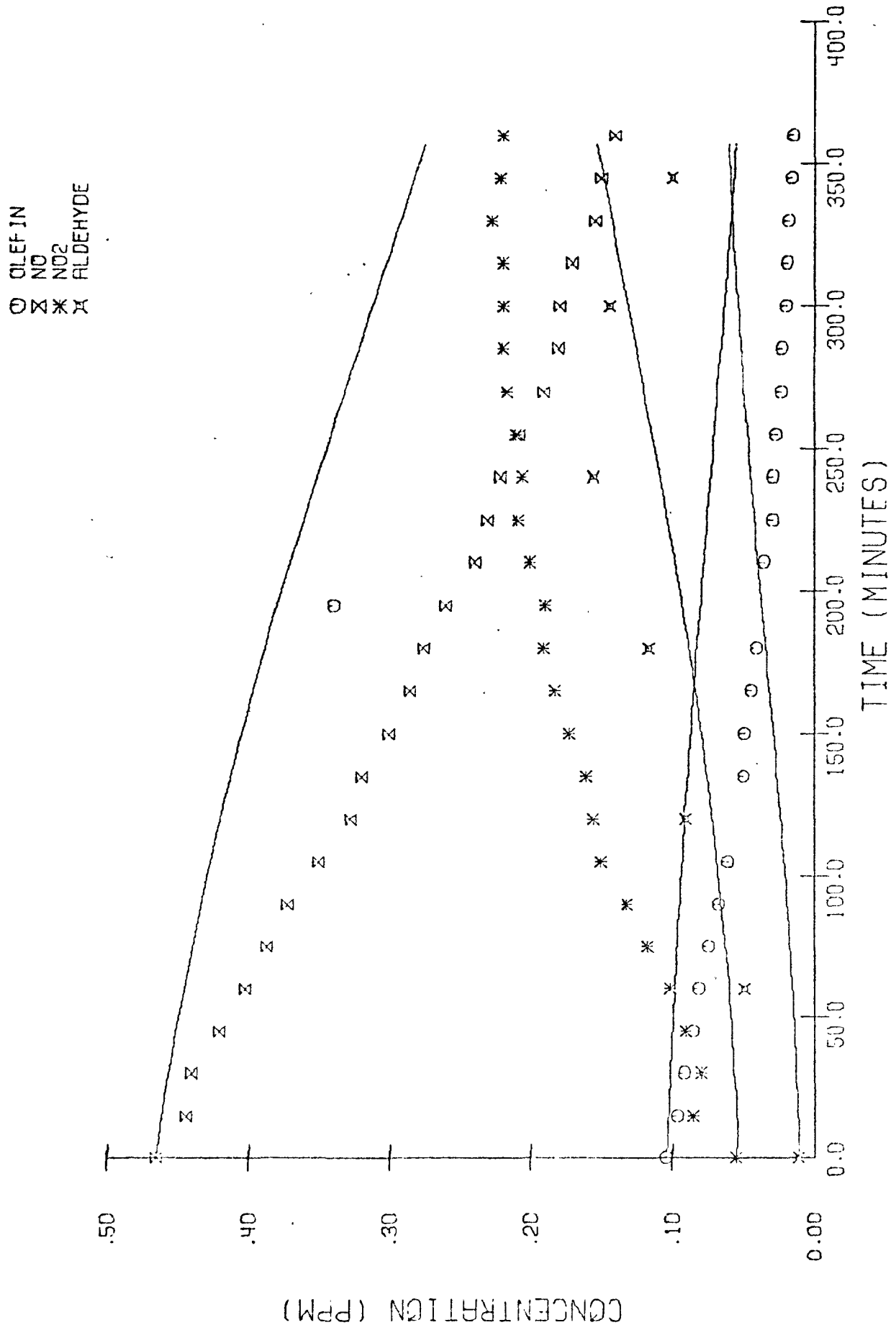


FIGURE 37. SIMULATION OF RUN EC-21 USING THE MECHANISM IN TABLE 1--  
PREDICTIONS FOR OLEFIN, NO, NO<sub>2</sub>, AND ALDEHYDE

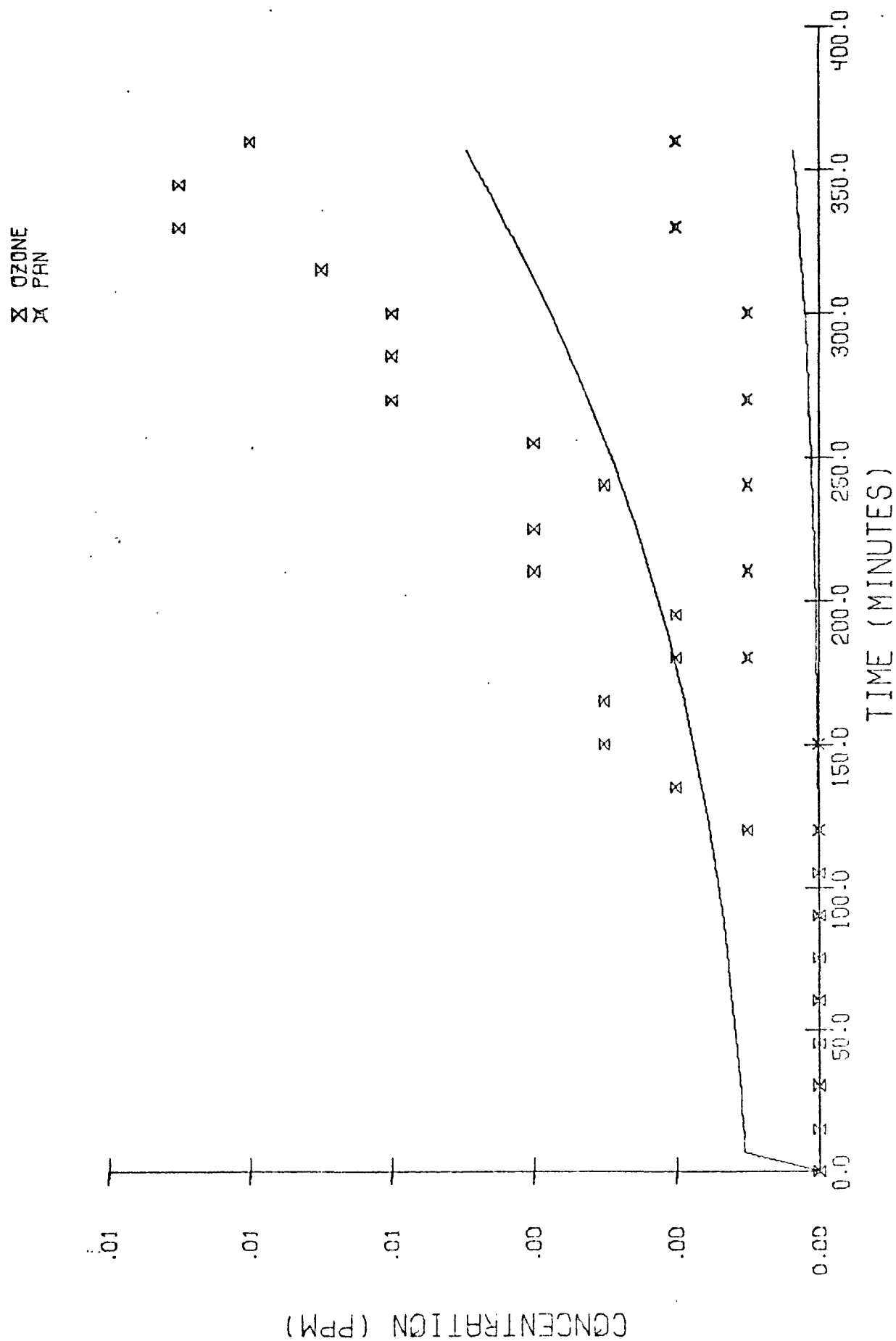


FIGURE 38. SIMULATION OF RUN EC-21 USING THE MECHANISM IN TABLE 1--  
 PREDICTIONS FOR  $O_3$  AND PAN

PART 2  
METHODOLOGY

## VI TECHNIQUES FOR EVALUATION THE KINETIC MECHANISM

Without methods for testing, analyzing, and proving the chemists' conjectures, proposing kinetic mechanisms is an empty exercise in theoretical chemistry. In this portion of the report, we present techniques that we have developed to assist in the all-important task of evaluating a proposed mechanism in light of the available experimental data.

Chapter VII discusses the types of analytical tools that are necessary in this evaluation and describes a computer program that embodies these tools. In addition, Appendix A (bound separately) is a complete user's manual and programmer's guide to the computer program that was developed under this contract.

Two of the tools useful in the analysis of chemical mechanisms, the steady-state assumption and the "lumping" of similar species, are dealt with in detail in Chapters VIII and IX, respectively. Both of these topics have engendered controversy in the past, and, since both are present in our analysis programs, we felt that an in-depth treatment of their justification as a means of simplifying the calculation of chemical kinetics was appropriate. In both cases, actual numerical examples are offered in defense of the validity of the techniques.

## VII AN AUTOMATIC COMPUTER PROGRAM FOR EVALUATION OF KINETIC MECHANISMS

Once a set of reactions for the formation of photochemical smog has been proposed, it is necessary to demonstrate that the mechanism is correct; i.e., it is able to account for, within experimental error, the actual concentration of each species present in the reaction mixture at any point during the time span of the reaction. This evaluation process involves, in its simplest form, the formulation and solution of the set of coupled differential equations that describe the variation in the formation and consumption of each species in the reaction mixture as a function of time. This set of equations can be expressed as

$$\frac{dy_i}{dt} = \sum_{j=1}^J R_{f,i,j} - \sum_{k=1}^K R_{c,i,k} \quad , \quad (8)$$

where the following definitions apply:

$Y_i$	the concentration of Species $i$
$t$	time
$R_{f,i,j}$	the rate of formation of Species $i$ in Reaction $j$ of the set of $J$ reactions that form Species $i$
$R_{c,i,k}$	the rate of consumption of Species $i$ in Reaction $k$ of the set of $K$ reactions that consume Species $i$ .

The concentrations thus calculated can be compared with those measured experimentally in the reaction mixture.

Unfortunately, the real world presents experimental, computational, and operational obstacles to the pursuit of this simple validation scheme. First, for the integrity of the reaction mixture to be preserved, the

mixture must be contained in some sort of reaction chamber, which in turn gives rise to two side effects: leaks (intentional, as in sampling, or unintentional) and wall reactions. Second, when the most efficient computer codes are used, the time needed to solve the coupled differential equations increases as the square of the number of species. Moreover, certain sets of rates lead all too often to sets of "stiff" equations, for which the solution times can approach infinity. Finally, the urge always exists to "improve" a reaction mechanism, no matter how closely it approximates the experimental data; the computer code must allow these changes to be performed with a minimum amount of effort. In dealing with these realities, the researcher is called upon to display his mettle and to tax his ingenuity. The approaches we used in this study are described in this chapter.

#### A. CHAMBER EFFECTS

With few exceptions, reaction chambers are not completely airtight. Under normal operating conditions, this does not create a serious problem, since almost all chambers are maintained at atmospheric pressure, and since the small amount of interchange by diffusion can usually be ignored. However, a problem does arise when samples are removed from the chamber for analysis. Since the species that comprise smog exist in the atmosphere in minute (1 to 1000 ppb) concentrations, sample sizes on the order of a few liters are commonly needed to obtain enough material for an accurate analysis. Moreover, samples must be withdrawn fairly frequently during the reaction to monitor species concentrations that are changing rapidly. As a result, it is not unusual for 10 to 20 percent of the chamber volume to be withdrawn through sampling procedures. The reaction simulation technique must take this "dilution" of the reaction medium into account.

In the ideal case, the gas used for replacement of withdrawn samples is inert with respect to the reaction (e.g., pure nitrogen in a smog system), or it contains only reactive species whose concentrations are so large--relative to the amounts consumed or produced by the reactions--that they can be assumed to be constant throughout the reaction (e.g., oxygen or water vapor in "clean" air). In this case, it is sufficient to

apply a "dilution factor" to the concentrations of all the species (inert diluent) or to those that do not remain constant (clean air diluent). If samples of more or less constant size are removed at reasonably uniform time intervals, the dilution factor can be considered to be a constant,  $Q$ , and the equation for the rate of change of the concentration of Species  $i$  becomes

$$\frac{dy_i}{dt} = \sum_{j=1}^J R_{f i, j} - \sum_{k=1}^K R_{c i, k} - y_i Q \quad (9)$$

In some chamber experiments, however, the incoming medium is just the natural atmosphere in the laboratory, which may contain concentrations of pollutant species as high as or higher than those being followed in the reaction chamber. Moreover, it may be desirable in some cases to inject pollutants or pollutant precursors deliberately into the chamber to simulate the effect of fresh emissions on the reaction mechanism. As long as the concentration of Species  $i$ ,  $y_{in}$ , in the incoming medium is known, the effect of such inflowing species on the rate equation can be easily expressed:

$$\frac{dy_i}{dt} = \sum_{j=1}^J R_{f i, j} - \sum_{k=1}^K R_{c i, k} - (y_i - y_{in})Q \quad (10)$$

Unfortunately, wall effects cannot be handled as neatly. Wall absorption is best determined by placing the species in question,  $A$ , in a "nonreactive" environment within the chamber and following its decay with time. One can then include within the reaction mechanism an equation such as

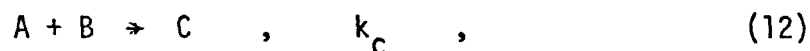


with an appropriate rate constant.

Heterogeneous catalysis by the reactor walls is even more troublesome. However, by determining reaction rates at several different surface-to-volume



ratios for the reactor (e.g., through the use of "artificial" walls to partition the chamber), the rate constants for the homogeneous and heterogeneous reactions can be obtained, and both reactions can be included in the mechanism:



## B. COMPUTATIONAL ASPECTS

As mentioned earlier, the computer time required to solve a set of differential equations increases at least as the square of the number of equations to be solved (or, in the present case, as the square of the number of distinct chemical species that appear in the reaction mechanism). Thus, any techniques that can be used to decrease the number of species concentrations that actually require coupled differential equations for their solution should be applied. Such techniques include the assumption of constant concentration; the uncoupling of product-only species; the invocation of the steady-state approximation; and the aggregation, or "lumping," of species that yield similar products. The last two techniques are the subjects of extensive discussion in Chapters VIII and IX and are thus not treated here.

As mentioned earlier, certain species that appear in the reaction mechanism either are present at truly constant concentrations (e.g., the reactor walls) or have concentrations so high--relative to the amounts of that species formed or consumed during the reaction--that they remain essentially constant with respect to time (e.g., oxygen). Since the change in concentration for these species is only negligibly different from zero, they can be excluded from the differential equation process.

A second category of species that need not be included in the set of coupled differential equations is comprised of those species that appear in the reaction mechanism only as products (e.g.,  $\text{CO}_2$  or  $\text{HNO}_3$ ). The rate of formation of these product species is, to be sure, represented by the

following differential equation:

$$\frac{dy_i}{dt} = \sum_{j=1}^J R_{f,i,j} \quad (14)$$

However, the presence of this species has no effect on the rate of formation of any other species; thus, the differential equation describing its formation can be uncoupled from the set of all differential equations and solved independently, at a significant savings in overall computer time.

### C. EASE OF CHANGING REACTIONS

Most computer codes used in the simulation of reaction kinetics incorporate, in one form or another, the features described above. The major advantage offered by the present program is the ease of preparation and, particularly, the ease of alteration of the mechanism and its associated species concentrations. The user need know nothing about computer programming or the solution of differential equations, and very little about chemical reaction mechanisms, to obtain meaningful results from the program.

On the first line of input, the user specifies the run identification, the number of reactions in the mechanism to be studied, how many of these are lumped reactions, the number of each of the various types of species described in Section VII-B, and an indication as to whether the reaction rates should be printed. The second line continues this specification of parameters with an indication of the frequency of printout, the time step sizes, and the dilution factor.

The user then submits his reaction mechanism, one reaction per line, restricted only by one requirement on ordering: The lumped reactions must appear last. Each reaction appears as an ordinary chemical equation, with a list of reactants, a list of products, and a rate constant. The products can have coefficients (either fractions or integers), but the reactants

cannot--each reactant molecule must be entered separately. The user can choose any four-letter mnemonic he wishes for the species names.

If there are any lumped reactions, the sets of individual reactions comprising each "lump" are then entered. Their formulation is exactly the same as that of the lumped reaction, except that the name of each species that contributes to the composition of the lump appears in place of the lumped species as the first reactant.

The user then provides the list of species and their initial concentrations--one per line. The order of their types must be the same as that given on the initial parameter line, but no particular order is required within each species type.

Should any of the species be present in the gas flowing into the reaction chamber, their concentrations in the inflowing stream and, if needed, the time and new values of any change in this concentration are entered next. Finally, the user can request concentration-time plots of any species. If he so desires, these plots can contain experimental points with which those points calculated by the proposed mechanism can be compared.

To change a rate constant or chemical reaction, the user need merely alter the corresponding input line. New reactions can be added by insertion; old ones can be removed by deletion. A similarly easy process can be used to change an initial species concentration or to add or remove species names from the list. Species can be transferred among species types (e.g., differential to steady state) by a single interchange of lines.

As previously noted, a complete user's guide to the computer program is included in Appendix A. This appendix (bound separately) provides detailed information on each of the features described above, descriptions and listings of all of the computer routines, and sample inputs and outputs.

## VIII THE QUASI-STEADY-STATE ASSUMPTION OF CHEMICAL KINETICS

The use of the quasi-steady-state assumption (QSSA) is probably as old as the theory of chemical kinetics itself. First developed by Bodenstein in 1913, this method essentially replaces the differential equations by algebraic ones in the rate equations for certain intermediate or transient species (Benson, 1960). Consequently, it considerably simplifies the rate equations, since the solution of differential equations is, in general, more difficult than the solution of comparable algebraic equations. Thus, the quasi-steady-state assumption has often been invoked not only in the early stages of the development of kinetic models for photochemical smog to simplify the complex system of rate equations (Westberg and Cohen, 1969; Friedlander and Seinfeld, 1969; Hecht and Seinfeld, 1972), but also in the literature (Smith and Urone, 1974).

With the recent development of increasingly high-speed digital computers and with the availability of ingenious software packages designed to solve systems of stiff ordinary differential equations [e.g., the Gear method (Gear, 1971)], the desirability of invoking the quasi-steady-state assumption has been questioned (Gelinas, 1972; Farrow and Edelson, 1974). In view of this controversy, we review the QSSA in this chapter.

We first discuss the reasons why the quasi-steady-state assumption must be invoked under certain specific situations. The reasons (or the needs) for the QSSA obviously cannot alone justify its use if unacceptably inaccurate or erroneous results are obtained by invoking the QSSA. The rest of the chapter is devoted to a quantitative assessment of the validity of the quasi-steady-state assumption.

## A. THE NEED FOR THE QUASI-STEADY-STATE ASSUMPTION

Regardless of its validity, the quasi-steady-state assumption is only an approximation of the full set of differential equations. Thus, this assumption should not be invoked without a legitimate reason. Although the most compelling reason for using the QSSA is always its simplicity, its applications in the past can be conveniently grouped into two categories of uses: analytical solutions and numerical solutions.

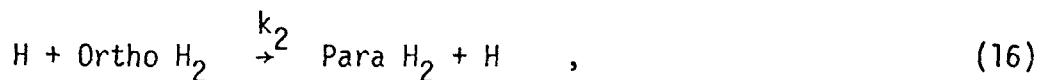
For many complex problems, it is often desirable to obtain analytical solutions, possibly at the expense of accuracy. In these cases, drastic simplifications have to be made; the quasi-steady-state assumption, when applicable, has been the most powerful tool available to simplify the kinetic equations. An example of this type of application appears in the analysis of laminar flames (Williams, 1965). In the so-called fundamental approaches, the quasi-steady-state assumption has been invoked in a non-isothermal system that involves molecular transport processes and multiple chemical reactions. After other suitable approximations have been introduced, closed-form solutions for the radical distributions and burning velocity can be obtained from the simplified set of equations. This procedure has proved to be extremely useful in the study of the ozone decomposition flame (Von Karman and Penner, 1954), the hydrogen-oxygen flame, and the hydrogen-bromine flame (Milan and da Riva, 1962).

With the availability of high-speed digital computers, the number of problems that are solved by directly seeking numerical solutions has been rising. Although the use of the quasi-steady-state assumption in such cases is not uncommon, its application is frequently suspect and has thus been the subject of controversy. The major advantage of introducing the quasi-steady-state assumption apparently lies in the savings in computational effort that can be realized because solving a system of algebraic equations is, in general, easier than solving a comparable system of differential equations. In cases where explicit solutions can be obtained for species for which the quasi-steady-state assumption has been invoked, the savings can be particularly substantial.

For kinetic mechanisms, such as those employed to delineate the photochemical transformations in urban atmospheres, which may involve as many as 50 elementary reaction steps, a typical simulation requires only a few tens of seconds of computing time on a modern computer, even when the full set of equations is used. Since the savings in computational time resulting from the use of the QSSA can amount to, at best, only a fraction of this relatively small amount of computing time, the invocation of the assumption is not justifiable per se in a kinetic study. However, studies of chemical kinetics are often imbedded in a larger and more complicated system that involves both physical and chemical processes. A superb example is the role played by photochemistry in the study of urban air pollution. Since the numerical solution of the entire problem requires considerably larger amounts of computing time (for instance, the SAI airshed model presently uses one hour of 360/165 computing time for a ten-hour simulation), the savings achieved by invoking the quasi-steady-state assumption in the repeated solution of the chemical kinetics is by no means trivial. Preliminary estimates indicate that a savings in computing time of up to 30 percent can be realized if a moderately complex kinetic mechanism (involving, say, 50 elementary steps) is incorporated into the urban airshed model. Therefore, the QSSA certainly ought to be an important consideration in the development of a more complex kinetic model if the eventual application is to be coupled with an urban airshed model.

#### B. THE VALIDITY OF THE QUASI-STEADY-STATE ASSUMPTION WHEN APPLIED TO A SIMPLE KINETIC MECHANISM

In addition to its success when applied to short-lived intermediates in straight-chain reactions, the quasi-steady-state assumption has been shown to be a valid approach for many other cases that cannot be strictly classified as chain reactions. However, the exact conditions under which the quasi-steady-state assumption is valid have been extremely difficult to delineate. To illustrate the major features that are involved in this approach, we discuss here a simple example concerning the conversion of ortho-hydrogen to para-hydrogen. The reaction mechanism for the initial phase of the conversion can be described (Williams, 1965) by



If we denote the concentrations of the following species by

$$[\text{Ortho H}_2] = \alpha \quad ,$$

$$[\text{Para H}_2] = \beta \quad ,$$

$$[\text{H}] = \gamma \quad ,$$

the rate equations for the product  $\beta$  and the intermediate  $\gamma$  can be written as

$$\frac{d\beta}{dt} = k_2\alpha\gamma \quad , \quad (18)$$

$$\frac{d\gamma}{dt} = 2k_1'(\alpha + \beta) - 2k_3'\gamma^2 \quad . \quad (19)^*$$

In Eq. (19), the conservation law for hydrogen is invoked:

$$[\text{H}_2] = [\text{Ortho H}_2] + [\text{Para H}_2] \approx \text{constant} \quad .$$

---

\* We use  $k_1'$  and  $k_3'$  to represent the quasi-first-order and quasi-second-order reaction rates for reaction Steps 1 and 3, respectively.

Through a differentiation of this relationship, a rate equation for  $\alpha$  can be found:

$$\frac{d\alpha}{dt} = -k_2\alpha\gamma \quad . \quad (20)$$

We now consider Eqs. (18) through (20), subject to the following initial conditions:

$$\alpha = A \quad , \quad (21)$$

$$\beta = 0 \quad , \quad (22)$$

$$\gamma = 0 \quad . \quad (23)$$

### 1. Exact Solutions

Analytical solutions for the system of equations posed above can be obtained. By eliminating  $\alpha$  and  $\beta$  from Eqs. (18) through (20) and by invoking the initial conditions given in Eqs. (21) and (22), we find that

$$\frac{d\gamma}{dt} = -2k_3'\gamma^2 + 2k_1' A \quad . \quad (24)$$

This is a Riccati equation, the exact solution to which, subject to Eq. (23), is the following (Kamke, 1971):

$$\gamma_{\text{exact}} = \sqrt{\frac{k_1'}{k_3'}} \sqrt{A} \tanh \left( 2\sqrt{k_1' k_3'} A t \right) \quad . \quad (25)$$

By substituting this solution for  $\gamma$  in Eq. (20), we can obtain the exact solution for  $\alpha$ :



$$\alpha_{\text{exact}} = A \cdot \left[ \cosh \left( 2 \sqrt{k_1' k_3'} A t \right) \right]^{-\frac{k_2}{2k_3'}} \quad (26)$$

## 2. Quasi-Steady-State Solutions

In this section, we seek the corresponding solutions for the system of equations when the quasi-steady-state assumption is applied to the reaction intermediate H. Thus, by setting the left-hand side of Eq. (19) equal to zero, we immediately obtain the solution for  $\gamma$ :

$$\gamma_{\text{QSSA}} = \sqrt{\frac{k_1'}{k_3'}} \cdot \sqrt{A} \quad (27)$$

Using this solution in Eq. (18), we can easily find the quasi-steady-state solution for  $\alpha$ :

$$\alpha_{\text{QSSA}} = A \cdot e^{\left( -k_2 \sqrt{\frac{k_1'}{k_3'}} \cdot \sqrt{A} t \right)} \quad (28)$$

These solutions [Eqs. (27) and (28)] can then be compared with their counterparts obtained above in Eqs. (25) and (26).

## 3. Comparison of the Exact and the Quasi-Steady-State Solutions

It is quite clear from a comparison of Eqs. (25) and (26), as shown in Figure 39, that differences between the two solutions depend upon the relative magnitudes of the time of interest and a characteristic time  $T$  defined by

$$T = \frac{1}{2 \sqrt{k_1' k_3'} A} \quad (29)$$

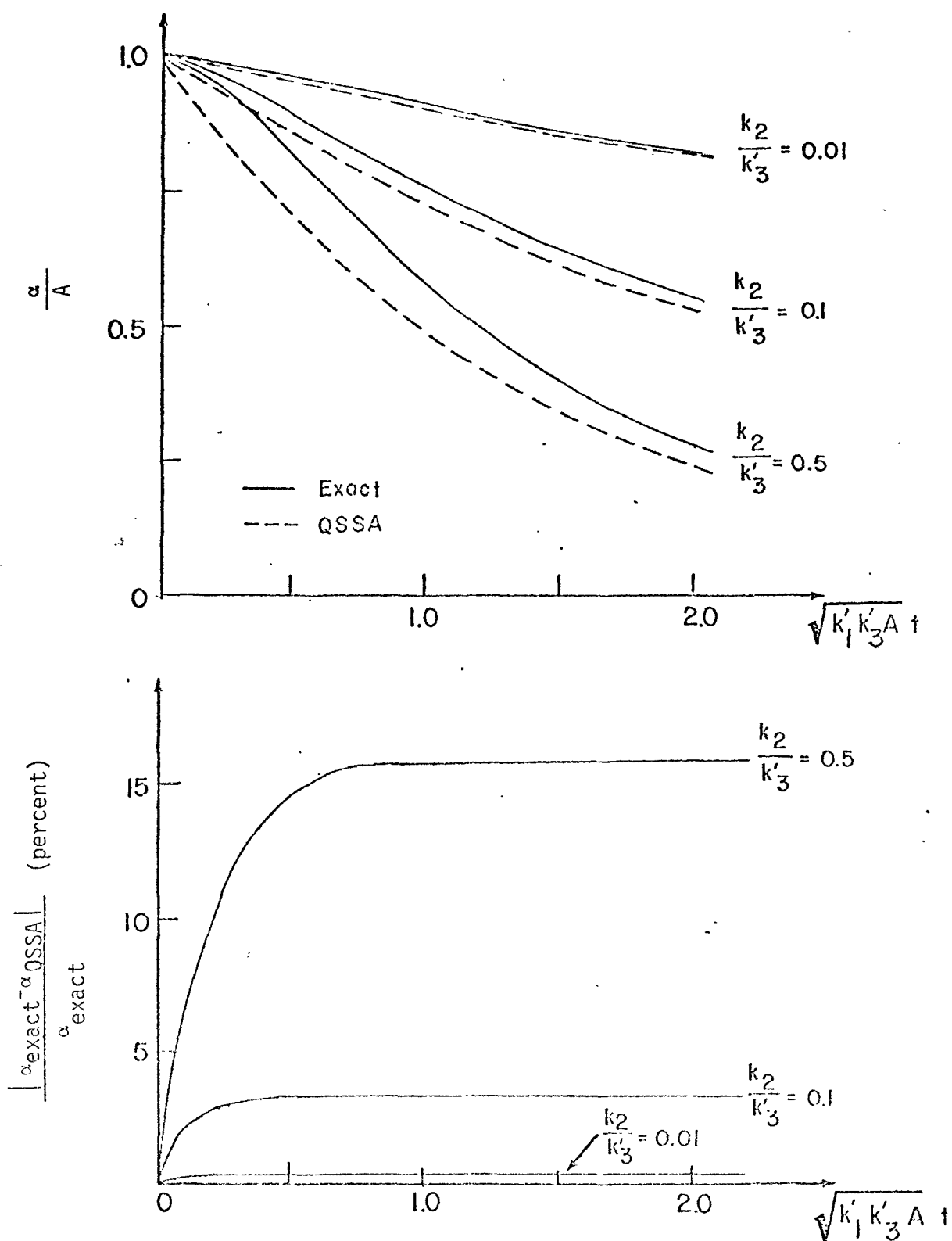


FIGURE 39. COMPARISONS OF THE EXACT AND THE QSSA SOLUTIONS FOR STABLE SPECIES

If the time of interest is considerably larger than this characteristic time,

$$t \gg T, \quad (30)$$

which is likely to occur if

$$k_3' \gg \frac{1}{k_1' A}, \quad (31)$$

then the analytical solution in Eq. (25) can be approximated by

$$r_{\text{exact}} \approx \sqrt{\frac{k_1'}{k_3'}} \cdot \sqrt{A}, \quad t \gg T, \quad (32)$$

which, of course, is the same as Eq. (27). Under the condition given in Eq. (30), the exact solution for  $\alpha$  [Eq. (26)] also reduces to

$$\begin{aligned} \alpha_{\text{exact}} &\approx A \cdot \left[ \frac{1}{2} e^{\left( 2 \sqrt{k_1' k_3'} A t \right)} \right]^{-\frac{k_2}{2k_3'}} \\ &\approx A \cdot 2^{\left( \frac{k_2}{2k_3'} \right)} e^{\left( -k_2 \sqrt{\frac{k_1'}{k_3'}} \sqrt{A} t \right)}, \quad t \gg T. \end{aligned} \quad (33)$$

Comparing Eqs. (28) and (33), as illustrated in Figure 40, we find that the error committed by the invocation of the quasi-steady-state assumption in the calculation for a stable species is bounded by a constant. This constant is dependent upon the ratio of the two rate constants  $k_2$  and  $k_3'$ :

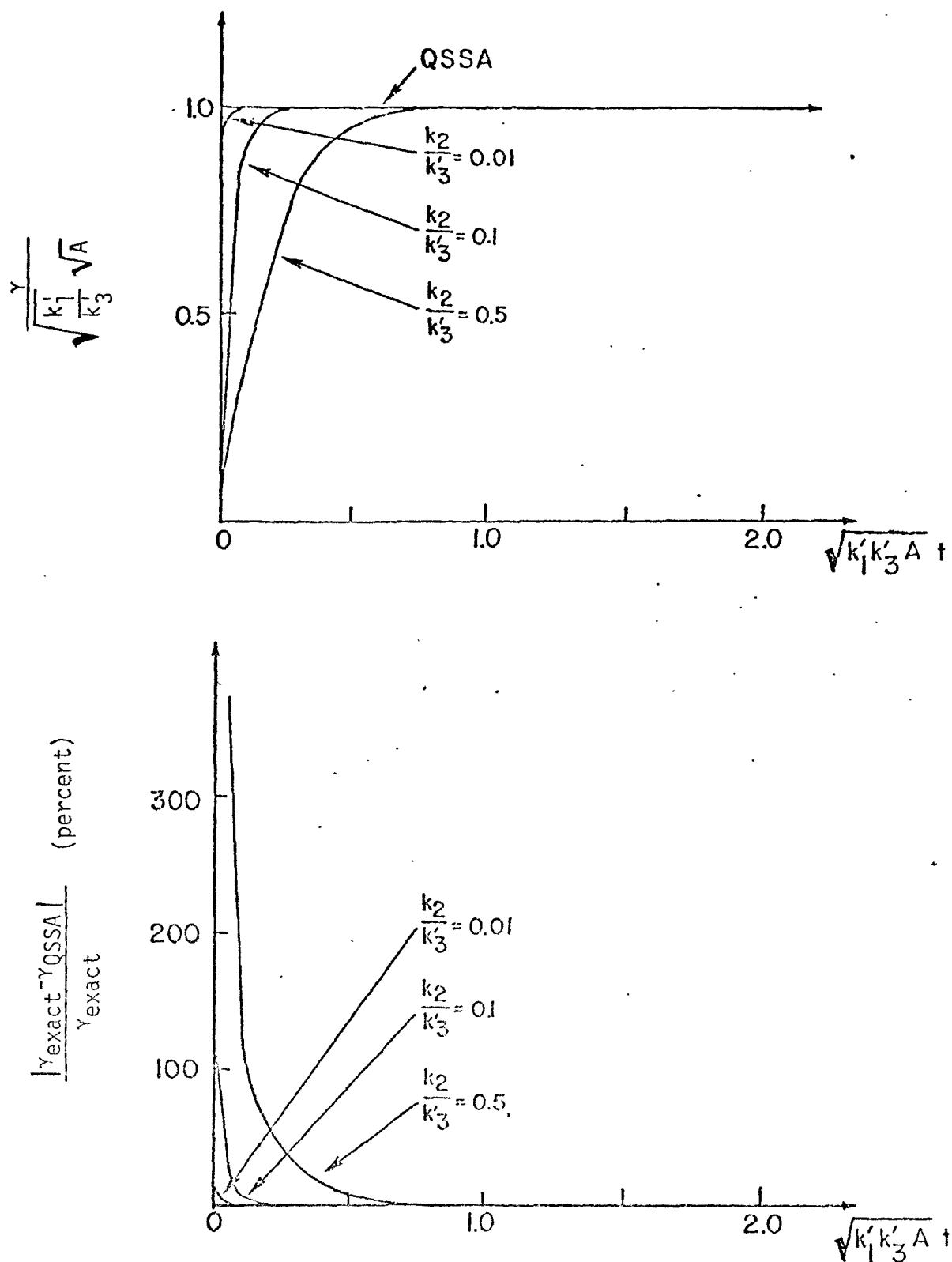


FIGURE 40. COMPARISONS OF THE EXACT AND THE QSSA SOLUTIONS FOR THE REACTION INTERMEDIATE

$$\text{Error} = 2 \left( \frac{k_2}{2k_3'} \right)^{-1} , \quad (34)$$

which tends to decrease to zero if

$$\frac{k_3'}{k_2} \gg 1 . \quad (35)$$

For finite but large  $k_3'/k_2$ , the values of the error are tabulated in Table 15. As Table 15 shows, for large values of  $k_3'/k_2$ , the quasi-steady-state solution is sufficiently accurate.

More insights can be gained if the above mathematical discussions are translated into physical descriptions. The validity of the quasi-steady-

Table 15  
ERROR RESULTING FROM THE USE OF THE QSSA

<u><math>(k_2/k_3')</math></u>	<u>Error (percent)</u>
1.0	41.4%
0.5	18.9
0.1	3.52
0.01	0.35
0.001	0.035

state assumption, according to this simple example, is always associated with a very large rate constant\* governing the consumption rate of the intermediate in question [in the above example,  $k_3'$ ; see Eqs. (31) and (35)]. Under this condition, the intermediate disappears as soon as it is formed; thus, after a short time period, the validity of neglecting the time derivative (i.e., justifying the invocation of the quasi-steady-state assumption) is evident. The invalidity of the quasi-steady-state assumption during this short time period, which might be called an "induction" period, is related to the boundary layer feature of the problem; a small parameter (in the above example,  $k_2/k_3'$ ) is associated with the highest derivative, a singular perturbation problem (Cole, 1968). Thus, the use of the quasi-steady-state assumption can be viewed as a formal procedure to obtain the zeroth order outer solution that is apparently invalid within the boundary layer (i.e., a short period of time). This aspect has been pointed out in a slightly different context by Bowen, Acrivos, and Oppenheim (1963).

According to the above analysis, the error incurred by invoking the quasi-steady-state assumption when it is valid remains constant or decays with time, in contrast to other types of errors, such as numerical errors due to finite differences, which generally grow with time because of accumulation. In fact, this feature has not only been demonstrated by Giddings and Shin (1961) for many other types of reaction mechanisms, but also it

---

\* This large rate constant will, on the other hand, inevitably introduce severe "stiffness" problems if the full set of equations is being used. In the limiting case, when this rate constant is extremely large, the invocation of the quasi-steady-state assumption is probably the only means of obtaining solutions, since it is doubtful that even the Gear method can reasonably deal with this situation.

has been confirmed by two numerical experiments--one reported by Gelinas (1972) and one carried out in the present study and discussed later.

### C. A GENERAL THEORY ON THE VALIDITY OF THE QUASI-STEADY-STATE ASSUMPTION

Despite the conclusive results, the findings presented in the last section are, rigorously speaking, applicable only to that specific mechanism; furthermore, the procedure used in the analysis cannot always be duplicated. This is particularly true for complex mechanisms where exact solutions are impossible to obtain and where interactions are expected. Based on this work, however, some of the logic involved in the derivation of the conclusions can be generalized to a certain extent. This section describes our preliminary efforts in this direction.

We consider the following general expression to be the full set of rate equations for the kinetic mechanism:

$$\frac{dy_i}{dt} = f_i(y_1, y_2, \dots, y_N; \epsilon) \quad , \quad i = 1, 2, \dots, N \quad . \quad (36)$$

A small parameter  $\epsilon$  was included because we know, from the last section, that an a priori condition for the validity of the quasi-steady-state assumption is the appearance of a very large rate constant. The reciprocal of this large number, properly nondimensionalized and designated here as  $\epsilon$ , was chosen in accordance with conventions used in the perturbation theory. Assuming that  $y_N$  is the species in the steady state, the solutions to Eq. (36) can be first expanded into power series in  $\epsilon$ :

$$y_i = y_i^{(0)} + \epsilon y_i^{(1)} + \epsilon^2 y_i^{(2)} + \dots \quad , \quad i = 1, 2, \dots, N \quad , \quad (37)^*$$

---

\* As pointed out by Bowen, Acrivos, and Oppenheim (1963), it may be necessary, under complicated situations, to invoke a noninteger power series in  $\epsilon$ . However, for the sake of simplicity, it probably suffices to consider a simple power series in the present study.

Substituting Eq. (37) into Eq. (36) and equating the likely power of  $\epsilon$ , we formally obtain the following for the zeroth order:

$$\begin{aligned}\frac{dy_i^{(0)}}{dt} &= f_i \left[ y_1^{(0)}, y_2^{(0)}, \dots, y_N^{(0)} \right], \quad i = 1, 2, \dots, N-1, \\ 0 &= f_N \left[ y_1^{(0)}, y_2^{(0)}, \dots, y_N^{(0)} \right].\end{aligned}\quad (38)$$

For the first order, we obtain

$$\frac{dy_i^{(1)}}{dt} = \sum_{j=1}^N a_{ij}^{(1)} y_j^{(1)}, \quad (39)$$

where  $a_{ij}^{(1)}$  can be a function of  $y_1^{(0)}, y_2^{(0)}, \dots, y_N^{(0)}$ .

Presumably, Eq. (38) will yield the quasi-steady-state solutions, and Eq. (39) will represent the first-order correction. If we can establish that the solutions to Eq. (39) are bounded, then we can conclude that the error incurred by invoking the quasi-steady-state assumption is at most on the order of  $\epsilon$ . With this objective in mind, we rewrite Eq. (39) in matrix form:

$$\frac{dY}{dt} = AY, \quad (40)$$

where  $Y$  is a column matrix with elements  $y_i^{(1)}$  and  $A = \left[ a_{ij}^{(1)} \right]$ . The solutions to Eq. (40) can be generally written as

$$y_i^{(1)} = \sum_{j=1}^N c_{ij} e^{\lambda_j t}, \quad (41)$$



where  $\lambda_j$  are the eigenvalues of Matrix A, defined by,

$$|\lambda I - A| = 0 \quad . \quad (42)$$

Our objective, however, is not to seek the general solutions of Eq. (40). Rather, we are interested in knowing only certain behavior characteristics of these solutions--particularly, whether they will grow or decay. This will, of course, depend on whether all of the characteristic roots have negative real parts, i.e., whether Matrix A is a stability matrix. The answer to this question is provided by the Hurwitz criterion (Bellman, 1960). According to this criterion, the condition for Matrix A being a stability matrix is that the following sequence of determinants must be positive:

$$\begin{vmatrix} b_1 \end{vmatrix} , \quad \begin{vmatrix} b_1 & 1 \\ b_3 & b_2 \end{vmatrix} , \quad \begin{vmatrix} b_1 & 1 & 0 \\ b_3 & b_2 & b_1 \\ b_5 & b_4 & b_3 \end{vmatrix} , \dots \quad . \quad (43)$$

The elements in these determinants are obtained from the characteristic polynomial of A ,

$$|\lambda I - A| = \lambda^N + b_1 \lambda^{N-1} + \dots + b_{N-1} \lambda + b_N \quad . \quad (44)$$

To illustrate the use of the above theory, we again use the example in Section VIII-B. First of all, recognizing that  $k_3'$  is relatively large compared with the other two rate constants, we let

$$\epsilon = \frac{k_2}{k_3'} ,$$

where  $k_2$  is arbitrarily chosen to form a nondimensional parameter. To create a proper balance of each term in Eqs. (18) through (20), the following transformations are required:

$$\lambda = \frac{\Gamma}{\sqrt{k_3'}} ,$$

$$t = \sqrt{k_3'} \tau .$$

Then, Eqs. (18) through (20) become

$$\frac{d\alpha}{d\tau} = -k_2 \Gamma \alpha , \quad (45)$$

$$\frac{d\beta}{d\tau} = k_2 \Gamma \alpha , \quad (46)$$

$$\epsilon \frac{d\Gamma}{d\tau} = 2k_1' k_2 (\alpha + \beta) - 2k_2 \Gamma^2 . \quad (47)$$

By assuming that

$$\alpha = \alpha^{(0)} + \epsilon \alpha^{(1)} + \epsilon^2 \alpha^{(2)} + \dots ,$$

$$\beta = \beta^{(0)} + \epsilon \beta^{(1)} + \epsilon^2 \beta^{(2)} + \dots ,$$

$$\Gamma = \Gamma^{(0)} + \epsilon \Gamma^{(1)} + \epsilon^2 \Gamma^{(2)} + \dots ,$$

we obtain the following for the zeroth order:

$$\frac{d\alpha^{(0)}}{d\tau} = -k_2 \Gamma^{(0)} \alpha^{(0)} , \quad (48)$$

$$\frac{d\beta^{(0)}}{d\tau} = k_2 \Gamma^{(0)} \alpha^{(0)} , \quad (49)$$

$$0 = 2k_1' k_2 [\alpha^{(0)} + \beta^{(0)}] - 2k_2 \Gamma^{(0)2} . \quad (50)$$

These equations are identical to the set of equations obtained from a direct invocation of the quasi-steady-state assumption for Eqs. (18) through (20). Similarly, the equations for the first-order correction can be found:

$$\frac{d\alpha^{(1)}}{d\tau} = -k_2 \Gamma^{(0)} \alpha^{(1)} - k_2 \alpha^{(0)} \Gamma^{(1)} ,$$

$$\frac{d\beta^{(1)}}{d\tau} = k_2 \Gamma^{(0)} \alpha^{(1)} + k_2 \alpha^{(0)} \Gamma^{(1)} ,$$

$$\frac{d\Gamma^{(1)}}{d\tau} = 2k_1' k_2 \alpha^{(1)} + 2k_1' k_2 \beta^{(1)} - 4k_2 \Gamma^{(0)} \Gamma^{(1)} ,$$

using a coefficient matrix A,

$$A = \begin{bmatrix} -k_2 \Gamma^{(0)} & 0 & -k_2 \alpha^{(0)} \\ k_2 \Gamma^{(0)} & 0 & k_2 \alpha^{(0)} \\ 2k_1' k_2 & 2k_1' k_2 & -4k_2 \Gamma^{(0)} \end{bmatrix} .$$

The characteristic polynomial is then given by

$$\begin{aligned} |\lambda I - A| &= \begin{vmatrix} \lambda + k_2 \Gamma^{(0)} & 0 & -k_2 \alpha^{(0)} \\ k_2 \Gamma^{(0)} & \lambda & k_2 \alpha^{(0)} \\ 2k_1' k_2 & 2k_1' k_2 & \lambda + 4k_2 \Gamma^{(0)} \end{vmatrix} , \\ &= \lambda^3 + 5k_2 \Gamma^{(0)} \lambda^2 + 4k_2^2 \Gamma^{(0)^2} \lambda - 4k_1' k_2^3 \alpha^{(0)} \Gamma^{(0)} . \end{aligned}$$

Hence, the sequence of determinants, as expressed in Eq. (43), is

$$\left| 5k_{2\Gamma}(0) \right|, \left| \begin{array}{cc} 5k_{2\Gamma}(0) & 1 \\ -4k_1'k_{2\alpha}^3(0)_{\Gamma}(0) & 4k_{2\Gamma}^2(0)^2 \end{array} \right|.$$

Since both of these determinants are positive irrespective of the zeroth-order solutions, we conclude that under all conditions the error incurred by invoking the quasi-steady-state assumption is on the order of  $\epsilon$ . The reader will recall that, according to the analysis presented in Section VII-B, the error is given by

$$\begin{aligned} \text{Error} &= 2^{\left(\frac{k_2}{2k_3'}\right) - 1} \\ &= 2^{\left(\frac{\epsilon}{2}\right) - 1} \\ &= e^{\left(\frac{\ln 2}{2} \epsilon\right) - 1} \\ &\approx \frac{\ln 2}{2} \epsilon, \quad \text{if } \epsilon \ll 1. \end{aligned}$$

This confirms the conclusion we obtained above.

The application of the theory derived in this section to more complex kinetic mechanisms is certainly possible. Although in principle there is no limit to the number of equations,  $N$ , that can be treated using the theory, algebraic manipulations can become extremely tedious if the number of equations exceeds five. For this reason, we do not employ the theory we derived above to assess the validity of the quasi-steady-state assumption for intermediates in the mechanism discussed in Table 1. Rather, a set of

"head-to-head" numerical experiments was carried out. Nevertheless, we can demonstrate through these numerical experiments that phenomena and conclusions obtained from the theoretical analysis still hold, albeit qualitatively, in cases where more complex kinetic mechanisms are involved.

#### D. SOME NUMERICAL EXPERIMENTS USING THE GENERAL MECHANISM

In this section, we describe a set of "head-to-head" numerical experiments we conducted to assess the validity of introducing the quasi-steady-state assumption. Because of our familiarity with it, the general kinetic mechanism (Table 1) was chosen for this test. The experiments, also used by Gelinas (1972) for the same purpose, simply consist of two sets of numerical simulations,\* one that invokes the quasi-steady-state assumption and one that does not. The conditions are otherwise identical. Comparisons of the two sets of predictions yield information regarding the errors incurred by invoking the quasi-steady-state assumption.

For the experiments, the following four species in the general mechanism were chosen to test the validity of the quasi-steady-state assumption:  $\text{RCO}_3$ ,  $\text{RO}_2$ ,  $\text{O}$ , and  $\text{O}_3$ . Initial conditions corresponding to EPA smog chamber Run 325 were used (Hecht, Seinfeld, and Dodge, 1974). The differences, in percentages, between the predictions calculated with and without the quasi-steady-state assumption for each individual species are presented in Table 16. The large deviation between the solution obtained through the use of the quasi-steady-state assumption and the exact solution, as shown in the last column of Table 16, clearly indicates that ozone is probably not a good candidate for the application of the quasi-steady-state assumption. This conclusion, however, should not be confused with the well-known photostationary state assumption (Leighton, 1961; O'Brien, 1974) in the study of photochemistry. The photostationary state assumption postulates that an approximate balance exists between the photolysis of nitrogen dioxide and the reverse reaction of nitric oxide oxidation by

---

\* The Gear technique (1971) was used to integrate the system of ordinary differential equations.

Table 16

PERCENTAGE ERRORS INCURRED BY USING THE QUASI-STEADY-STATE ASSUMPTION

Time (minutes)	Species			
	$\text{RCO}_3$	O	$\text{RO}_2$	$\text{O}_3$
0.2128	-1.29	2.04	-15.78	27.77
0.5128	0.17	0.04	- 0.45	7.72
1.013	-0.40	-0.04	0.32	4.61
4.013	0.01	0.01	0.24	4.67
9.413	0.02	0.01	0.13	5.19
18.92	0.18	-1.10	1.03	5.42
28.92	0.14	-1.32	- 0.89	6.78
43.92	0.11	-1.49	- 0.89	11.10
53.92	0.15	-1.42	2.82	16.81
63.92	0.17	-1.25	0.47	33.87
78.92	0.20	-0.87	- 1.24	400.33
93.92	0.08	-0.06	- 1.00	384.76
108.9	0.05	0.20	- 0.53	193.31
123.9	0.01	0.38	- 0.15	119.51
138.9	-0.02	0.52	0.01	81.50
163.9	0.06	0.56	0.07	45.02
188.9	0.08	0.66	0.21	18.26
213.9	0.15	0.72	0.43	-10.62

ozone. The differences (in percentages) between ozone concentrations calculated under the photostationary assumption and those resulting from the exact solution in the same numerical experiment are shown in Table 17. A comparison of Tables 16 and 17 shows that the photostationary state assumption works quite well for the time span of interest.\*

On the other hand, Table 16 shows that, for  $\text{RCO}_3$ ,  $\text{O}$ , and  $\text{RO}_2$ , the errors incurred by invoking the quasi-steady-state assumption are all within 1 percent after an initiating time period, implying that the quasi-steady-state assumption is apparently acceptable for this specific case. Also, the errors for these three cases tend to decrease with time. This verifies one of the key features we derived in the theoretical studies: The quasi-steady-state solution, when applicable, will converge to the exact solution. This same behavior has also been observed by Gelinas (1972) in a similar experiment.

#### E. CONCLUSIONS

Although the quasi-steady-state assumption clearly should not be invoked indiscriminately, its use can be fruitful in certain cases. A potential example is the application of the kinetic model to the urban airshed model. In these cases, however, care must be taken to ascertain that the species for which the quasi-steady-state assumption is invoked are judiciously chosen and that their validities are thoroughly assessed.

---

\* The accuracy of the photostationary state at later times can, of course, be further improved if one includes the ozone-nitrogen dioxide and ozone-hydrocarbon reactions.

Table 17  
PERCENTAGE ERRORS INCURRED  
BY USING THE PHOTOSTATIONARY STATE ASSUMPTION

<u>Time (minutes)</u>	<u>Percentage Error in Ozone Concentrations</u>
5.925	0.45%
18.92	0.76
23.92	0.92
28.92	0.97
43.92	1.35
53.92	1.82
63.92	2.81
78.92	7.19
93.92	12.47
108.9	13.55
123.9	14.02
138.9	14.44
163.9	15.24
188.9	16.06
213.9	17.17



## IX TREATMENT OF COMPLEX MIXTURES OF ORGANIC REACTANTS IN THE KINETIC MECHANISM

One of the major difficulties in the study of photochemical air pollution is that the contaminated atmosphere consists of a multitude of organic species with widely varying capabilities of participating in photochemical reactions. Because a kinetic model of reasonable size for atmospheric applications cannot individually incorporate all organic species that participate in the photochemical reactions, a means must be found to lump the organics together. This chapter presents an analytic technique for approaching this problem.

To illustrate the principles of the proposed technique, we chose the general kinetic model (Table 1) as the basis for the following discussion. In the kinetic mechanism, the reactive hydrocarbons are grouped into the following four categories:

- >  $HC_1$  = olefins
- >  $HC_2$  = aromatics
- >  $HC_3$  = paraffins
- >  $HC_4$  = aldehydes.

Since the atmosphere contains a variety of species having widely varying rate constants and stoichiometric coefficients within each group, a scheme is needed to evaluate the lumped rate constants and stoichiometric coefficients for these four lumped hydrocarbons.

To begin, consider as an example a mixture of  $M$  individual olefins, denoted by  $OL_1, OL_2, \dots, OL_M$ , and represented as one lumped olefin,  $HC_1$ .

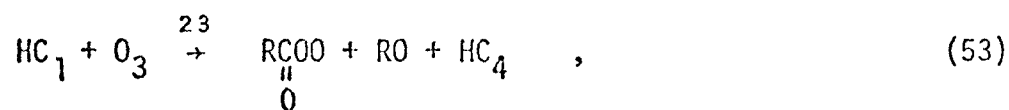
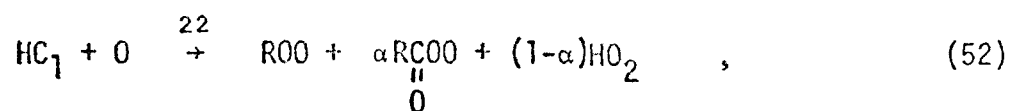
We assume that the concentrations (in moles), as well as the respective rate constants and stoichiometric coefficients, are all known. The following tabulation summarizes the characteristics of this example:

<u>Species</u>	<u>Concentration</u>	<u>Rate Constants*</u>			<u>Stoichiometric Coefficient</u>
$OL_1$	$[OL_1]$	$r_{22,1}$	$r_{23,1}$	$r_{24,1}$	$\alpha_1$
$OL_2$	$[OL_2]$	$r_{22,2}$	$r_{23,2}$	$r_{24,2}$	$\alpha_2$
.	.	.	.	.	.
.	.	.	.	.	.
.	.	.	.	.	.
$OL_M$	$[OL_M]$	$r_{22,M}$	$r_{23,M}$	$r_{24,M}$	$\alpha_M$

The objective is to obtain lumped rate constants ( $r_{22}$ ,  $r_{23}$ ,  $r_{24}$ ) and a lumped stoichiometric coefficient ( $\alpha$ ) for the lumped olefin whose concentration is

$$[HC_1] = \sum_{i=1}^M [OL_i] \quad (51)$$

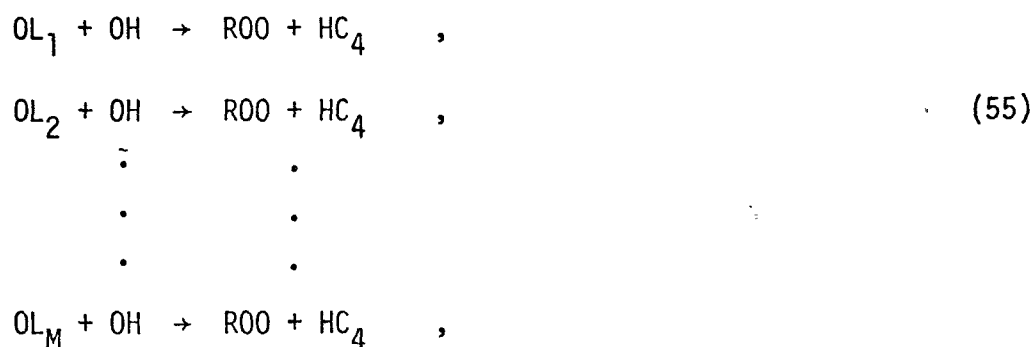
The pertinent chemical reactions for the olefins are




---

\* The numbers 22, 23, and 24 refer to reaction numbers in the mechanism (Table 1).

Consider the last reaction first. For each individual olefin, the reaction steps can be expressed by



with the overall reaction step represented by Eq. (54). The rates of depletion of olefins due to Eqs. (54) and (55) can be written, respectively, as

$$\frac{\delta[\text{HC}_1]}{\delta t} = -r_{24} [\text{HC}_1] [\text{OH}] \quad , \quad (56)$$

$$\left. \begin{array}{rcl}
 \frac{\delta[\text{OL}_1]}{\delta t} & = & -r_{24,1} [\text{OL}_1] [\text{OH}] \\
 \frac{\delta[\text{OL}_2]}{\delta t} & = & -r_{24,2} [\text{OL}_2] [\text{OH}] \\
 \cdot & & \cdot \\
 \cdot & & \cdot \\
 \cdot & & \cdot \\
 \frac{\delta[\text{OL}_M]}{\delta t} & = & -r_{24,M} [\text{OL}_M] [\text{OH}]
 \end{array} \right\} \quad (57)$$

However, because other oxidants ( $\text{O}$  and  $\text{O}_3$ ) are continuously in competition with  $\text{OH}$  for depletion of the olefins [Eqs. (52) and (53)], these equalities can hold only instantaneously. Therefore, we use a different symbol for the time derivative,  $\delta/\delta t$ , to emphasize this fact. Now, if we sum both the left- and right-hand sides of Eq. (57) and invoke Eq. (51), we find that

$$\begin{aligned}
\frac{\delta[\text{HC}_1]}{\delta t} &= - \left\{ r_{24,1}[\text{OL}_1] + r_{24,2}[\text{OL}_2] + \dots + r_{24,M}[\text{OL}_M] \right\} \cdot [\text{OH}] \\
&= - \sum_{i=1}^M \left\{ r_{24,i}[\text{OL}_i] \right\} \cdot [\text{OH}] \\
&= - \sum_{i=1}^M \left\{ r_{24,i} Y_i \right\} \cdot [\text{HC}_1] \cdot [\text{OH}] \quad . \quad (58)
\end{aligned}$$

Comparing Eqs. (56) and (58), we immediately obtain

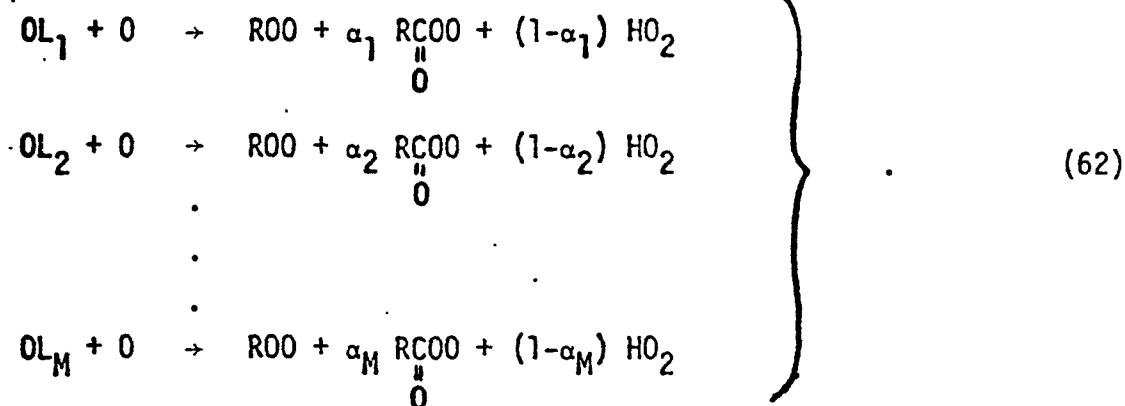
$$r_{24} = \sum_{i=1}^M r_{24,i} Y_i \quad , \quad (59)$$

where  $Y_i$  denotes the mole fraction of  $\text{OL}_i$ . One can similarly show that for the reactions in Eqs. (52) and (53),

$$r_{22} = \sum_{i=1}^M r_{22,i} Y_i \quad , \quad (60)$$

$$r_{23} = \sum_{i=1}^M r_{23,i} Y_i \quad . \quad (61)$$

To obtain the lumped stoichiometric coefficient  $\alpha$  in Eq. (52), we can repeat the same procedures. The individual reactions can be written as



The rate equations for production of  $\underset{\text{O}}{\underset{\parallel}{\text{RCOO}}}$  due to Eqs. (52) and (62) are, respectively,

$$\frac{\delta}{\delta t} [\underset{\text{O}}{\underset{\parallel}{\text{RCOO}}}] = \alpha r_{22} [\text{OL}_1] \cdot [\text{O}] \quad , \quad (63)$$

$$\begin{array}{rcl}
 \frac{\delta}{\delta t} [\underset{\text{O}}{\underset{\parallel}{\text{RCOO}}}]^{(1)} & = & \alpha_1 r_{22,1} \cdot [\text{OL}_1] \cdot [\text{O}] \\
 \frac{\delta}{\delta t} [\underset{\text{O}}{\underset{\parallel}{\text{RCOO}}}]^{(2)} & = & \alpha_2 r_{22,2} \cdot [\text{OL}_2] \cdot [\text{O}] \\
 & \cdot & \\
 & \cdot & \\
 & \cdot & \\
 \frac{\delta}{\delta t} [\underset{\text{O}}{\underset{\parallel}{\text{RCOO}}}]^{(M)} & = & \alpha_M r_{22,M} \cdot [\text{OL}_M] \cdot [\text{O}]
 \end{array} \quad \left. \vphantom{\begin{array}{c} \frac{\delta}{\delta t} [\underset{\text{O}}{\underset{\parallel}{\text{RCOO}}}]^{(1)} \\ \frac{\delta}{\delta t} [\underset{\text{O}}{\underset{\parallel}{\text{RCOO}}}]^{(2)} \\ \cdot \\ \cdot \\ \cdot \\ \frac{\delta}{\delta t} [\underset{\text{O}}{\underset{\parallel}{\text{RCOO}}}]^{(M)} \end{array}} \right\} \quad (64)$$

Again, if we sum both sides of Eq. (64) and use the identity

$$\frac{\delta}{\delta t} [\underset{\text{O}}{\underset{\parallel}{\text{RCOO}}}] = \sum_{i=1}^M \frac{\delta}{\delta t} [\underset{\text{O}}{\underset{\parallel}{\text{RCOO}}}]^{(i)} \quad ,$$

we finally find that

$$\alpha = \frac{1}{r_{22}} \sum_{i=1}^M \alpha_i r_{22,i} Y_i = \frac{\sum_{i=1}^M \alpha_i r_{22,i} Y_i}{\sum_{i=1}^M r_{22,i} Y_i} \quad (65)$$

Thus, we have obtained the desired formulas for computing the lumped rate constants and stoichiometric coefficient for the olefins.

In appearance, Eqs. (59) through (61) are similar to the type of formula first proposed by Jackson (1963), who used a linear summation of the products of mole fractions and the corresponding rates of individual component hydrocarbons to calculate the overall reactivity for the mixture. In his calculation, reactivities were based on the initial mole fractions of the reactants. He then assumed that the relative mole fractions of the individual components remain constant as the reactions take place; this, of course, is incorrect, except in the degenerate case when the reactivities of all the various components are identical. In all other cases, as the reactions proceed, the more reactive species are depleted at a faster rate. Consequently, the influence of these species diminishes most rapidly with time. Therefore, it is obvious that the straightforward linear summation method tends to overpredict the overall reaction rate.

The essence of the present scheme lies in its recognition of the temporal variations of the hydrocarbon concentrations. Two procedures, one exact and one approximate, have been proposed to update the mole fractions.

#### A. EXACT SOLUTIONS

With a kinetic model available, the updating of the hydrocarbon mole fractions can be achieved analytically. For example, the exact concentration history of  $[OL_i]$  can be shown as

$$[OL_i]_t = [OL_i]_0 e^{-\int_0^t \left\{ r_{22,i}[O](\tau) + r_{23,i}[O_3](\tau) + r_{24,i}[OH](\tau) \right\} d\tau} \quad (66)$$

We should emphasize that no assumption whatsoever has been used in deriving Eq. (66). The application of this equation, however, requires the continuous knowledge of the concentration levels of  $O$ ,  $O_3$ , and  $OH$ . This can be achieved approximately in the numerical kinetic model as follows.

Assume that the time steps used in the numerical model are, in sequence,

$$\Delta t_1, \Delta t_2, \Delta t_3, \dots, \Delta t_N$$

(we have allowed for a variable step-size numerical scheme, such as the one now being used). Then, using the initial concentrations (at the beginning of time step  $\Delta t_n$ ) of  $O$ ,  $O_3$ ,  $OH$ , denoted by  $[O]_{(n)}$ ,  $[O_3]_{(n)}$ ,  $[OH]_{(n)}$  for the time interval,  $\Delta t_n$ , Eq. (66) becomes

$$[OL_i]_t = [OL_i]_0 \cdot \exp \left\{ -r_{22,i} \left( \sum_{n=1}^N [O]_{(n)} \Delta t_n \right) - r_{23,i} \left( \sum_{n=1}^N [O_3]_{(n)} \Delta t_n \right) - r_{24,i} \left( \sum_{n=1}^N [OH]_{(n)} \Delta t_n \right) \right\} \quad (67)$$

Or, more simply, the updating of  $[OL_i]_{(n+1)}$  can be accomplished by computing

$$[OL_i]_{(n+1)} = [OL_i]_{(n)} \exp \left( - \left\{ r_{22,i} \cdot [O]_{(n)} + r_{23,i} \cdot [O_3]_{(n)} + r_{24,i} \cdot [OH]_{(n)} \right\} \Delta t_n \right) \quad (68)$$

which can readily be implemented in the kinetic model.

To test the validity of the proposed scheme, we carried out the following numerical experiment. Employing our kinetic model, we used three different methods to treat the binary hydrocarbon mixture (propylene and ethylene):

- > Propylene and ethylene were modeled as two distinct olefins (each represented by a different equation). This scheme is, therefore, an "exact" means of modeling a binary hydrocarbon system with the general mechanism.
- > Propylene and ethylene were lumped together using the linear scheme (Jackson, 1963).
- > Propylene and ethylene were lumped together using the proposed lumping scheme.

The initial conditions, identical for all three, are listed below:

<u>Species</u>	<u>Concentration (ppm)</u>
NO	1.25
NO <sub>2</sub>	0.08
Paraffin	3.41
Ethylene	0.184
Propylene	0.046

Comparisons of the predicted hydrocarbon consumption rates and ozone production rates are presented in Tables 18 and 19. The accuracy of the proposed scheme is demonstrated by the small deviations between it and the exact scheme: less than 0.3 percent after 375 minutes of simulation. In contrast, during the same interval, the linear scheme overpredicted (as expected) the hydrocarbon consumption by 4 percent and the ozone production by 15.2 percent.

As a further example, we also carried out tests for two kinetic simulations discussed in Sections III-B and III-C. The first run involved a group of five individual paraffins, and the second, six olefins. Because of the large number of hydrocarbon species involved and the wide disparity in reactivity (at least in the case of the olefins), these runs provide a more severe test for our proposed lumping scheme.



Table 18

## COMPARISON OF HYDROCARBON CONSUMPTION FOR DIFFERENT LUMPING SCHEMES

<u>Time (minutes)</u>	<u>Exact Scheme (ppm)</u>	<u>Linear Scheme* (ppm)</u>	<u>Present Scheme* (ppm)</u>
0	0.2300	0.2300	0.2300
130	0.1949	0.1947 (0.1%)	0.1948 (0.05%)
300	0.1485	0.1459 (1.8%)	0.1482 (0.2%)
375	0.1292	0.1240 (4.0%)	0.1288 (0.3%)

---

\* Percentages in parentheses indicate deviations from the exact scheme.

Table 19

## COMPARISON OF OZONE PRODUCTION FOR DIFFERENT LUMPING SCHEMES

<u>Time (minutes)</u>	<u>Exact Scheme (pphm)</u>	<u>Linear Scheme* (pphm)</u>	<u>Present Scheme* (pphm)</u>
0	0	0	0
130	0.2539	0.2550 (4.3%)	0.2539 (0%)
300	1.924	2.033 (5.7%)	1.926 (0.1%)
375	6.948	8.005 (15.2%)	6.970 (0.3%)

---

\* Percentages in parentheses indicate deviations from the exact scheme.

Tables 20 and 21 compare the predictions for the paraffins and ozone derived from the exact scheme with those from the proposed scheme. The maximum differences observed during a six-hour simulation were 0.53 percent for ozone and 0.16 percent for the paraffins. The computational time for the two runs was 1.524 seconds for the exact scheme and 1.420 seconds for the lumping scheme. Thus, the lumping scheme results in a 7 percent savings in computation time for the paraffin run.

Tables 22 and 23 present the results for the olefins. These data again confirm the accuracy of the proposed scheme; the maximum differences are 1.08 percent for ozone and 0.31 percent for the olefins for a six-hour simulation period. The extremely small differences for the two predictions for the olefins are particularly noteworthy because, at the end of six hours, the five most reactive species were depleted by more than 99.9 percent! The wide range of rate constants for the six olefins is also apparently responsible for the impressive savings of computing time; lumping apparently reduced the stiffness of the system of equations. The computational times were 3.236 seconds for the exact scheme and 2.402 seconds for the lumping scheme. Thus, the lumping scheme resulted in a 25.8 percent savings in computing time.

## B. APPROXIMATE SOLUTIONS

In the absence of a kinetic model, the lumped rate constant of a hydrocarbon mixture can be obtained in the following manner. Consider as an example the species  $OL_i$ . If we invoke the steady-state assumption for  $[O]$ ,  $[O_3]$ ,  $[OH]$ , which, for the time being, we interpret as

$$[O], [O_3], [OH] \approx \text{constant} \quad , \quad (69)$$

we can write the solution for  $[OL_i]$  as

$$[OL_i]_t = [OL_i]_0 e^{-k_i t} \quad , \quad (70)$$

with

$$k_i = r_{22,i} [O] + r_{23,i} [O_3] + r_{24,i} [OH] \quad , \quad (71)$$

Table 20

## COMPARISON OF HYDROCARBON CONSUMPTION IN THE MULTIPARAFFIN RUN

<u>Time (minutes)</u>	<u>Exact Scheme (ppm)</u>	<u>Present Scheme (ppm)</u>	<u>Difference (percent)</u>
0	1.770	1.770	--%
102.8	1.639	1.638	-0.06
202.8	1.457	1.455	-0.14
302.8	1.305	1.303	-0.15
362.8	1.235	1.233	-0.16

Table 21

## COMPARISON OF OZONE PRODUCTION IN THE MULTIPARAFFIN RUN

<u>Time (minutes)</u>	<u>Exact Scheme (pphm)</u>	<u>Present Scheme (pphm)</u>	<u>Difference (percent)</u>
0	0	0	--%
102.8	0.5250	0.5245	-0.10
202.8	7.779	7.738	-0.53
302.8	30.23	30.17	-0.20
362.8	39.10	39.05	-0.13

Table 22

## COMPARISON OF HYDROCARBON CONSUMPTION IN THE MULTIOLEFIN RUN

<u>Time (minutes)</u>	<u>Exact Scheme (ppm)</u>	<u>Present Scheme (ppm)</u>	<u>Difference (percent)</u>
0	6.505	6.505	--%
51.49	4.034	4.028	-0.15
100.1	2.842	2.845	+0.11
200.1	1.672	1.675	+0.18
361.6	0.759	0.757	-0.26

Table 23

## COMPARISON OF OZONE PRODUCTION IN THE MULTIOLEFIN RUN

<u>Time (minutes)</u>	<u>Exact Scheme (pphm)</u>	<u>Present Scheme (pphm)</u>	<u>Difference (percent)</u>
0	0	0	--%
51.49	0.5649	0.5608	-0.73
100.1	0.5921	0.5857	-1.08
200.1	0.6686	0.6674	-0.18
361.6	0.7039	0.7061	+0.31

where  $[OL_i]_t$  is the instantaneous concentration of  $OL_i$  at Time  $t$  and  $[OL_i]_0$  is the initial value. Thus, an expression for the time-dependent mole fractions can be derived:

$$y_i = \frac{[OL_i]_0 e^{-k_i t}}{\sum_{j=1}^M [OL_j]_0 e^{-k_j t}} \quad (72)$$

Equation (72) takes care of only the "aged" olefins injected at Time 0; any fresh addition of olefins at a subsequent time should, of course, be included in computing this mole fraction.

As an illustration of the use of the approximate technique, consider the following example. For a binary mixture of ethylene and propylene, we have the following information:

Species	$[OL]_0$ (ppm molar)	$r_{22}$ (ppm <sup>-1</sup> min <sup>-1</sup> )	$r_{23}$ (ppm <sup>-1</sup> min <sup>-1</sup> )	$r_{24}$ (ppm <sup>-1</sup> min <sup>-1</sup> )
Ethylene	0.060	722	0.004	2,500
Propylene	0.015	4,000	0.016	25,000

Using this information, we can calculate the lumped rate constants from Eqs. (59), (60), (61), (71), and (72), provided that we know  $[O]$ ,  $[O_3]$ , and  $[OH]$  levels. For example,

$$r_{22} = \frac{[Eth]_0 e^{-k_{Eth} t} \cdot r_{22, Eth} + [Prop]_0 e^{-k_{Prop} t} \cdot r_{22, Prop}}{[Eth]_0 e^{-k_{Eth} t} + [Prop]_0 e^{-k_{Prop} t}} \quad (73)$$

where

$$k_{\text{Eth}} = r_{22,\text{Eth}} \cdot [\text{O}] + r_{23,\text{Eth}} \cdot [\text{O}_3] + r_{24,\text{Eth}} \cdot [\text{OH}] \quad ,$$

$$k_{\text{Prop}} = r_{22,\text{Prop}} \cdot [\text{O}] + r_{23,\text{Prop}} \cdot [\text{O}_3] + r_{24,\text{Prop}} \cdot [\text{OH}] \quad .$$

Similar expressions can be derived from  $r_{23}$  and  $r_{24}$ . These results are plotted in Figures 41 through 43. The time-dependent feature of these rate constants is apparent.

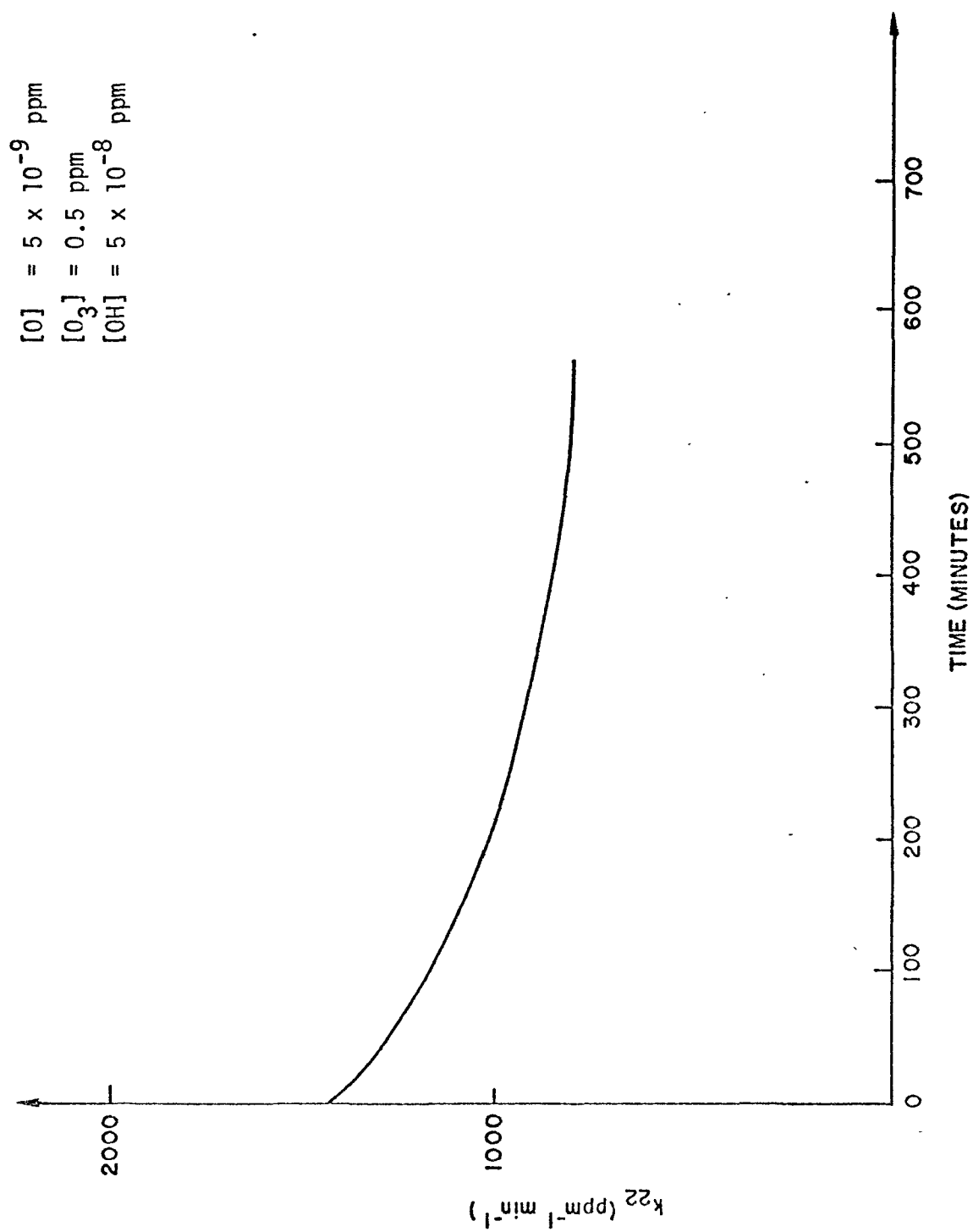
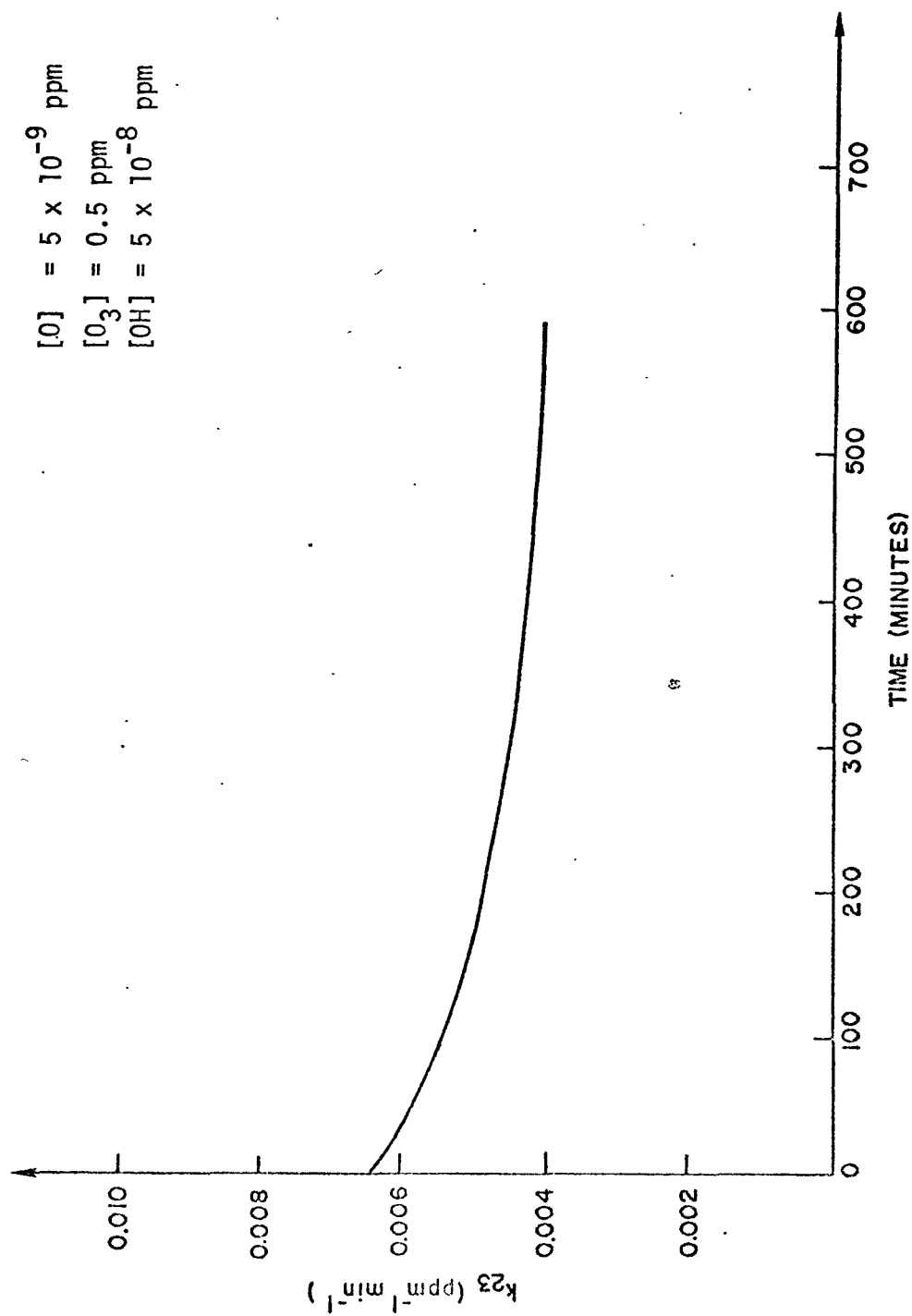


FIGURE 41. THE RATE CONSTANT FOR HC + O

FIGURE 42. THE RATE CONSTANT FOR  $HC + O_3$





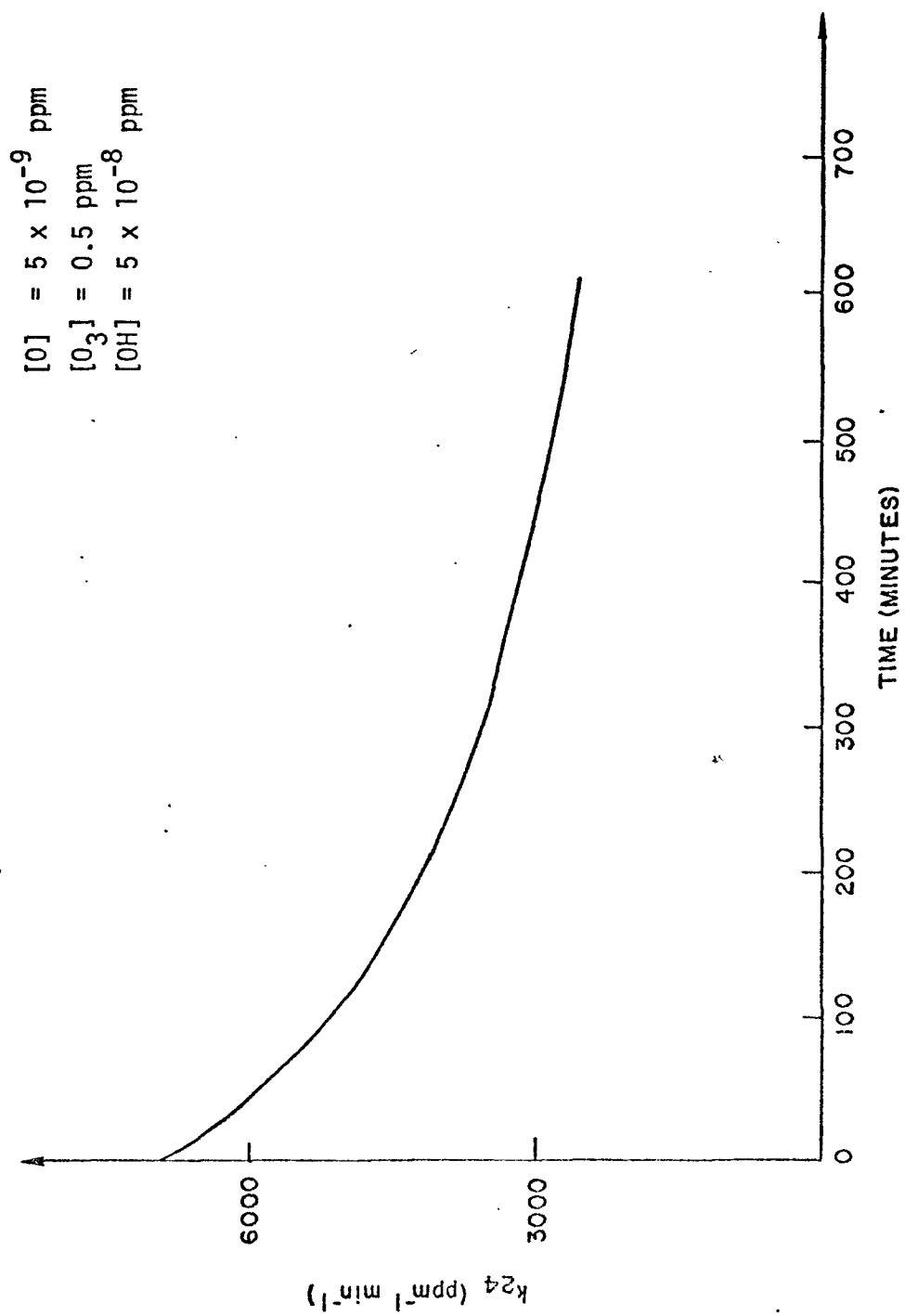


FIGURE 43. THE RATE CONSTANT FOR HC + OH

PART 3  
OVERVIEW AND PROSPECT

## X OVERVIEW AND PROSPECT

Our formulation of the general kinetic mechanism is limited in exactness by uncertainties in the kinetics of elementary reactions, and the thoroughness of our evaluation suffers from incomplete measurements in smog chambers. For the many inorganic reactions in the mechanism that have been studied by several different investigators over the years, there is virtually no doubt about the nature of the reactants and products, and the rate constants are "known" within a factor of 1.5 or less of the true values. However, although the rate constants of many other reactions in the general mechanism have been measured by at least one group, too often little effort has been made to identify the products of the elementary reactions (at times, because mechanistic studies are difficult or impossible using the kinetic techniques employed). In such cases, we know the importance of the specific reactions as loss mechanisms for the reactants involved, but we can only speculate as to the intermediates and subsequent reactions of the intermediates. Finally, there are some reactions in the mechanism that have never been studied experimentally. These are reactions that should occur, according to thermochemical considerations, but have not yet been observed directly. Thus, both the mechanism and the rate constants are, at best, intelligent speculation.

The smog chamber data base possesses a similar mix of strengths and weaknesses. If we specifically consider the UCR evacuable chamber system, one of the newest and most technically advanced systems presently in use, we can cite a long list of attributes, such as the following:

- > Measurements of most organics, PAN, NO, NO<sub>2</sub>, and O<sub>3</sub>, with an accuracy of better than  $\pm 5$  percent, even at pphm concentrations.
- > Characterization of the rate of NO<sub>2</sub> photolysis.

- > Characterization of the rate of  $O_3$  decay on the walls.
- > Control of the temperature within the chamber.

Yet, the magnitude and nature of many other chamber effects and operating parameters are poorly characterized, and some of the most important chemical species in the smog system, the free radicals, are not measurable routinely, if at all.

Consequently, the development of a kinetic mechanism might be viewed as a quest to piece together a puzzle showing a blurred and evolving picture, with some pieces that are rigid and well shaped, others that are moldable, and still others (possibly) that are missing. Smog chamber scientists are continually striving to improve the picture, kineticists are adding and changing pieces, and the modelers are ordering and re-arranging the pieces in new ways to complete the picture as much as possible. But every time that either our perception of the picture or our set of pieces changes, the model may also have to be changed.

We are speaking of a picture as though there were only one. In fact, we showed in Figure 21 that the model can predict the behavior of reactants under a single set of initial conditions very well. If we were interested only in that one case, we would probably conclude that the general mechanism is quite satisfactory.

But in actual fact our expectations and needs are broader, and every smog chamber experiment that uses a different set of initial reactant ratios provides a new and stiffer test for the kinetic mechanism. Once we have shown that a particular formulation of the general reaction scheme works well, we construct new ways to stress the model--to test the completeness and accuracy of the reactions and the values of the rate constants. As inadequacies appear, steps are taken to resolve the deficiencies, and a new and stronger formulation of the general mechanism results.

We shall continue this type of development work next year. If predictions do not appear to improve substantially from one year to the next,

it is partly because the tests of the model are growing increasingly broad. But new information is continually being introduced into the mechanism, new reactions are being studied in kinetics laboratories, and new species and effects are being measured in smog chambers.

In short, we are well along the path from ignorance to knowledge, and the roots of the general mechanism are being based increasingly on fact rather than speculation. We are confident that the combination of experimental and theoretical research being performed will result in an accurate, reliable mechanism for photochemical smog formation.

## REFERENCES

- Beauchene, J. H., et al. (1973), Proceedings of the Seventh Conference on Space Simulation, Los Angeles, California (12-14 November 1973).
- Bellman, R. (1960), Introduction to Matrix Analysis (McGraw-Hill Book Company, Incorporated, New York).
- Benson, S. W. (1960), The Foundations of Chemical Kinetics (McGraw-Hill Book Company, Incorporated, New York).
- \_\_\_\_\_ (1968), Thermochemical Kinetics (John Wiley and Sons, New York).
- Bowen, J. R., A. Acrivos, and A. K. Oppenheim (1963), "Singular Perturbation Refinement to Quasi-Steady State Approximation in Chemical Kinetics," Chem. Engrg. Sci., Vol. 18, pp. 177-188.
- Bufalini, J. J., S. L. Kopczynski, and M. C. Dodge (1972), Environ. Letters, Vol. 3, p. 101.
- Calvert, J. G., et al. (1972), Science, Vol. 175, p. 751.
- Cole, J. D. (1968), Perturbation Methods in Applied Mathematics (Blaisdell Publishing Company, Waltham, Massachusetts).
- Cvetanovic, R. J. (1963), Adv. in Photochemistry, Vol. 1, p. 115.
- Davis, D. D., et al. (1972), "A Kinetics Study to Determine the Importance of HO<sub>2</sub> in Atmospheric Chemical Dynamics: Reaction with CO," presented at the Symposium on Sources, Sinks, and Concentrations of CO and CH<sub>4</sub> in the Earth's Environment, St. Petersburg Beach, Florida (August 1972).
- Demerjian, K. L., J. A. Kerr, and J. G. Calvert (1974), Advances in Environmental Sciences and Technology, J. N. Pitts and R. L. Metcalf, eds., Vol. 4, pp. 1-262 (John Wiley and Sons, New York).
- Doyle, G., and A. M. Winer (1974), private communication, University of California, Riverside, California.
- Elias, L. (1963), J. Chem. Phys., Vol. 38, p. 989.
- Farrow, L. A., and D. Edelson (1974), "The Steady State Approximation: Fact or Fiction?," to appear in Int'l. J. Chem. Kinetics.
- Friedlander, S. K., and J. H. Seinfeld (1969), "A Dynamic Model of Photochemical Smog," Environ. Sci. Technol., Vol. 3, pp. 1175-1181.

- Garvin, D., and R. F. Hampson, eds. (1974), "Chemical Kinetics Data Survey VII. Tables of Rate and Photochemical Data for Modelling the Stratosphere," Report NBSIR 74-430, National Bureau of Standards, Washington, D. C. (January 1974).
- Gay, B. W., Jr., and J. J. Bufalini (1971), Environ. Sci. Technol., Vol. 5, p. 422.
- Gear, C. W. (1971), "The Automatic Integration of Ordinary Differential Equations," Comm. of the Assoc. for Comput. Machinery, Vol. 14, pp. 176-179.
- Gelinas, R. J. (1972), "Stiff Systems of Kinetic Equations - A Practitioner's View," J. Comput. Phys., Vol. 9, pp. 222-236.
- Ghormley, J. A., R. L. Ellsworth, and C. J. Hochanadel (1973), J. Phys. Chem., Vol. 77, p. 1341.
- Giddings, J. C., and H. K. Shin (1961), "Departure from the Steady State in Complex Reactions with a Reactive Intermediate," Trans. Faraday Soc., Vol. 57, pp. 468-483.
- Golden, D., D. Hendry, and D. Mendenhall (1974), private communication, Stanford Research Institute, Menlo Park, California.
- Greiner, N. R. (1970a), J. Chem. Phys., Vol. 53 p. 1070.
- \_\_\_\_\_ (1970b), ibid, P. 1284.
- Hanst, P. L. (1971), J. Air Pollut. Contr. Ass., Vol. 21, p. 269.
- Hecht, T. A., and J. H. Seinfeld (1972), "Development and Validation of a Generalized Kinetic Mechanism for Photochemical Smog," Environ. Sci. Technol., Vol. 6, pp. 47-57.
- Hecht, T. A., J. H. Seinfeld, and M. C. Dodge (1974), "Further Development of a Generalized Kinetic Mechanism for Photochemical Smog," Environ. Sci. Technol., Vol. 8, pp. 327-339.
- Hecht, T. A., P. M. Roth, and J. H. Seinfeld (1973), "Mathematical Simulation of Atmospheric Photochemical Reactions: Model Development, Validation, and Application," Report R73-28, Systems Applications, Incorporated, San Rafael, California.
- Herron, J. T., and R. E. Huie (1969), J. Phys. Chem., Vol. 73, p. 3327.
- Holmes, J. R., et al. (1973), Environ. Sci. Technol., Vol. 7, p. 519.



- Jackson, M. W. (1963), "Effects of Some Engine Variables and Control Systems on Composition and Reactivity of Exhaust Hydrocarbons," SAE Prog. in Technol., Vehicle Emissions, Vol. 12, Part II (Selected SAE Papers, 1963-1966), pp. 241-267 (1967).
- Jaffe, S., and H. W. Ford (1967), J. Phys. Chem., Vol. 71, p. 1832.
- Jaffe, R. J. (1972), "Study of Factors Affecting Reactions in Environmental Chambers," Report LMSC/A997745, Lockheed Missiles and Space Company, Sunnyvale, California (May 1972).
- Johnston, H. S., et al. (1970), "Atmospheric Chemistry and Physics," Vol. 4, Project Clear Air, Task Force Assessments, University of California.
- Kamke, E. (1971), Differentialgleichungen Lösungsmethoden und Lösungen (Chelsea Publishing Company, New York).
- Leighton, P. A. (1961), The Photochemistry of Air Pollution (Academic Press, Incorporated, New York).
- Millan, G., and I. da Riva (1962), Eighth International Symposium on Combustion (Williams and Wilkins Company, Baltimore, Maryland).
- Morris, E. D., Jr., and H. Niki (1973), J. Phys. Chem., Vol. 75, p. 3640 (1971).  
\_\_\_\_\_, J. Phys. Chem., Vol. 77, p. 1929.
- Niki, H., E. E. Daby, and B. Weinstock (1972), Advan. Chem., Vol. 113, p. 16.
- O'Brien, R. J. (1974), "Photostationary State in Photochemical Smog Studies," Environ. Sci. Technol., Vol. 8, pp. 579-583.
- O'Neal, H. E., and C. Blumstein (1973), Int. J. Chem. Kinetics, Vol. V, p. 397.
- Roth, P. M., et al. (1974), "Development of a Second Generation of Photochemical Air Quality Simulation Models: Interim Report," Systems Applications, Incorporated, San Rafael, California.
- Schuck, E. A., E. R. Stephens, and P. R. Schrock (1966), J. Air Pollut. Contr. Ass., Vol. 16, p. 695.
- Schuck, E. A., et al. (1972), "Reaction of Peroxyacetyl Nitrate with Nitric Oxide," Statewide Air Pollution Research Center, Riverside, California.
- Seinfeld, J. H., T. A. Hecht, and P. M. Roth (1973), "Existing Needs in the Experimental and Observational Study of Atmospheric Chemical Reactions: A Recommendations Report," Report EPA-R4-73-031, Environmental Protection Agency, Research Triangle Park, North Carolina.

- Smith, J. P., and P. Urone (1974), "Static Studies of Sulfur Dioxide Reactions," Environ Sci. Technol., Vol. 8, pp. 742-746.
- Stephens, E. R. (1969), "Advances in Environmental Sciences and Technology," Interscience, Vol. 1, p. 119.
- Von Karman, T., and S. S. Penner (1954), Selected Combustion Problems, Fundamentals and Aeronautical Applications (AGARD, Butterworths Scientific Publications, London).
- Wei, Y. K., and R. J. Cvetanovic (1963), Can. J. Chem., Vol. 41, p. 913.
- Westberg, K., and N. Cohen, "The Chemical Kinetics of Photochemical Smog as Analyzed by Computer," Report ATR-70 (8107)-1, Aerospace Corporation, El Segundo, California.
- Westberg, K. (1973), private communication, Aerospace Corporation, El Segundo, California.
- Williams, F. A. (1965), Combustion Theory (Addison-Wesley Publishing Company, Incorporated, Reading, Massachusetts).

TECHNICAL REPORT DATA (Please read Instructions on the reverse before completing)			
1. REPORT NO. EPA-650/4-74-040		3. RECIPIENT'S ACCESSION NO.	
4. TITLE AND SUBTITLE Mathematical Simulation of Smog Chamber Photochemical Experiments		5. REPORT DATE November 1974	
7. AUTHOR(S) Thomas A. Hecht, Mei-Kao Liu, David C. Whitney		6. PERFORMING ORGANIZATION CODE	
9. PERFORMING ORGANIZATION NAME AND ADDRESS Systems Applications, Inc. 950 Northgate Drive San Rafael, California 94903		8. PERFORMING ORGANIZATION REPORT NO. R74-9	
12. SPONSORING AGENCY NAME AND ADDRESS U. S. Environmental Protection Agency Office of Research and Monitoring National Environmental Research Center Research Triangle Park, N. C. 27711		10. PROGRAM ELEMENT NO. 1A1008	
		11. CONTRACT/GRANT NO. 68-02-0580	
		13. TYPE OF REPORT AND PERIOD COVERED Final (June 1973 - June 1974)	
15. SUPPLEMENTARY NOTES		14. SPONSORING AGENCY CODE	
16. ABSTRACT <p>The continual development and testing of a kinetic mechanism for photochemical smog is described. Several rate constant values were updated, in line with recent experimental measurements, and simulations of several EPA smog chamber runs were repeated. The predictions vary in their agreement with experimental observations but tend to be best at high initial hydrocarbon-to-NO<sub>x</sub> ratios. The mechanism also reproduced the behavior of a complex mixture of paraffins and NO<sub>x</sub> and a mixture of six olefins and NO<sub>x</sub>. A sensitivity analysis of the mechanism was carried out. The results were combined with uncertainty estimates of the rate constants to quantify the importance of determining individual rate constants with greater accuracy. Preliminary modeling of smog chamber data collected at the University of California, Riverside, was also undertaken.</p> <p>This report was submitted in fulfillment of Contract No. 68-02-0580 by Systems Applications, Incorporated under the sponsorship of the Environmental Protection Agency.</p>			
17. KEY WORDS AND DOCUMENT ANALYSIS			
a. DESCRIPTORS	b. IDENTIFIERS/OPEN ENDED TERMS	c. COSATI Field/Group	
Photochemical modeling Chemical kinetics Atmospheric chemical modeling			
18. DISTRIBUTION STATEMENT Unlimited	19. SECURITY CLASS (This Report) Unclassified	21. NO. OF PAGES 178	
	20. SECURITY CLASS (This page) Unclassified	22. PRICE	

ENVIRONMENTAL PROTECTION AGENCY  
Technical Publications Branch  
Office of Administration  
Research Triangle Park, N.C. 27711

OFFICIAL BUSINESS

AN EQUAL OPPORTUNITY EMPLOYER

POSTAGE AND FEES PAID  
ENVIRONMENTAL PROTECTION AGENCY  
EPA - 335



Return this sheet if you do NOT wish to receive this material ☐,  
or if change of address is needed ☐ (Indicate change, including  
ZIP code )

PUBLICATION NO. EPA-650/4-74-040